(NASA-CR-158032) CONCENTRATOR ENHANCED SOLAR ARRAYS DESIGN STUDY Final Report (Lockheed Missiles and Space Co.) 114 p HC A06/MF A01 CSCL 10A

N79-14546

Unclas
G3/44 41947

CONCENTRATOR ENHANCED SOLAR ARRAYS

DESIGN STUDY

FINAL REPORT

LMSC-D665407
JPL955110

OCTOBER 1978

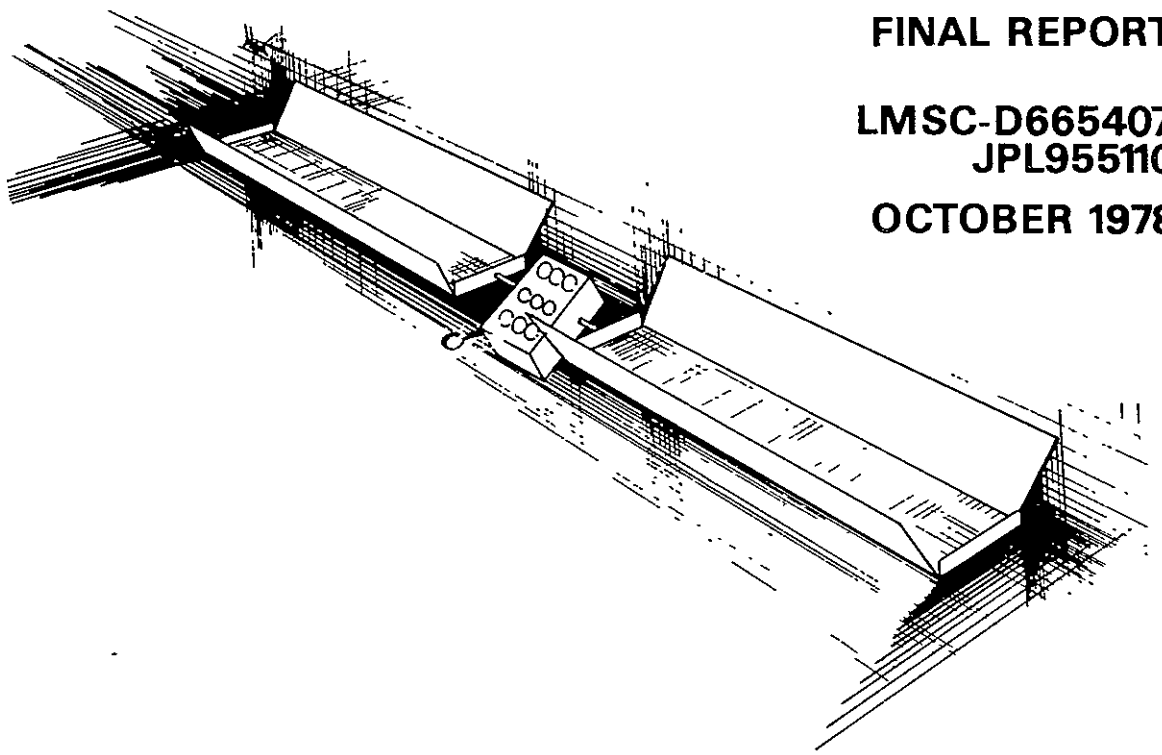

PERFORMED BY *Lockheed* **MISSILES & SPACE COMPANY, INC.**

FOR JET PROPULSION LABORATORY—PASADENA, CALIFORNIA

LMSC-D665407
October 1978

CONCENTRATOR ENHANCED SOLAR ARRAYS DESIGN STUDY

FINAL REPORT

JPL955110

Prepared By

D. R. LOTT
W. R. SZMYD
K. L. JOHNSON

This work was performed for the Jet Propulsion Laboratory, California Institute of Technology, sponsored by the National Aeronautics and Space Administration under Contract NAS7-100.

LOCKHEED MISSILES & SPACE COMPANY, INC.

FOREWORD

The findings of a study which was performed to evaluate the feasibility and the advantages associated with incorporating trough reflectors on the NASA-MSFC (LMSC) lightweight SEP Solar Array are summarized in this final report. The baseline design developed is for a concentrator enhanced solar array which will provide 25 kW at 1 AU. This document was prepared in compliance with the JPL Contract No. 955110 Statement of Work. Its content is not necessarily endorsed by the Jet Propulsion Laboratory, California Institute of Technology, or the National Aeronautics and Space Administration.

CONTENTS

CONTENTS (Continued)

(III IV)

ILLUSTRATIONS

ILLUSTRATIONS (continued)

ILLUSTRATIONS (continued)

TABLES

Section 1
SUMMARY

The work reported herein pertains to the analysis and preliminary design of a 25 kW concentrator enhanced lightweight flexible solar array. The design and analysis activity were based on adaptation and minor modification of the NASA-MSFC lightweight Solar Electric Propulsion (SEP) array technology for reflector augmentation. The JPL Contract Technical Manager for this study was Mr. J. H. Stevens. The study was organized into five major tasks which ran somewhat concurrently during the four month study span. The tasks were: (1) assessment and specification of design requirements, (2) mechanical design, (3) electrical design, (4) concentrator design, and (5) cost projection. The study incorporated three oral working reviews at LMSC and a final study presentation at JPL in September 1978. The tasks were conducted in an iterative manner so as to best derive a baseline design selection. The objectives of the study are discussed in Section 2 and comparative configuration and mass data on the SEP array design, concentrator array design options, and configuration/mass data on the selected concentrator enhanced solar array baseline design are presented. In Section 3, which is the major section of this report, design requirements, supporting design analysis and detailed baseline design data are discussed. Section 4 contains the results of the cost projection analysis and Section 5 contains a discussion of new technology.

1.1 STUDY CONCLUSIONS

The primary finding of this study is that it is feasible mechanically with modifications to incorporate concentrators on the SEP array, and that the resultant system is more effective from a weight and cost standpoint. A 25 kW Concentrator Enhanced Solar Array (CESA) system provides 81.5 watts/kg whereas an equivalent planar SEP provides 69.5 watts/kg, for over 17% increase in power density associated with the mass of the systems. Through reflected energy augmentation it is possible to reduce the number of solar cell panels in the CESA array, 22 panels less, and realize over 22% reduction in cost from (ROM) 11.057 million for a SEP flight set to (ROM) 8.548 million for a CESA flight set.

The other significant conclusions of this study are as follows:

- The problems associated with reflector distortion and poor planiarity can be eliminated by the use of reflector guide wires, intermediate reflector joint ribs, and proper reflector blanket tensioning.

- A trough type reflector is the simplest type to use with the SEP array without adversely impacting array aspect ratio.

- Unbalanced reflected illumination on solar arrays can have as significant a power throttling effect on concentrator arrays as does shadowing. However, this effect can be eliminated by greater reflector width or preferably, with minor power reduction, lower reflector angles.

- For 1 AU to 3 AU the SEP baseline circuit module and panel design can be used directly with CESA and will comply with the 200 to 400 volt system requirement.

- A counterbalance/cable system can be used to offset the eccentric loads that trough reflectors impose on the array deployment mast, and result in an overall lighter system.

- Fixed position (concentrator angle) reflector mechanisms are inherently less complex and more reliable than adjustable angle systems that would be required with defocussing.

1.2 RECOMMENDATIONS

To technically substantiate the very high payoffs associated with the use of a CESA type of lightweight array for a variety of missions including the comet ion drive applications, the following work should be initiated.

- A full-scale reflector blanket design and suspension design should be fabricated to evaluate producibility and deployment-planiarity factors.

- Root section full scale models of the reflector box hinge-staging mechanisms should be fabricated and subjected to static load tests.

- A three dimensional model should be set up for the CESA and dynamic analysis run for selected systems in 5 kW increments from 15 to 40 kW.

- Work should be initiated on spectrally selective reflector surfaces to assess technology readiness on this approach to enhanced power gain without adverse temperature penalties.

Section 2

INTRODUCTION

2.1 OBJECTIVES

The purpose of the study was to conduct a conceptual design and analysis associated with incorporating a concentrator system on the NASA-MSFC (LMSC) SEP Solar Array. The concentrated solar array system thus derived is intended for use on ion drive propelled Comet mission spacecraft. It can, however, have application on a variety of mission applications where solar photovoltaic power systems are required and it will result in lower weight and lower aspect ratios. In this general power domain the use of concentrator augmented solar arrays will also result in lower cost, photovoltaic power systems now and for the future until significant price reductions occur for solar cells.

The major study objectives were as follows:

- Develop conceptual designs for a solar array concentrator - Using the SEP solar array as a baseline, a primary objective was to assess concentrator concepts that could be integrated with the basic array in a manner which would have minimum impact on the developmental and qualification status of the SEP array.

- Perform supporting concentrator analysis - Another major objective was to conduct an extensive analysis of conceptual concentrators to assess the effects on performance of a broad category of geometrical parameters of the concentrator reflectors such as size, concentrator angle, and concentrator distortion.

- Select a baseline 25 kW design - A paramount objective in the study was to perform iterative mechanical configuration tradeoffs with the findings of concentrator analysis to derive the most feasible baseline concentrator enhanced solar array which would provide 25 kW at 1 AU. As a part of

baseline selection it was also necessary to perform supporting dynamic, thermal, structural, and electrical analysis to verify the design integrity of the baseline.

- Generate performance and mass data for the baseline - Taking the baseline selected, an objective was to develop BOL power performance characteristics from 1 AU to 3 AU based on solar cell characteristics and temperature projections. It was also an objective to develop the design in sufficient detail so that a detailed weight summary could be prepared.

- Perform a cost projection analysis - The last objective, based on the baseline concentrator enhanced solar array, was to develop a preliminary cost projection incorporating relative nonrecurring and recurring cost projections. These projections were prepared to provide an input for technical and management assessment of concentrator vs planar array relative advantages, and to provide ROM cost numbers for planning purposes.

2.2 CONCENTRATOR ENHANCED SOLAR ARRAY (CESA) OVERVIEW

A brief discussion is provided here of the NASA-MSFC Lightweight (SEP) Solar Array, concentrator configurations which were reviewed as possible candidates for power enhancement via the use of reflectors with planar arrays, and an overview description of the selected baseline CESA concept. A summary is thus provided early in this study report of the basic design that was to be modified for incorporation of reflectors, concentrator/reflector concepts available for consideration and a description of the baseline concentrator enhanced solar array that evolved.

2.2.1 NASA-MSFC Lightweight Solar Array (SEP) Design

The baseline SEP array is described briefly herein to identify the design which was studied and modified to incorporate concentrator (side trough) reflector enhancement. This array is a flat-pack as opposed to a drum type array. The array folds in "firehose" fashion and is contained within a rectangular storage box, the lid or cover providing the interface with the deployment mast to which the outboard panel is attached. The development of this array has been under the technical direction of NASA-MSFC and

it was originally configured for SEP missions and is referred to within this study, interchangeably, as the NASA-MSFC Lightweight Array and the SEP array. At this time this report was prepared, the array was under consideration for multiple mission applications including the JSC-Payload Extension Package (PEP), Shuttle-associated Power Module (PM) arrays, plus the original SEP mission.

The major assemblies and components of the SEP array are shown in Figure 2-1. To more easily depict the extension/retraction mast and guide wire systems, the view is from the back or inactive (electrically) side of the solar array. The basic building blocks of the solar array are independent but identical solar cell panels containing 3060 each 2 x 4 cm wraparound solar cells. The panels are interconnected mechanically along their long axis, transverse to the major deployment axis, at panel hinge lines. They are connected electrically at each of their outer edges to power feeder harnesses routed along each edge of the array. A detailed description of this basic planar array is incorporated in paragraph 3.3.1.

2.2.2 Solar Array Concentrator Configuration Options

Several concentrator-enhanced solar array configurations were considered for design selection. The simple trough configuration is preferred due to lowest complexity of implementation.

A. The trough configuration is a flexible cell blanket which has planar reflectors adjacent to each side of the blanket. These side reflectors can be canted at angles of 45° to 90° to add illumination intensity to the cell blanket.

B. The sawtooth configuration uses reflectors labeled "in-blanket" reflectors. These reflectors are also effective at angles from 45° to 90°.

C. The double trough configuration is two troughs side by side, but the same area as A.

D. The side and in-blanket reflectors of the previous configurations may be combined to form a 3-dimensional reflector system or a sawtooth/trough configuration. This system offers high geometric concentration possibilities.

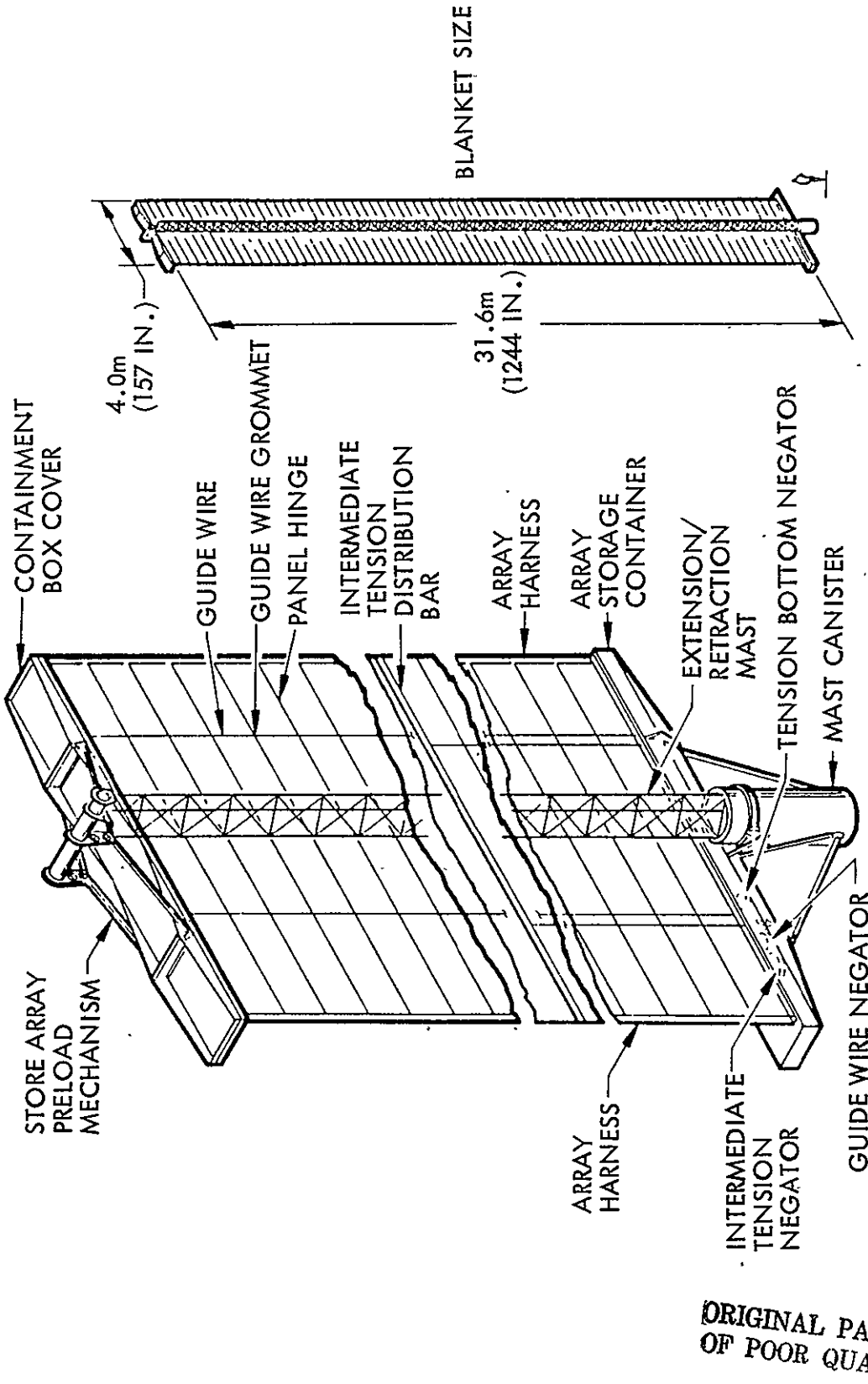

Figure 2-1 NASA-MSFC (LMSC) 25 kW Solar Array

E. Compound parabolic concentrators are attractive because of their high average concentration. The precise curved reflector shapes required and the inherent intensity variations associated with this system are a drawback to this configuration. To overcome this disadvantage and to eliminate the complexity of deploying the compound reflectors a segmented compound reflector (SCR) system can be considered.

F. The W configuration has planar reflectors which are perpendicular to the cell blanket. The reflector/cell blanket is then positioned to a sun angle between 0° and 45°. A feature of this system is that the light both directly incident on the cell and reflected onto the cell arrives at the same angle of incidence.

All of the foregoing configurations are depicted in Figure 2-2 with their geometric concentration ratios, CR's, indicated. Effective ratios are lower due to reflection and surface losses.

2.2.3 CESA Baseline Conceptual Design

The effort described in this report resulted in a conceptual design of a 25 kW, 1 AU, (BOL) concentrated solar array for use on space missions. The array is composed of two wings with a total mass of 306.92 kg (including tiedown pyrotechnics, erection trunnions, and actuators). Each wing is stowed in a package with overall dimensions of 163.348 inches wide by 35.50 inches deep by 45.20 inches high. When deployed, the 27 panels of the flat-folded array wing become planar and are augmented by two flat aluminized Kapton reflectors in a trough configuration. The deployed CESA system is shown in Figure 2-3.

A continuous coilable longeron mast provides the necessary rigidity and motive power to withdraw the solar array and reflector blankets from their stowed condition. When fully deployed, the mast provides support and tension to the three blankets ensuring planarity and adequate fundamental natural frequency.

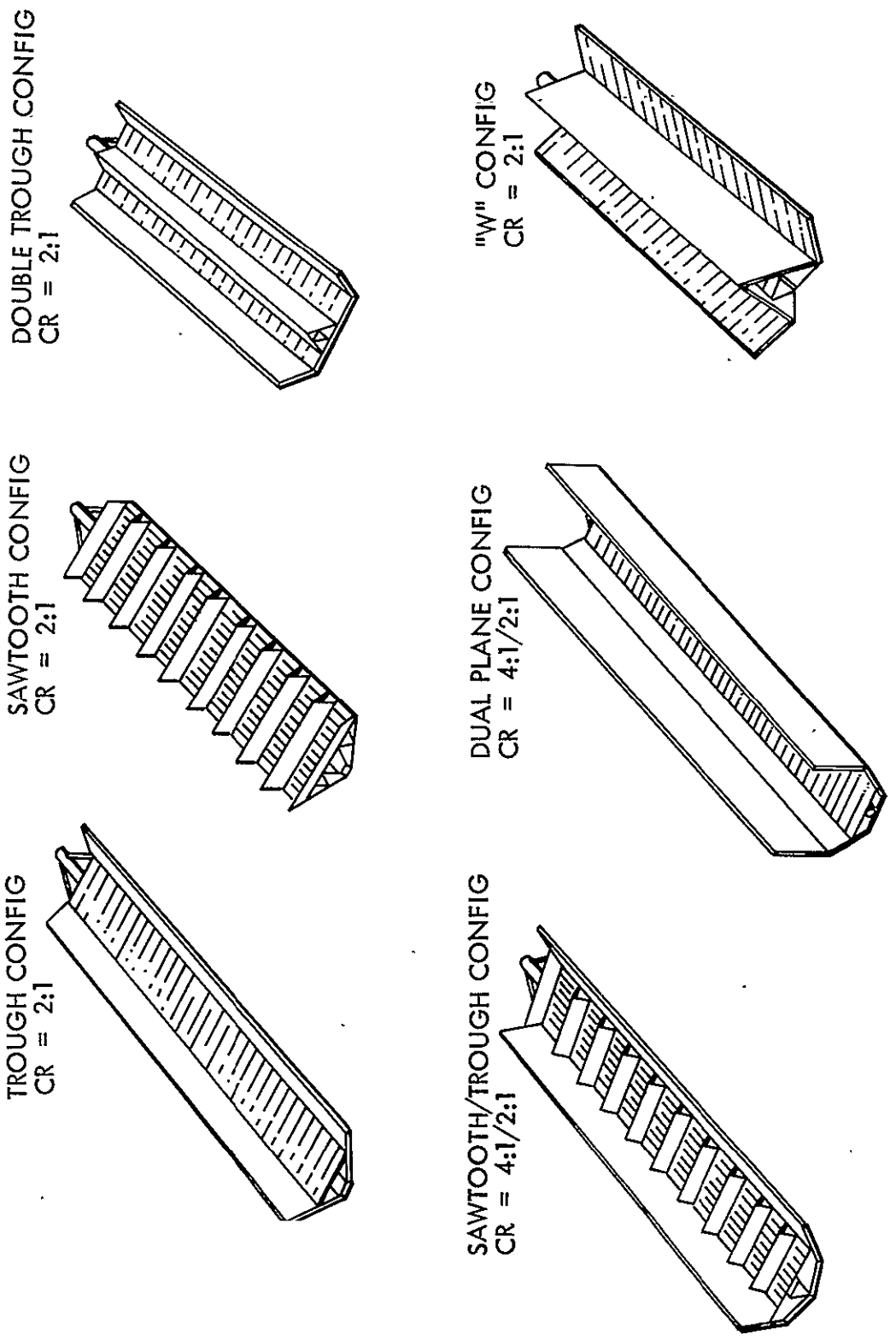

Figure 2-2 Concentrator Solar Array Configuration Options

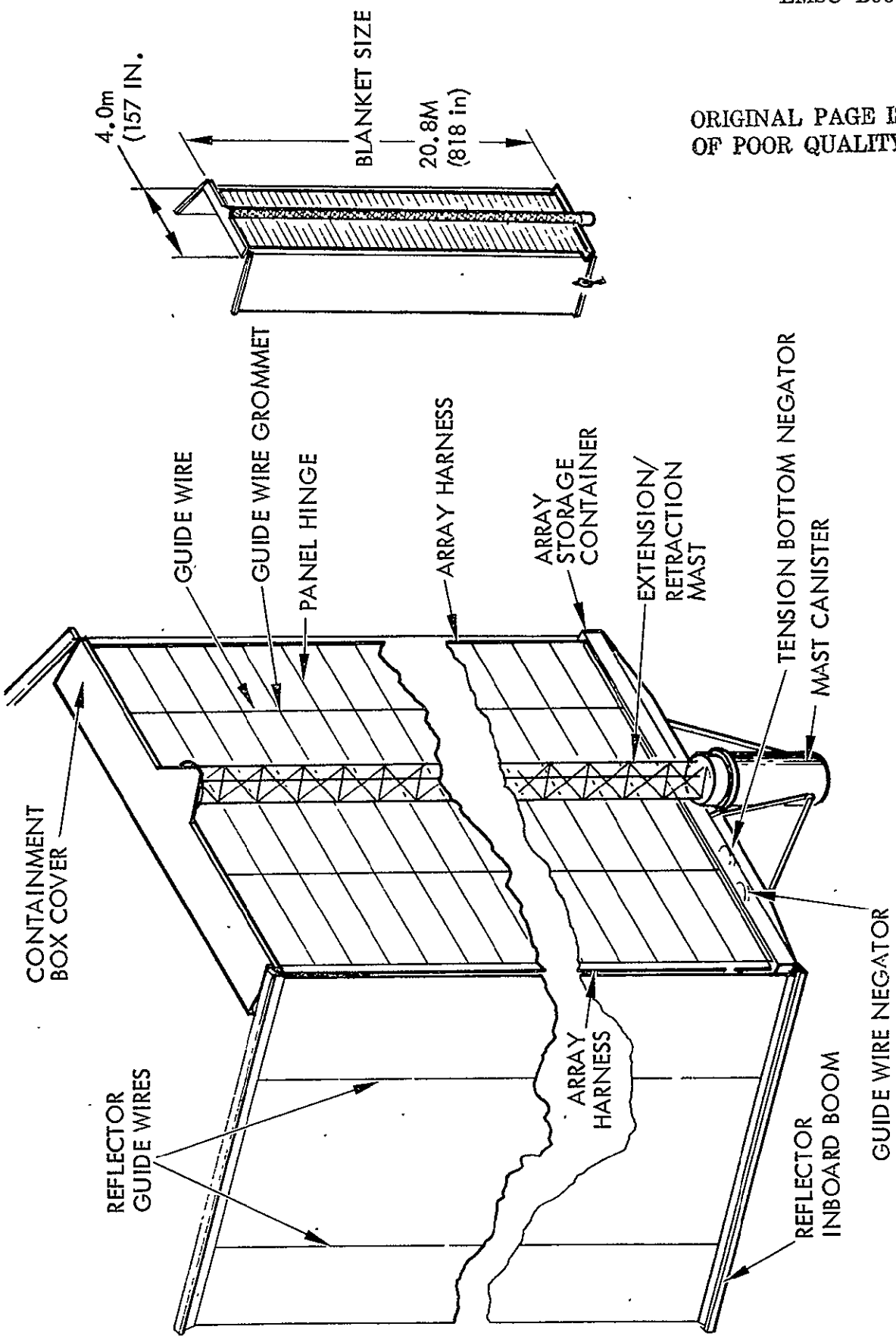

Figure 2-3 Deployed CESA System Wing

The total spacecraft is carried aloft by STS/Twin Stage Inertial Upper Stage (IUS). The IUS spent 2nd stage is retained until full array deployment is complete to capitalize on the attitude control capability present.

The reflector is positioned 57° out of the array plane. It is sized to produce full solar array illumination with up to 4° total misalignment of the solar vector. It is constructed of 0.0003 inch thick aluminized Kapton by splicing 48 inch wide stock into a blanket 147.176 inches wide by 815 inches long.

Control of the solar array and reflectors during deployment is provided by tension cables stored on spring loaded storage reels.

The reflectors are stored in separate containment boxes which are swung out to the 57° angle prior to mast deployment. These boxes are divided into two parts and constructed of honeycomb. The two parts provide the structural support for the deployed reflector. One part deploys with the mast tip and the other remains behind with the array base.

A counterbalance, which provides cancellation of the moment introduced to the mast tip, is used to reduce overall system mass.

Support of the folded array blanket and reflectors during launch is provided by friction developed by a packing pressure of 1.5 psi. The packing pressure is developed by pyrotechnic release tiedowns which apply compression forces to the outer containment box squeezing all elements of the stack against the side of the spacecraft interstage adapter.

The concentrated array is constructed using most of the technology of the SEP array. Certain measures were taken to provide mounting provisions for the reflectors. Unneeded items associated with SEP peculiar requirements were removed. Concentrator peculiar items were added. The most significant feature of this concentrator array design over the planar SEP array is the major reduction in wing span accomplished by being able to remove 11 solar array panels from each wing and maintain the power level at 25 kW.

The stowed configuration of a SEP array is depicted in Figure 2-4. The stowed configuration of the CESA (concentrator enhanced solar array) is shown in Figures 2-5 and 2-6. A view of a fully deployed CESA is presented in Figure 2-7.

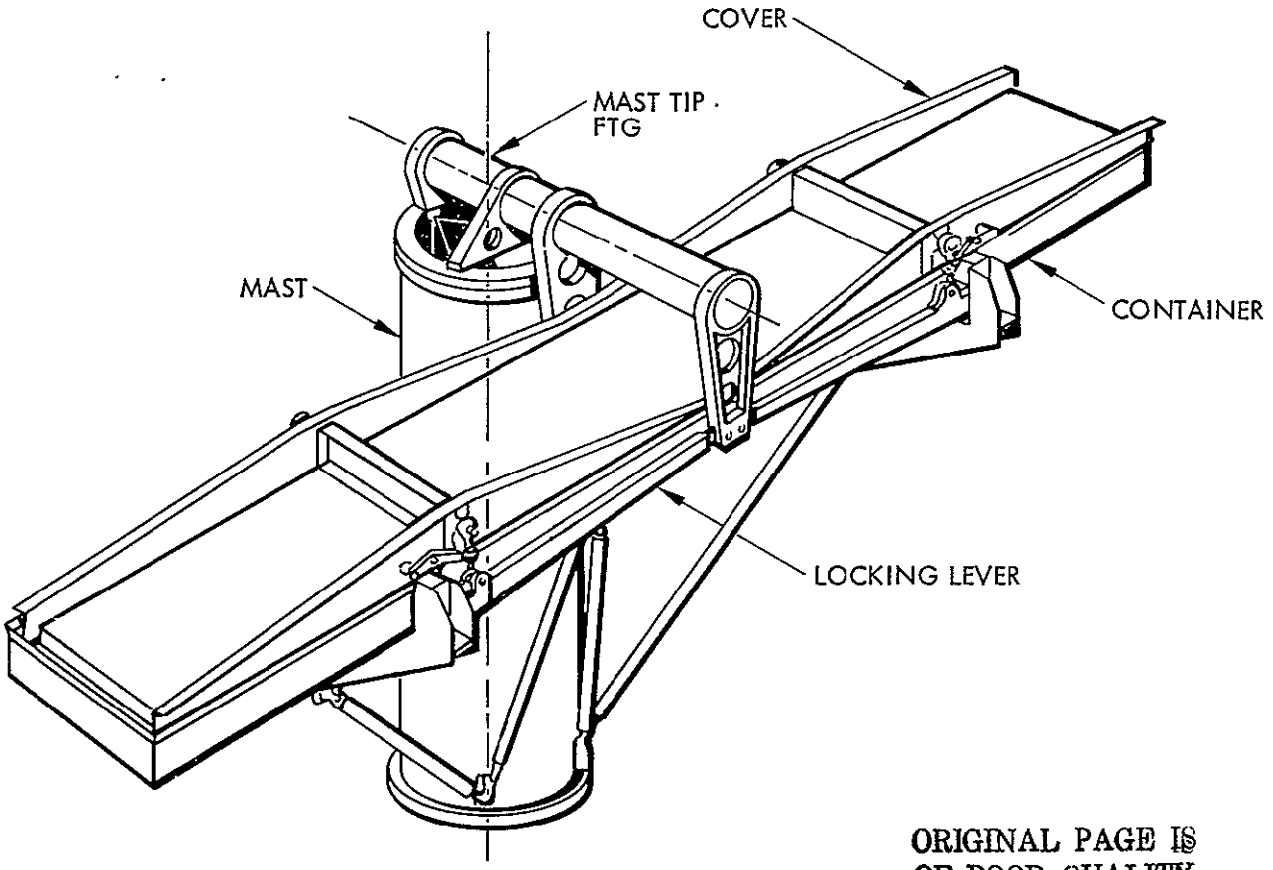

ORIGINAL PAGE IS
OF POOR QUALITY

Figure 2-4 Stowed SEP Solar Array

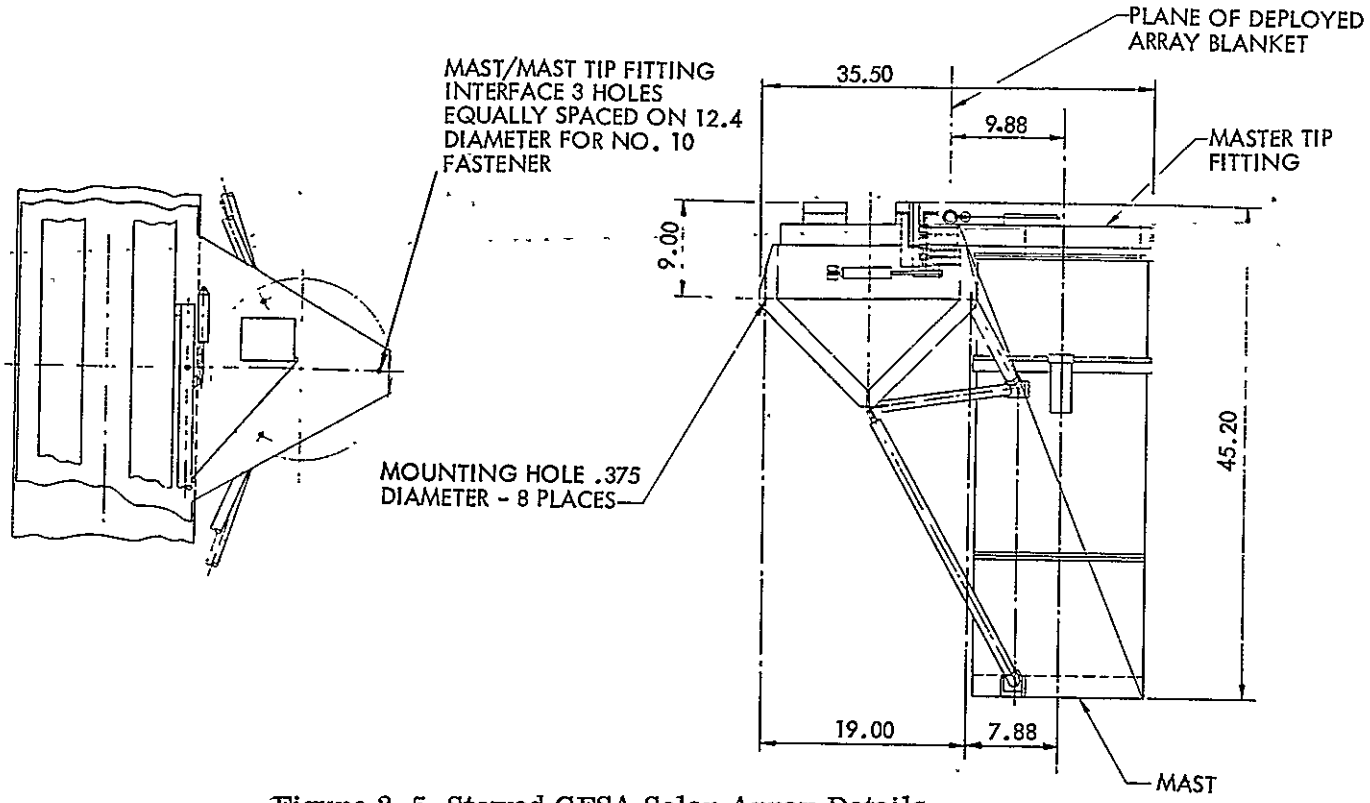

Figure 2-5 Stowed CESA Solar Array Details

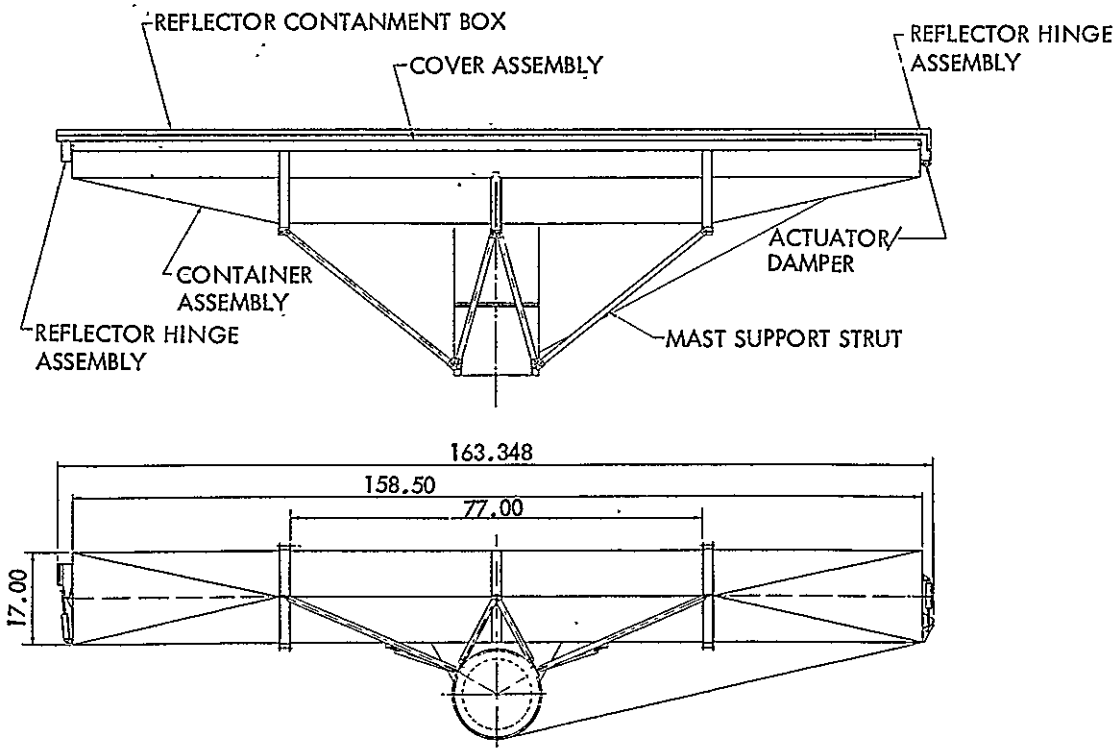

Figure 2-6 Stowed CESA Solar Array

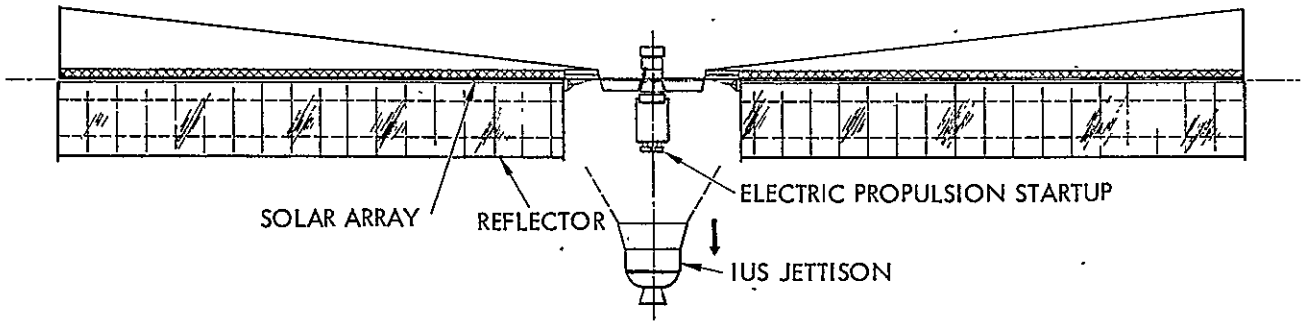

Figure 2-7 Fully Deployed Two-Wing CESA Array System

A summary of the weight of one CESA wing is provided in Table 2-1 and that of a 25 kW SEP wing in Table 2-2. The weight deltas for increasing or decreasing CESA array length in panel or meter increments are also listed as well as the delta (0.999 kg) associated with additional deployment of a 27 panel wing to place its center of pressure further outboard for total system center of pressure balancing or to avoid inboard shadowing. For a detailed baseline design description and a detailed CESA weight breakdown refer to paragraph 3.3.2. A 25 kW CESA array system, two wings, would weigh 306.92 kg and a 25 kW SEP 976 panels using 12 percent cells would weigh 359.64 kg, 81.45 watts/kg and 69.51 watts/kg respectively.

TABLE 2-1

MASS SUMMARY - CESA 25 kW ARRAY SYSTEM (27 PANEL WING)

	KG
MAST/CANISTER/COUNTERBALANCE	26.64
ARRAY GUIDEWIRE MECHANISMS (2)	1.53
REFLECTOR GUIDEWIRE MECHANISMS (4)	2.85
FULL TENSION MECHANISMS (2)	0.75
TENSION TRANSFER (8)	0.03
COVER ASSEMBLY (1)	7.33
CONTAINER (1)	12.72
SOLAR CELL BLANKET (1)	78.05
INTERCONNECT HARNESS	4.00
MISCELLANEOUS NUTS & BOLTS	0.99
REFLECTOR ASSEMBLY (2)	13.27
REFLECTOR ATTACHMENTS	1.89
DEPLOYMENT MECHANISM (1)	3.41
TOTAL	153.46

Δ MASS FACTORS PER MODULE (WING)	KG/M	KG/PANEL
CONCENTRATED ARRAY	4.912	3.716
UNCONCENTRATED ARRAY	4.692	3.549
ADDNL DEPLOYMENT OF FIXED SIZE CONCENTRATED ARRAY	0.999	

TABLE 2-2

MASS SUMMARY - SEP SOLAR ARRAY SYSTEM (38 PANEL WING)

	KG
MAST/CANISTER	36.85
ARRAY GUIDEWIRE MECHANISM (2)	1.66
INTERMEDIATE TENSION MECHANISM (2)	3.45
FULL TENSION MECHANISM (2)	.74
TENSION TRANSFER	.02
MAST TIP FITTING	.84
COVER ASSEMBLY	8.57
CONTAINER	11.62
SOLAR CELL BLANKET	109.64
INTERCONNECT HARNESS	5.44
MISCELLANEOUS NUTS & BOLTS	.99
TOTAL	179.82 kg

Section 3
CONCENTRATOR ARRAY DESIGN

The major results of the study are incorporated in this section. These results pertain to the basic design requirements, the findings of the analyses which were conducted to select the optimum design and the mechanical configuration of the selected baseline design. The major emphasis in the study was on concentrator design and analysis, and on developing a conceptual mechanical design to the extent that it could go directly into a definitive detail design phase in the future. The electrical portion of this design study was minimal and primarily in the area of system sizing analysis because the basic SEP solar cell module panel design and power harness design are directly applicable, without modification, to the CESA system.

3.1 DESIGN REQUIREMENTS

Incorporated into the study were two types of requirements, those which were established at the initiation of the study and those which were coordinated and agreed upon by JPL and LMSC during the engineering and technical interface at working reviews as the study progressed. The primary requirements are as follows:

1. The concentrator enhanced solar array baseline shall be configured such that it is modular in design for purposes of growth and for scale up or scale down to make it amenable for alternate mission applications.

2. The CESA shall be capable of multiple deployments and retractions but does not require intermediate deployment positions.

3. The design of the CESA shall be such that it can be simply and reliably integrated with the NASA-MSFC lightweight array.

4. The baseline design shall be compatible with shuttle launch and staging loads.

The three major derived requirements are as follows:

1. When the solar array is retracted it is not required that the ascent preloads be reapplied.

   This coordinated requirement resulted in major simplification and improved reliability of the design and greatly enhanced the interface of the reflector containers with the main array containment box.

2. The CESA reflector design shall be such that significant power reductions will not occur with solar vector misalignments up to ± 4°. This incorporates a ± 2° tracking sensor and drive link error plus a ± 2° deployed array wing twist.

   This requirement was derived as an outgrowth of early concentrator and conceptual mechanical design and analysis wherein it was found that severe power reductions occurred when tight off angles and high concentration ratio CR angles near 60° were mandated. It was found that two solutions were available, (a) holding the high reflector angle and folding the reflector back on itself so it had a higher deployed width or (b) reducing the reflector angle. The latter was selected because of reduced complexity, nominal impact on power output and adaptation of achievable tracking tolerances as denoted above. This analysis factor is discussed in more detail in the concentrator analysis section.

3. The CESA system sizing shall assume the use of 12% efficient solar cell assemblies.

   Both the SEP array and the CESA array cell assembly baseline is an 8 mil wraparound solar cell with a 6 mil cover. However, the SEP design has used an 11.4% cell efficiency. It was jointly decided that in the intervening years since the designation of the 11.4% that significant advances in cell performance have occurred and that 12% was a more realistic, yet still conservative, power conversion efficiency.

3.2 DESIGN SUPPORT ANALYSIS

An extensive concentrator analysis was conducted to develop parametric data on the broad variables associated with trough type concentrators. This enabled the activity on the mechanical design to avoid false starts and to eliminate effort being expended on reflector geometries that would result in imbalanced illumination. The second major category of analysis was on those variables associated with temperature, electrical performance, dynamics and stress that directly impact total system size, and size and configuration of subassemblies.

3.2.1 Concentrator Analysis

Several areas of concentrator evaluation including concentration ratio versus concentrator geometry, reflector materials and properties, various reflector distortions, and some suggestions for possible future studies are discussed in this paragraph. Considerable work has been done for terrestrial concentrator applications and some work has been done on space concentrators such as the "Extended Performance SEP Solar Array Study," NAS8-31352, done by LMSC for Marshall Space Flight Center. These studies pointed out some areas of concern in concentrator evaluation, particularly the importance of reflector material optical properties, the high degree of tracking accuracy required, and the need for uniform light intensity across the cell blanket.

As a result of the work done in this section, a baseline concentrator and concentrator performance were defined. The original baseline for this study was a 60° concentrator. After adding on the extra width to accommodate a misalignment of ± 4°, the reflector width became longer than the cell blanket width. This meant that the reflector now had to be folded, which added substantial complexity to the design.

A 57° concentrator was chosen to eliminate folding the reflector, as even after a 31 percent size increase to accommodate ± 4° misalignment, the reflector was shorter than the cell blanket width. There is actually still room for additional reflector width so that either a ± 5° misalignment could be tolerated or a 57.7° concentrator could be constructed.

At 57°, the geometric CR is 1.813. The reflector efficiency was assumed to be 92% and the angle-of-incidence effects were assumed to degrade the reflector performance by 6.5 percent. An effective CR of 1.7 was taken as the baseline.

The baseline SEP blanket is 159.50 inches wide. Allowing for ± 4° misalignment and offset for a five inch harness width, the reflector was calculated to be 147.176 inches wide. Since edge curl was found to not be a problem, no additional reflector width was required.

The reflector blanket is composed of 48 inch by 148 inch panels. The panels are joined with 1/2 inch reinforced seams every 47 inches. The seams provide beam-like stiffness to the reflectors and along with the reflector guide wires eliminate reflector buckling and convex or concave distortions.

Concentration Ratio. Considering the array to be a trough with both the reflectors and the cell blanket being essentially flat, the concentration ratio (CR) can be computed from $CR = (4 \sin^2 \theta - 2)(RE)(AI) + 1$ where:

θ	=	reflector angle (acute angle from cell blanket plane)
RE	=	reflector efficiency (reflectance)
AI	=	angle-of-incidence effects

The AI factor is the ratio of the incident light absorptance with a concentrator angle θ to normal incident light absorptance or $AI = \frac{1 - r_\theta}{1 - r_0}$. The relationship between CR and θ is shown in Figure 3-1.

The optimum reflector width, R, can be calculated from $R = L(2 \sin^2 \theta - 1)/\cos \theta$ where L is the cell blanket width. The optimum reflector width is the width where a light ray striking the upper end of a reflector ends up illuminating the opposite edge of the cell blanket.

As can be seen from the formulae the CR increases like the sine of the angle while the reflector width increases as the tangent (with increasing θ). A point of diminishing returns is soon reached after a concentrator angle of about 70° as the reflector width increases rapidly.

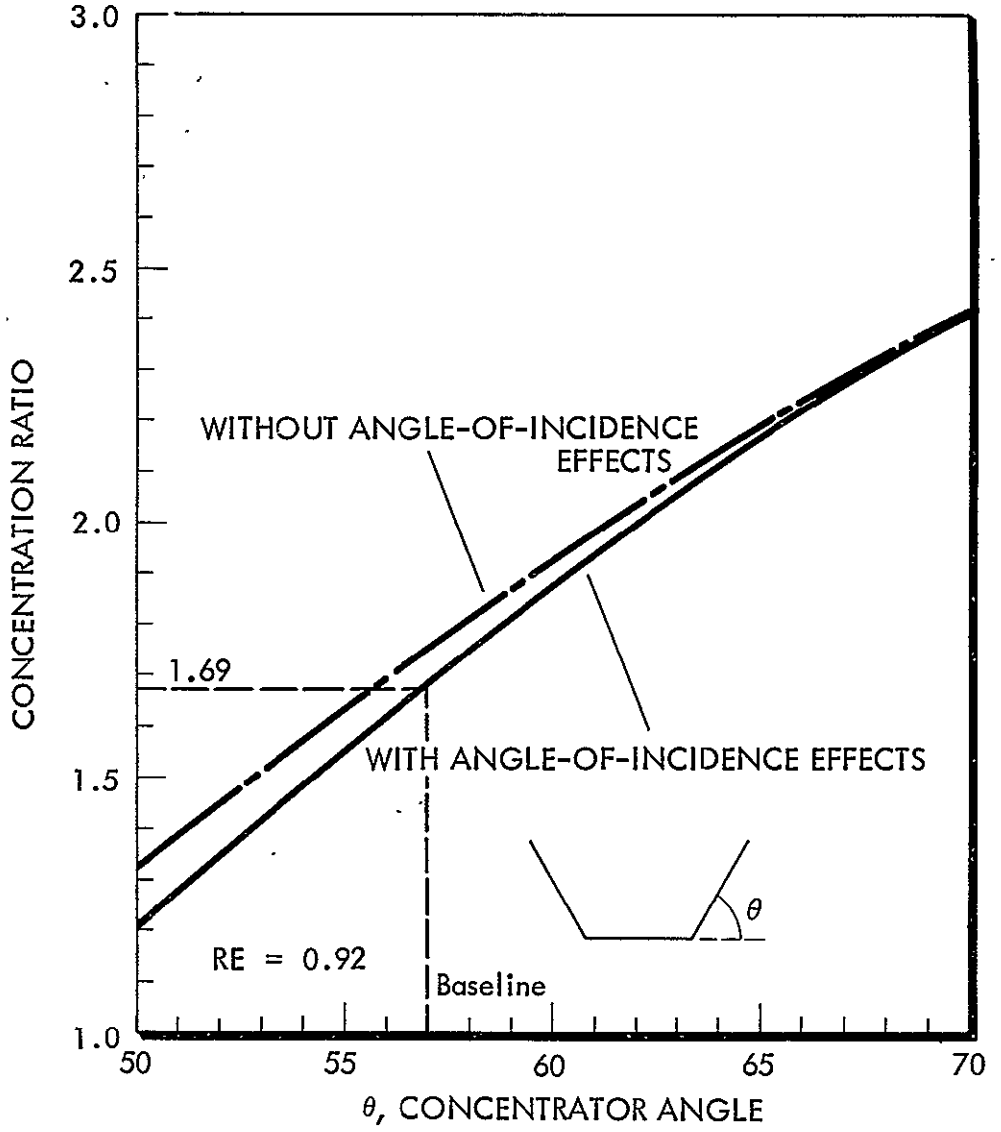

Figure 3-1 Concentration Ratio vs Angle

Reflector Materials. Metalized plastic films were chosen as the best reflector materials in a previous study with aluminized polyimide film being the most desirable. Aluminum was chosen over other metals because of its excellent reflectance and its environmental stability. A polyimide film was selected over polyester and other films due to its high strength and low creep properties and its ability to operate continuously in a -250 to 300°C temperature range.

Figure 3-2 plots the reflectance of a sample of aluminized Kapton ® over the wavelength range of 0.29 to 1.8 microns. The measurement was made using a Cary 14 spectophotometer with an integrating sphere. The solar reflectance was calculated using the Johnson solar spectrum and found to be 0.92. For cell power calculations, it would be more correct to integrate the reflectance curve over the cell response area (0.35 to 1.2 microns) factoring in the spectral response of a cell for reflectance rather than using ρ_S. This study, however, used ρ_S for both power and temperature calculations.

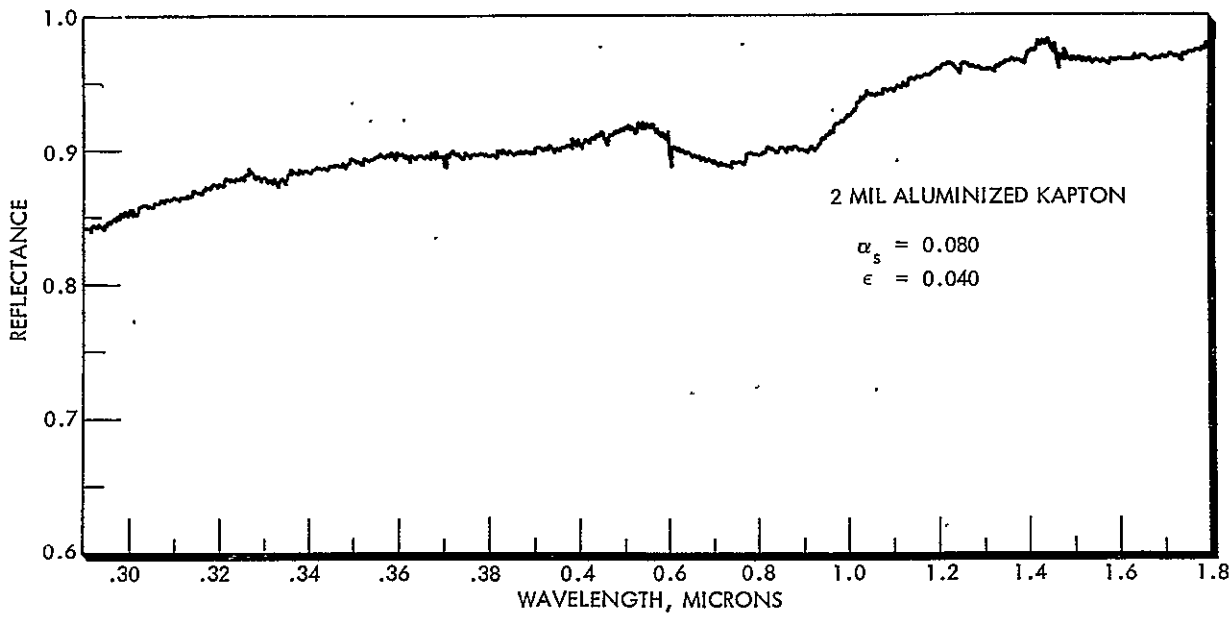

Figure 3-2 Aluminized Kapton Spectral Reflectance

The frontside emittance was measured using a Gier-Dunkle DB-100 reflectometer. The normal infrared emittance of this sample was 0.04.

® Registered trademark of DuPont

A program has been underway at NASA/MSFC to evaluate materials for advanced solar arrays and concentrator systems. Outgassing, UV, and proton tests were performed on 0.5 mil aluminized polyimide and reported on in "Evaluation of Materials for High Performance Solar Arrays," A. Whittaker, et al. These tests and their results are shown in Table 3-1. The performance criterion for the UV and proton tests were thermo/optical properties and the results of the tests showed no degradation of the samples.

TABLE 3-1
REFLECTOR MATERIAL ENVIRONMENTAL STABILITY

TESTS

- 500 SUN-HRS OF UV AT 1 SUN INTENSITY
- 1500 SUN-HRS OF UV AT 3 SUN INTENSITY
- 10^{16} P/SQ CM FLUENCE
- THERMAL/VACUUM OUTGASSING TEST

RESULTS

- ACCEPTABLE OUTGASSING
- NO UV DEGRADATION OF ALUMINIZED SIDE
- NO PROTON DEGRADATION OF ALUMINIZED SIDE

Coverslide Reflection. The reflection off the coverslide, r, was calculated using Fresnel's formula, the sine law, and considering the first surface reflection from the coverslide AR coating (MgF_2) only. Additional interface reflections or light polarization effects from the aluminized reflectors were not included in the calculations. Figure 3-3 shows the percentage of light reflected versus the concentrator angle, θ. For the baseline 57° concentrator r is equal to 10.5% for an AI factor of 0.92. This factor appears to be conservative; however, as previous solar cell angle-of-incidence data shows that for an incident angle of 66° (57° concentrator) the power loss is only 6.2 percent which would indicate an AI of only 0.938. An AI of 0.935 or 6.5 percent reflection will be used as the baseline.

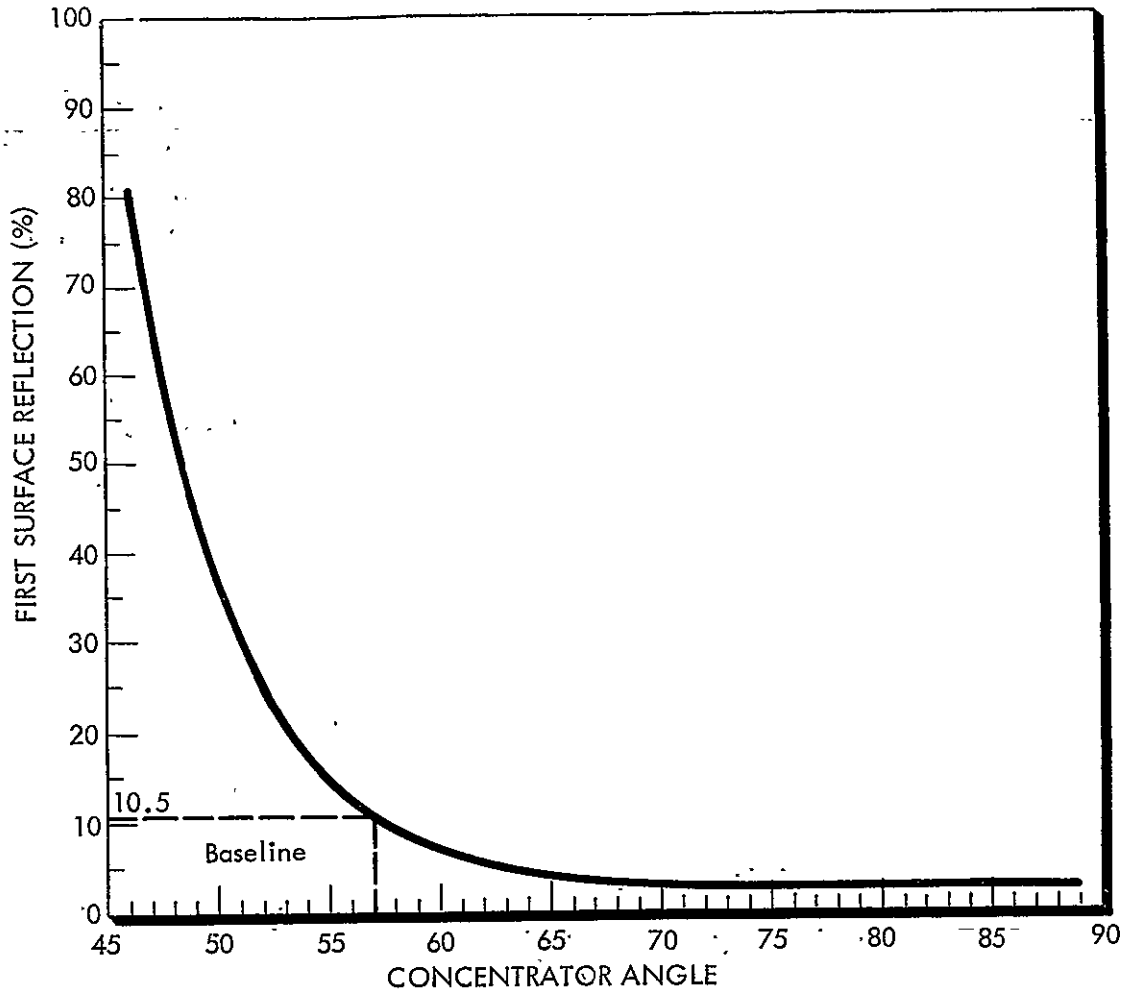

Figure 3-3 Coverslide Reflection vs Concentrator Angle

Array Misalignment. One of the array subsystems that is substantially impacted by a concentrating design is the array sun-tracking system. A planar array can deviate over 18° off sun normal before a 5 percent power reduction whereas an uncompensated concentrator array would lose more than 5 percent power for only a 2° non-normal position.

For a misalignment study, a 60° concentrator was chosen and sized for normally incident light. The light was then allowed to vary from 1 to 10 degrees off normal and the light intensity across the cell blanket was calculated and plotted in Figure 3-4. As can be seen in the figure, even a small misalignment produces a severe non-uniform intensity across the cell blanket.

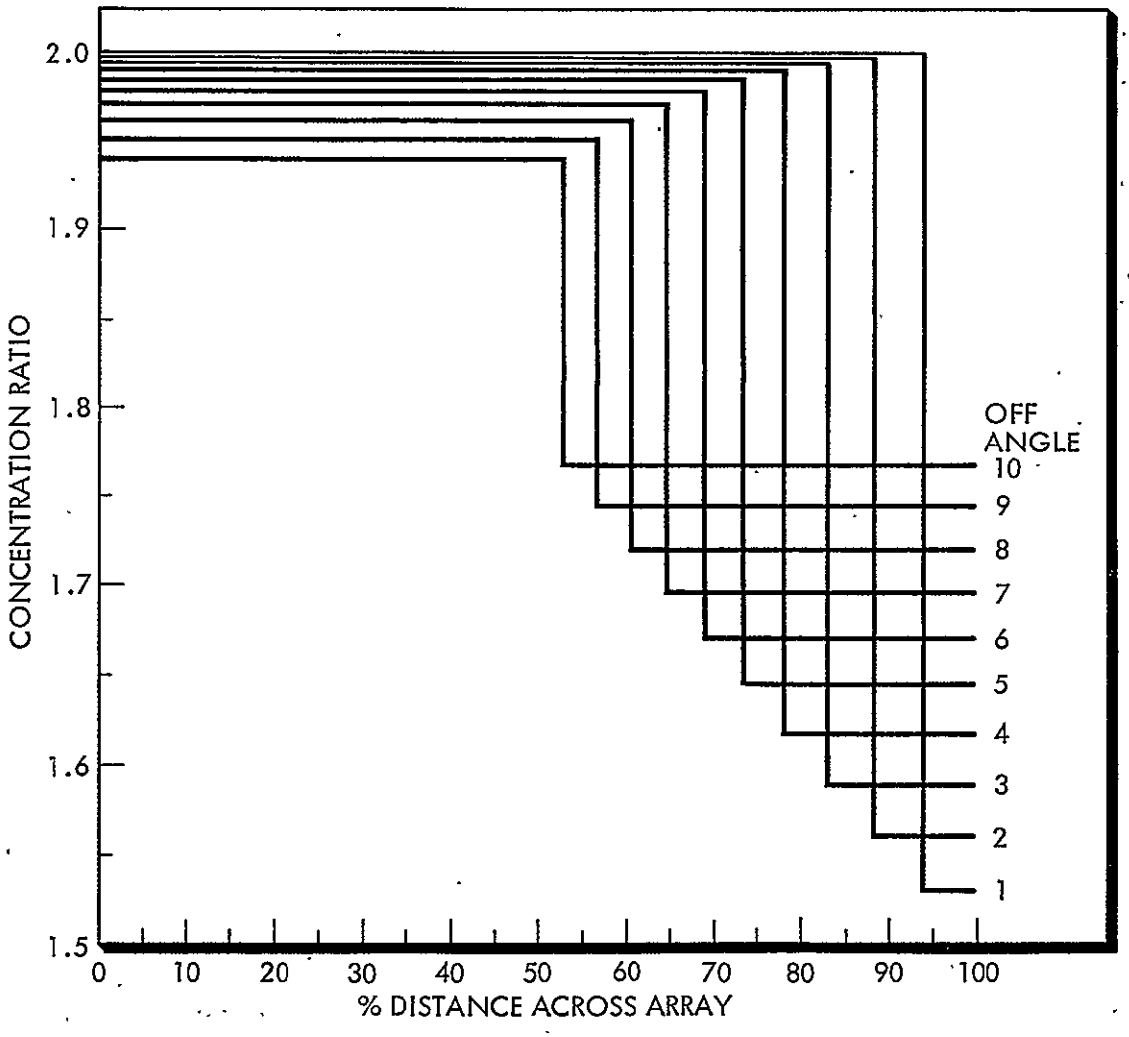

Figure 3-4 Effect of Array Misalignment

The array misalignment can be compensated for in two ways: oversizing the reflectors and/or allowing some inactive area on the cell blanket between the cells and the reflector edge. The current SEP blanket already had some inactive edge area taken up by the power harness but some reflector oversizing was necessary to compensate for a misalignment of ± 4°. Allowing for the approximately 5 inch harness dead space and the reflector box offsets, the reflector was oversized by 31 percent. The light intensity changes by less than 1 percent for a 4° misalignment with this concentrator geometry. The light intensity also remains uniform across the blanket.

Reflector Wrinkles. An attempt was made at quantifying the effect of wrinkled reflectors. A 60° concentrator angle was chosen as the baseline for this study. Some sinusoidal noise was added to the angle across the reflector to simulate wrinkles. The concentrator angle at location n is then described by $\theta_n = 60 + A \arcsin(B\, n\, W/100)$ where A = wrinkle amplitude (.1, .3, or .5 for this study), B = frequency (600 for 1 reflector, 450 for the other), and W = width of reflector. No angle-of-incidence effects, reflector efficiency, or polarization effects were included in this analysis. The CR across the blanket was calculated and plotted in Figure 3-5. The CR decreases with increasing wrinkle amplitude but remains relatively uniform across the blanket. With the baseline reflector tensioning there will probably be no wrinkles and no degradation losses are taken in the baseline design. If for some reason wrinkles do develop, they cause no severe degradation and are not a cause for concern.

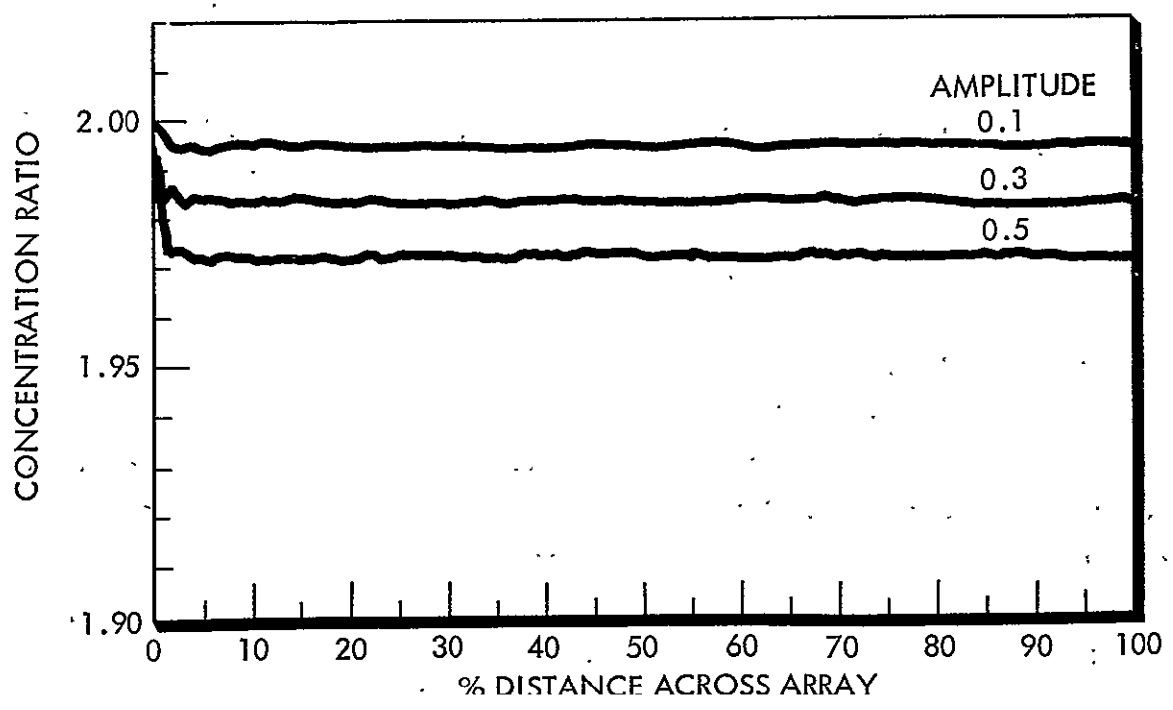

Figure 3-5 Effect of Wrinkled Concentrators

Mal Positioned Reflectors. Since focussing and defocussing of the reflectors has been considered in some programs as a way of regulating temperature and power, the effects of under- and over-extending the reflectors were determined. For this study the reflectors were sized for a 60° concentrator and then positioned at angles greater and less than 60°.

Figure 3-6 shows the effect of under-extended reflectors ($\theta < 60°$). The intensity decreases with decreasing θ but remains uniform across the cell blanket.

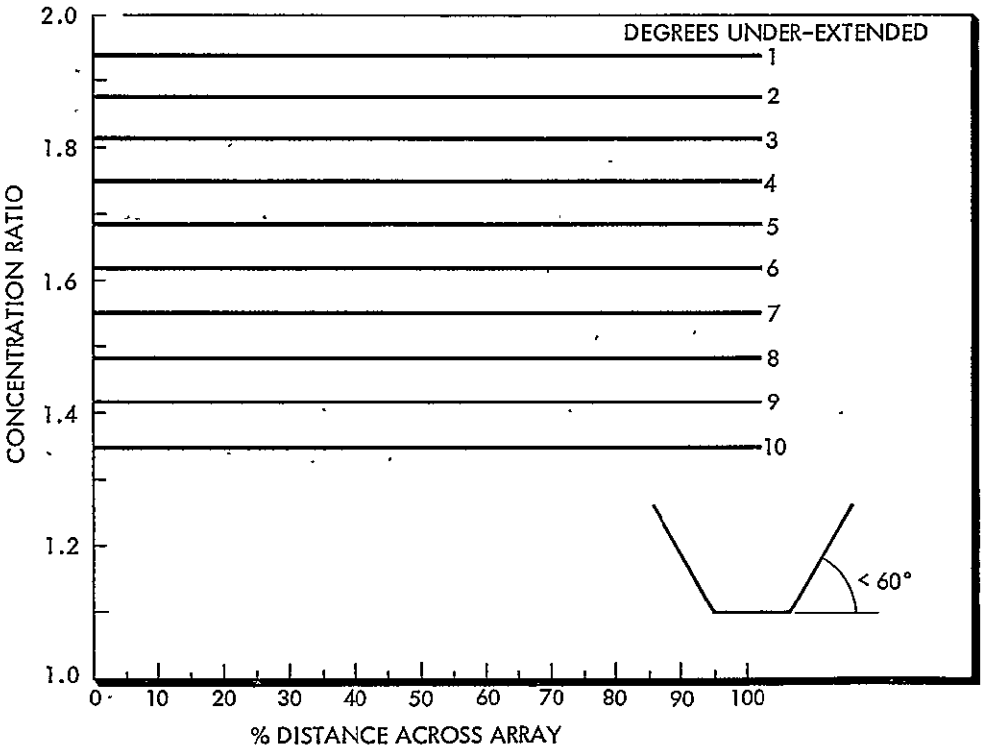

Figure 3-6 Effect of Under-Extended Concentrators

Figure 3-7 shows the effect of over-extending the reflectors ($\theta > 60°$). The average CR decreases with increasing θ but more significantly there is a step-function variation in the CR across the blanket.

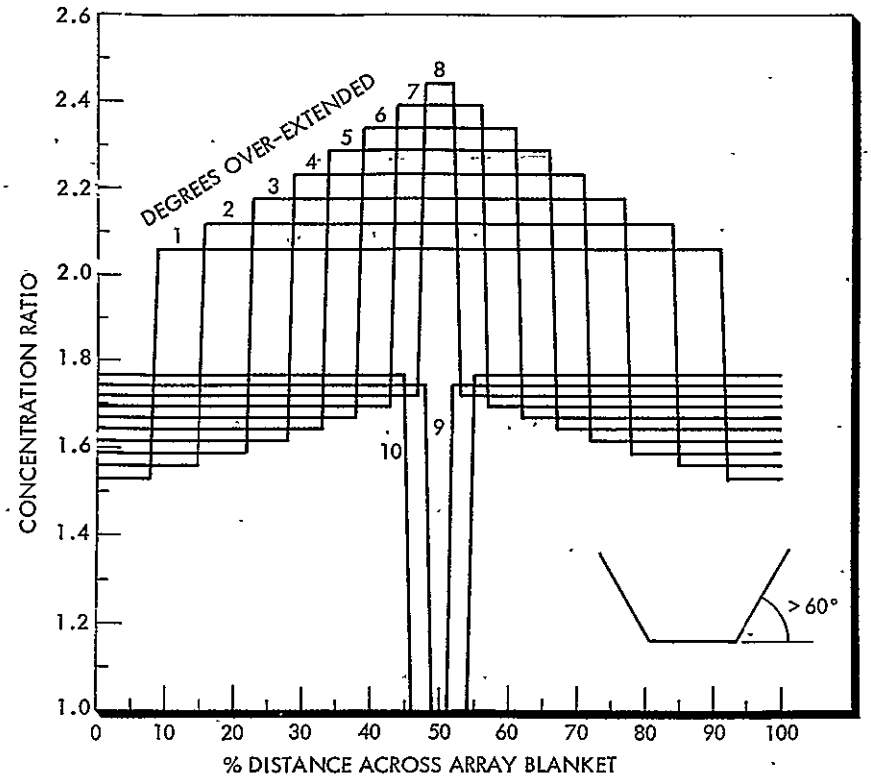

Figure 3-7 Effect of Over-Extended Concentrators

Malpositioning of the reflectors is not a problem with our 57° concentrator baseline as focussing and defocussing was determined to be not necessary. The reflectors can be locked into position and the deviation from 57° will only be the manufacturing tolerance.

Reflector Distortions. While all of the previous analysis and design dealt with essentially planar reflector surfaces, it is recognized that the reflectors have the potential to assume concave and convex surfaces without proper stiffening. This analysis deals with the effects of concave and convex reflector surfaces.

A convex reflector surface was modeled by allowing the reflector tops to flex away from the array centerline from 1° to 10°. The deflection varied linearly from the reflector root to its tip. The CR was calculated across the cell blanket and is shown in Figure 3-8. A convex distortion does decrease the average CR but the intensity remains relatively uniform across the blanket until deflections greater than 5°.

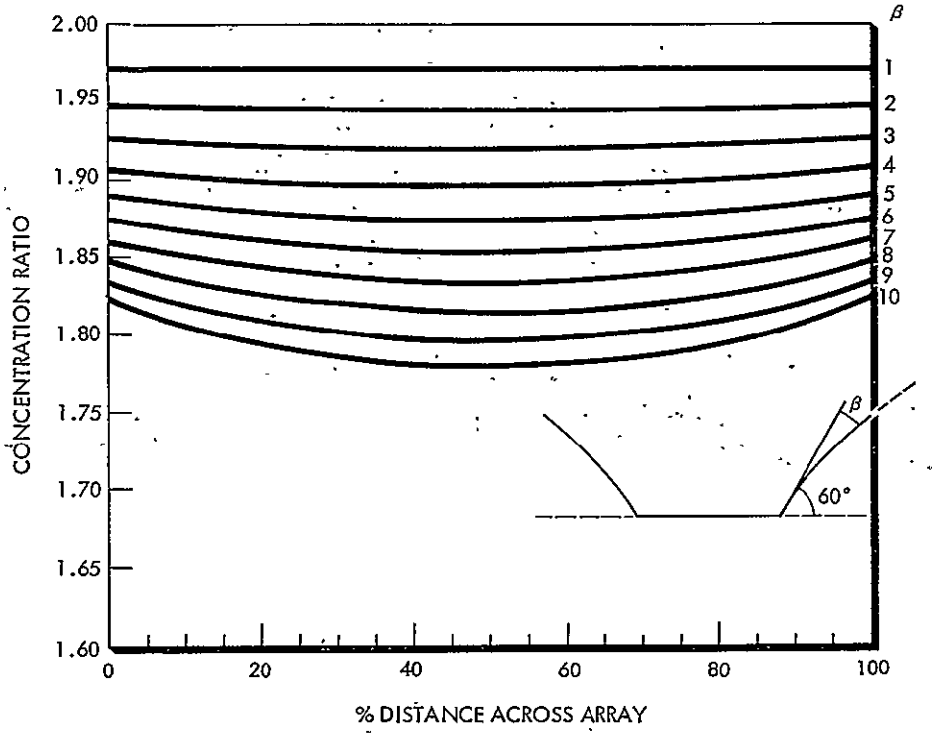

Figure 3-8 Effect of Convex Concentrator Distortion

A concave reflector distortion is modeled exactly like a convex reflector except that the reflector tips were allowed to flex towards the array centerline. This distortion causes much more severe problems, however, as not only is the overall CR reduced but the CR varies tremendously across the cell blanket. The concave case is depicted in Figure 3-9.

Concave and convex distortions can be avoided through the use of reflector stiffeners, adequate reflector outriggers, adequate reflector guidewire tension, and sufficient reflector tension. These items were considered during the baseline design of the array and it is felt that these distortions have been minimized or eliminated. In the event that further study or testing proves the design marginal, there is still room for additional stiffeners or tension.

Concentrator Tests. Several concentrator tests were conducted during the "Extended Performance SEP Solar Array Study" by both LMSC and NASA/MSFC to verify analytical predictions. Two of the five tests, shown in Table 3-2 had reflector material reflectance measured and all tests had a geometric CR, effective CR, and an overall efficiency

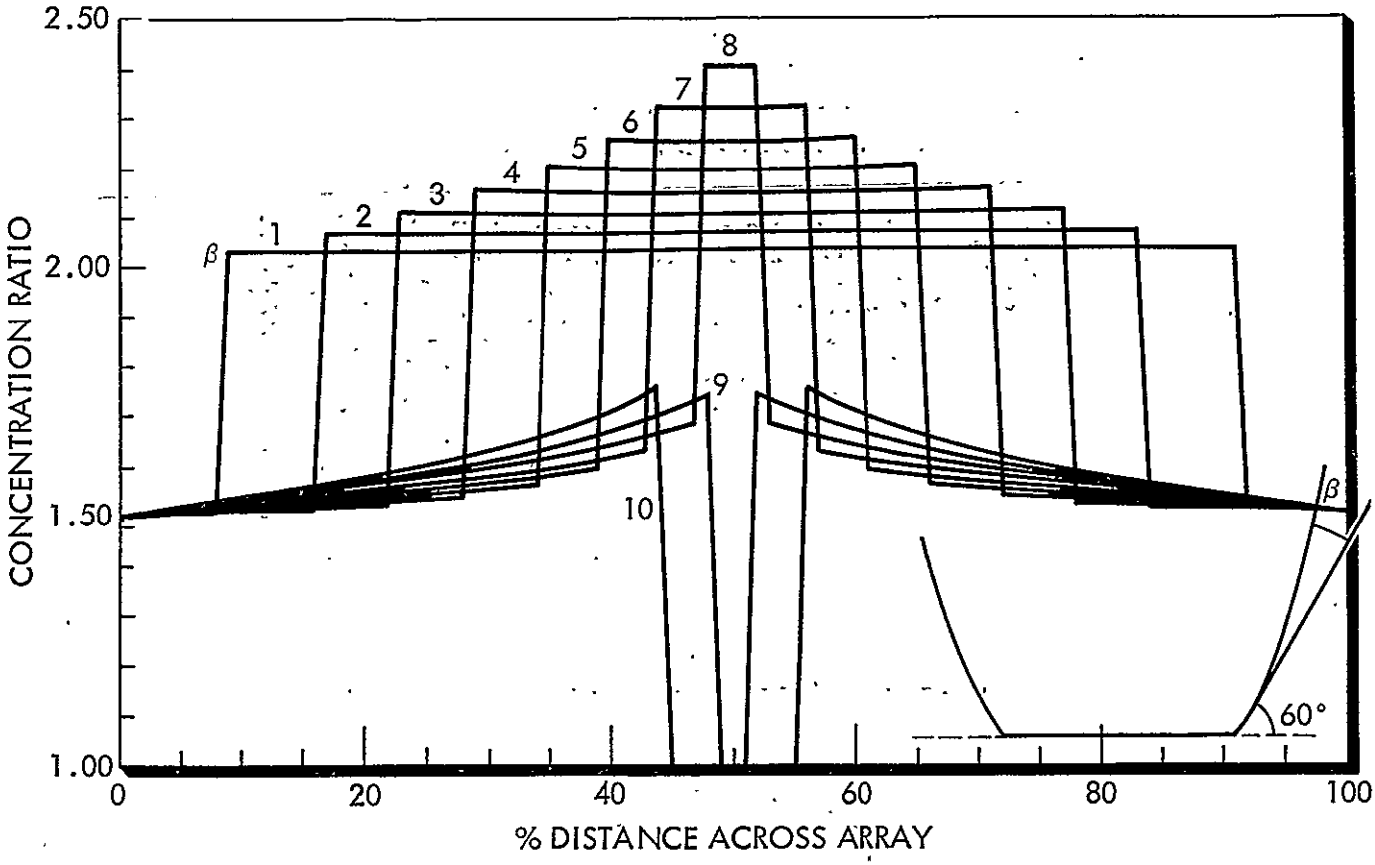

Figure 3-9 Effect of Concave Concentrator Distortion

TABLE 3-2
CONCENTRATOR TESTS CR RESULTS

CONCENTRATOR TEST	REFLECTOR ρ	GEOMETRIC CR	EFFECTIVE CR	OVERALL EFFICIENCY PERCENT
NASA/MSFC		2.0	1.71	71
NASA/MSFC	–	3.0	2.49	75
LMSC/36-CELL	0.9	3.83	3.4	85
LMSC/20-CELL	0.92	3.83	3.5	88
LMSC/10-CELL	–	2.0	1.73	73
BASELINE	0.92	1.81	1.7	86

calculated. The overall efficiency is actually the product of AI and RE, and is the percentage of light being utilized by the cells from what is intercepted by the reflectors. The two tests which had their reflector reflectance measured also had the highest overall efficiencies 85 and 88 percent. It is strongly suspected that the lower efficiencies of the other tests were due to poor reflectors; either non-specular or low reflectance.

Assuming a highly specular, reflective surface can be maintained for the baseline array, an overall efficiency of about 86% was estimated for the baseline array. This efficiency factor, again, is equal to (RE) times (AI). With RE equal to 0.92 and an AI of 0.935, the efficiency equals (0.92) (0.935) or 0.86.

Reflector Edge Curl. One problem encountered in tensioning thin plastic films is the tendency of the free edges to curl. On a concentrated array a curled reflector edge would have to be compensated for by increasing the reflector width. To assess this problem a simple reflector model was made as shown in Figure 3-10. Three 36 by 47 inch panels of 1/2 mil aluminized Kapton were jointed with 1/2 inch widths of double-sided Kapton tape. Of interest was the edge curl in the middle panel when a 2 lb load was applied to the edges of the outside panels.

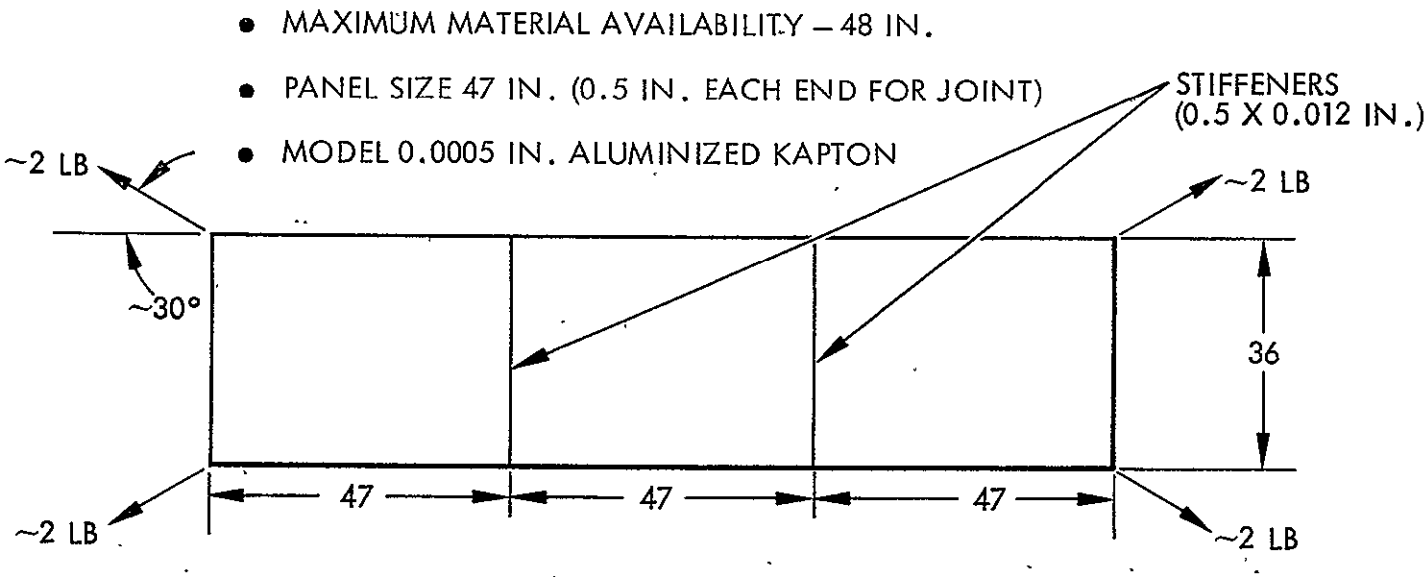

Figure 3-10 Reflector Edge Curl Investigations

Essentially no edge curl was observed in any of the panels and so the addition of compensating material is not necessary.

Future Studies. Future concentrator studies may want to include higher CR's, GaAs solar cells, and selective reflectors among other potential variations. Figures 3-11 and 3-12 show some preliminary work which helps scope the concentration ratios which should be considered.

Figure 3-11 shows relative power versus concentration ratio for a family of silicon solar cells operating at 1 AU. Both aluminized Kapton and a selectively reflecting surface are considered as reflectors. For an aluminized Kapton reflector a CR of 2 to 3 is optimal while a CR of 4 to 5.5 is best for a selective reflector.

Figure 3-12 shows relative power versus concentration ratio for a family of GaAs solar cells operating at 1 AU. For GaAs and aluminized Kapton reflectors a CR of about 15 is optimal. A CR range of 35 to 45 is maximum for GaAs cells and a selective reflector.

The selective reflector properties in this example are those of an OCLI product. The transmittance and reflectance of this material is shown in Figure 3-13. The reflector was assumed to reflect 60 percent of the light in the cell response area and 40 percent of the total solar spectrum.

One way to achieve the higher CR's indicated in Figures 3-11 and 3-12 is to go to parabolic concentrators. Using a reflector on four rather than two sides will also increase the CR. The parabolic concentrator has an inherent intensity variation problem which is undesirable, however. An approximation of that parabolic surface using two segments overcomes the intensity problems while still allowing higher CR's than a planar reflector. This dual-angle or compound trough concentrator is shown in Figure 3-14. For CR's above 2.5 a compound trough concentrator is a more area efficient concentrator than its single plane counterpart. Choosing a reflector area to cell blanket area ratio of 8, Figure 3-14 shows that a standard trough has a CR of about 2.8. A compound trough has a CR of 3.34 for the same amount of reflector material. A four-sided standard concentrator would have a CR

ORIGINAL PAGE IS
OF POOR QUALITY

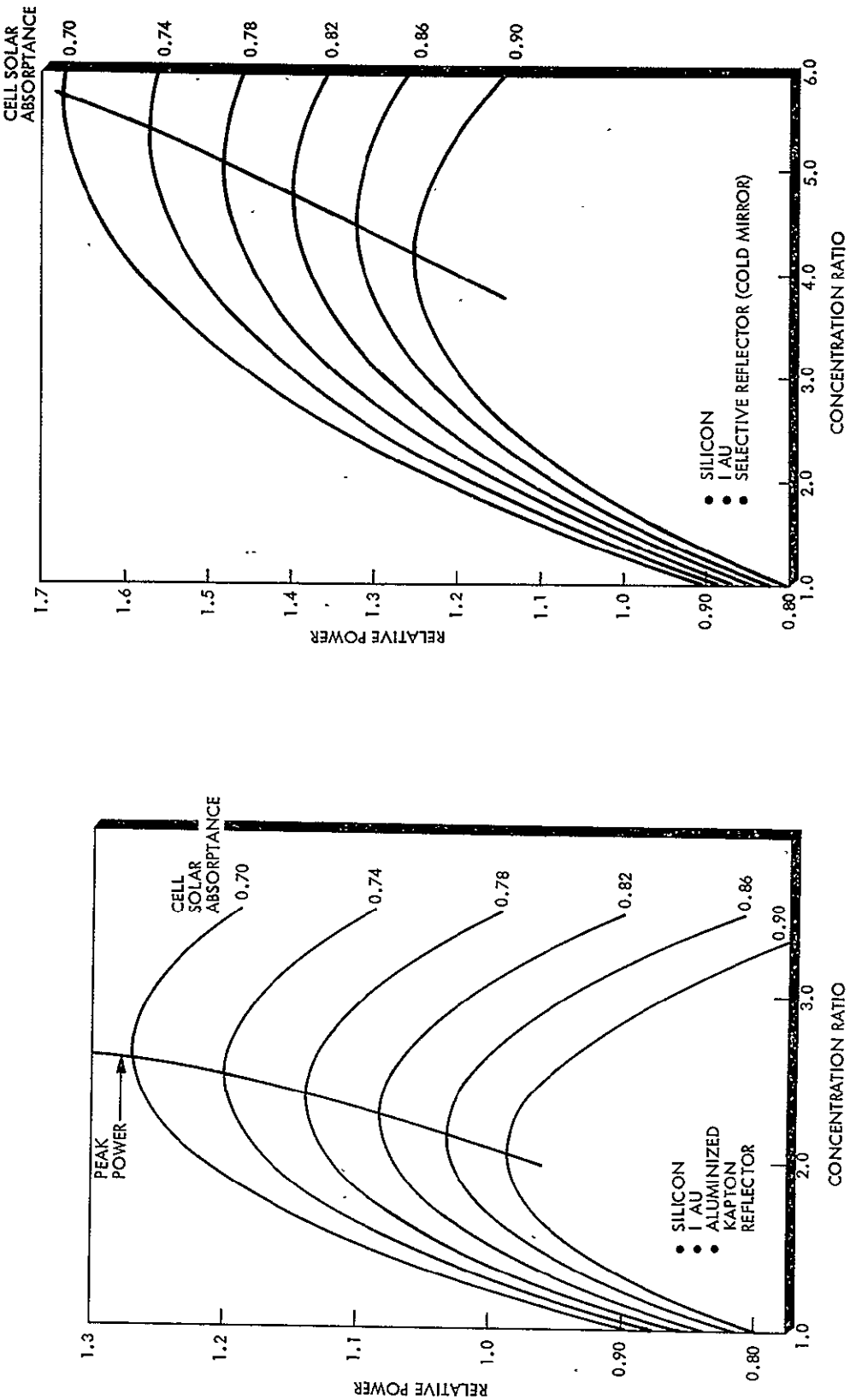

Figure 3-11 Optimum Concentration Ratio - Silicon Cells

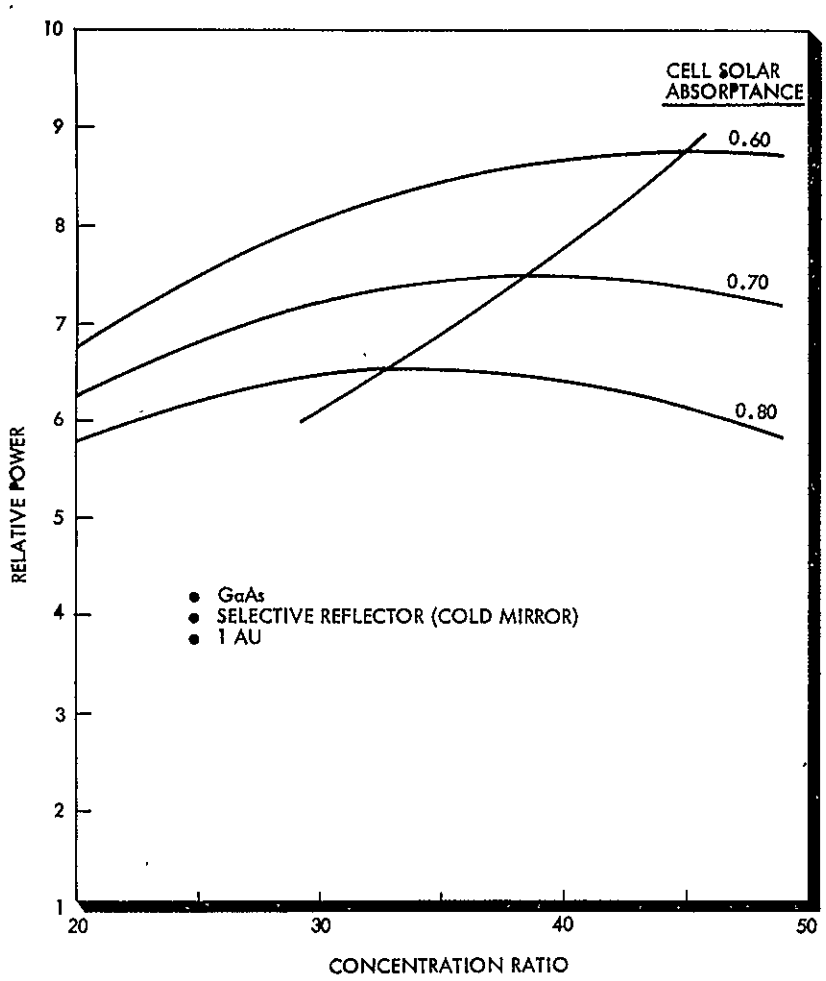

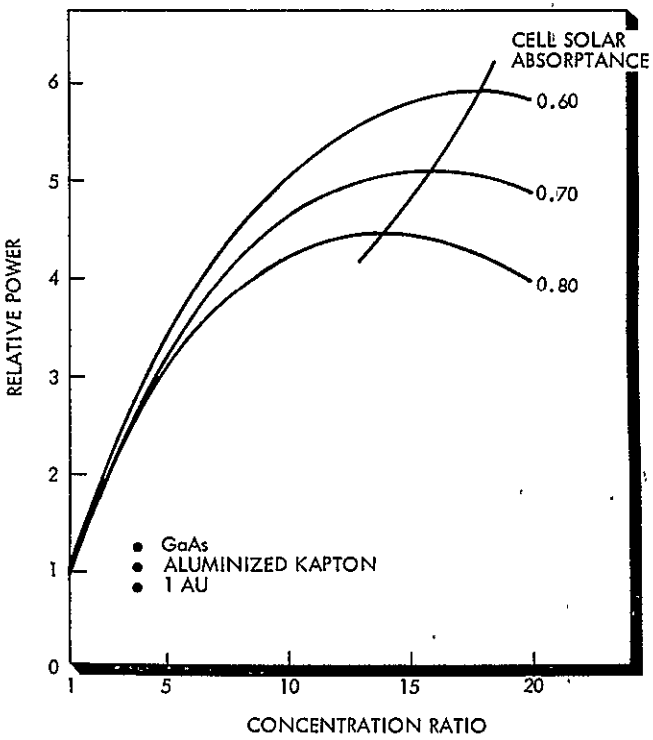

Figure 3-12 Optimum Concentration Ratio - GaAs Cells

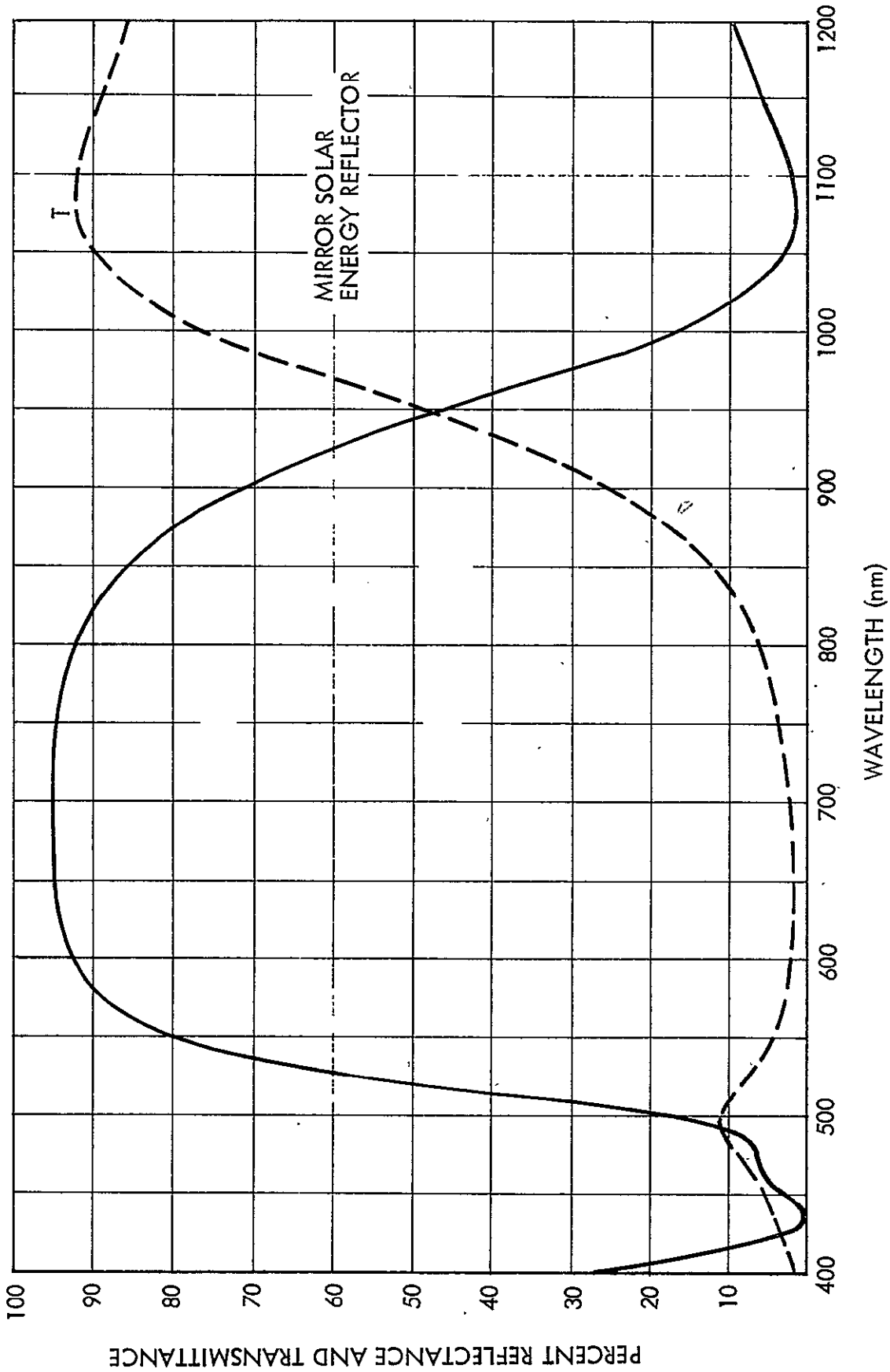

Figure 3-13 Transmission Characteristics of a Spectrally Selective Reflector

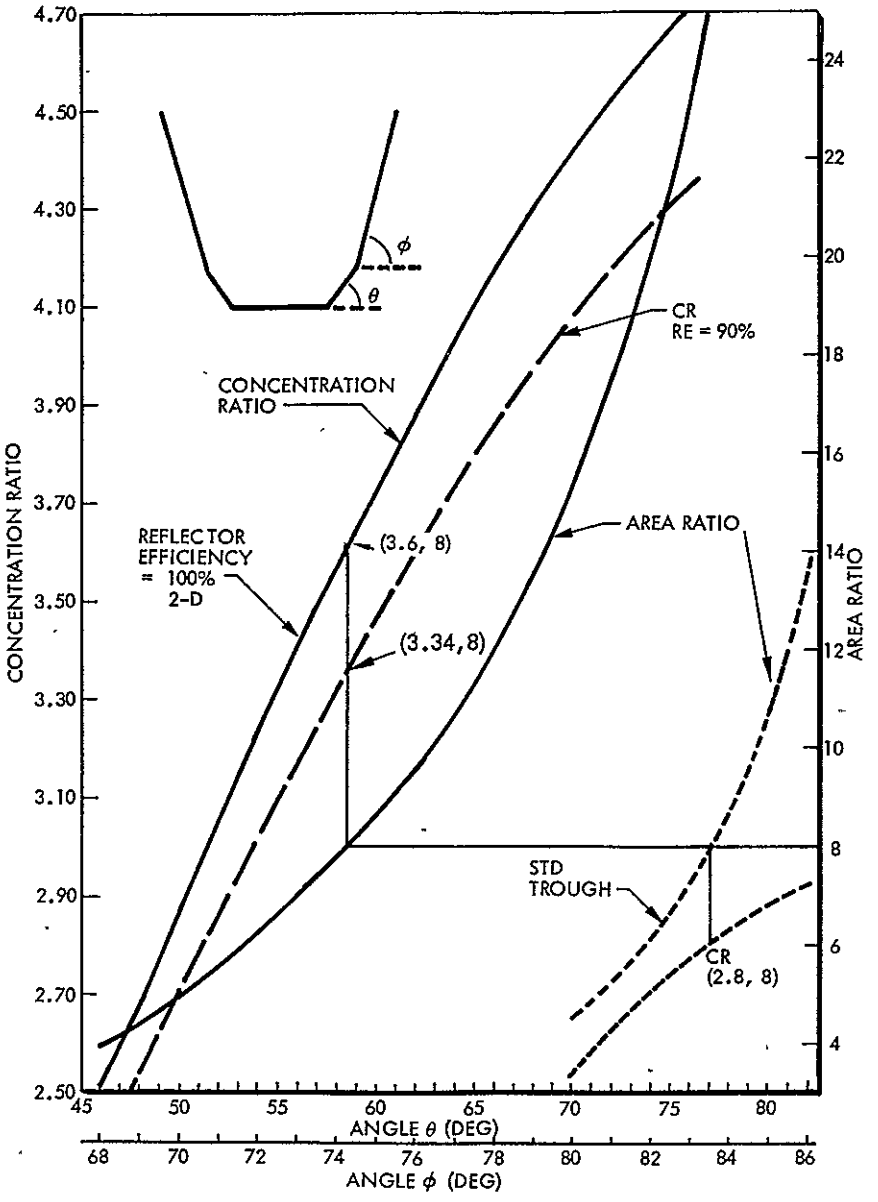

Figure 3-14 Compound Trough Concentrators

of 5.7 with the same area ratio. These CR's cover the silicon solar cell's optimum range only and it would still be necessary to go to single cell concentration with parabolic concentrators to achieve GaAs's optimum.

3.2.2 Dynamic Analysis

The mathematical model, shown in Figure 3-15, consists of a central cantilever boom, with rigid inboard and outboard lateral members that support the solar blanket and the two reflector panels. For modeling purposes, the reflectors are oriented in the plane of the blanket, and all offsets are ignored. The results of the 2-dimensional modeling will be conservative as no 3-dimensional array stiffening effects will be included. With the constraints of rigid member supports for the blanket and reflectors and uniform tensions for each, single-curved displacement patterns permit closed form solutions which are obtained in the form of four equilibrium equations (which are solved exactly) and twelve boundary conditions. The statement of the boundary conditions results in a 12 x 12 matrix whose determinant must be zero. This resulting frequency equation is solved by iteration. The rather simplified model used for this study does indicate that the desired frequency limit can be reached with reasonable pretensioning. The truly 3-dimensional nature of the array along with proper consideration of eccentricities will probably require finite element modeling. Still another aspect of the problem which ultimately must be addressed is the in-plane stiffness of very thin panels. Static testing of representative panels is suggested.

The torsional stiffness of this array has not been addressed as it requires a 3-dimensional model. Given that the array is a 3-dimensional system, however, with its reflector and mast counterbalance systems, torsional rigidity is not thought to be a problem.

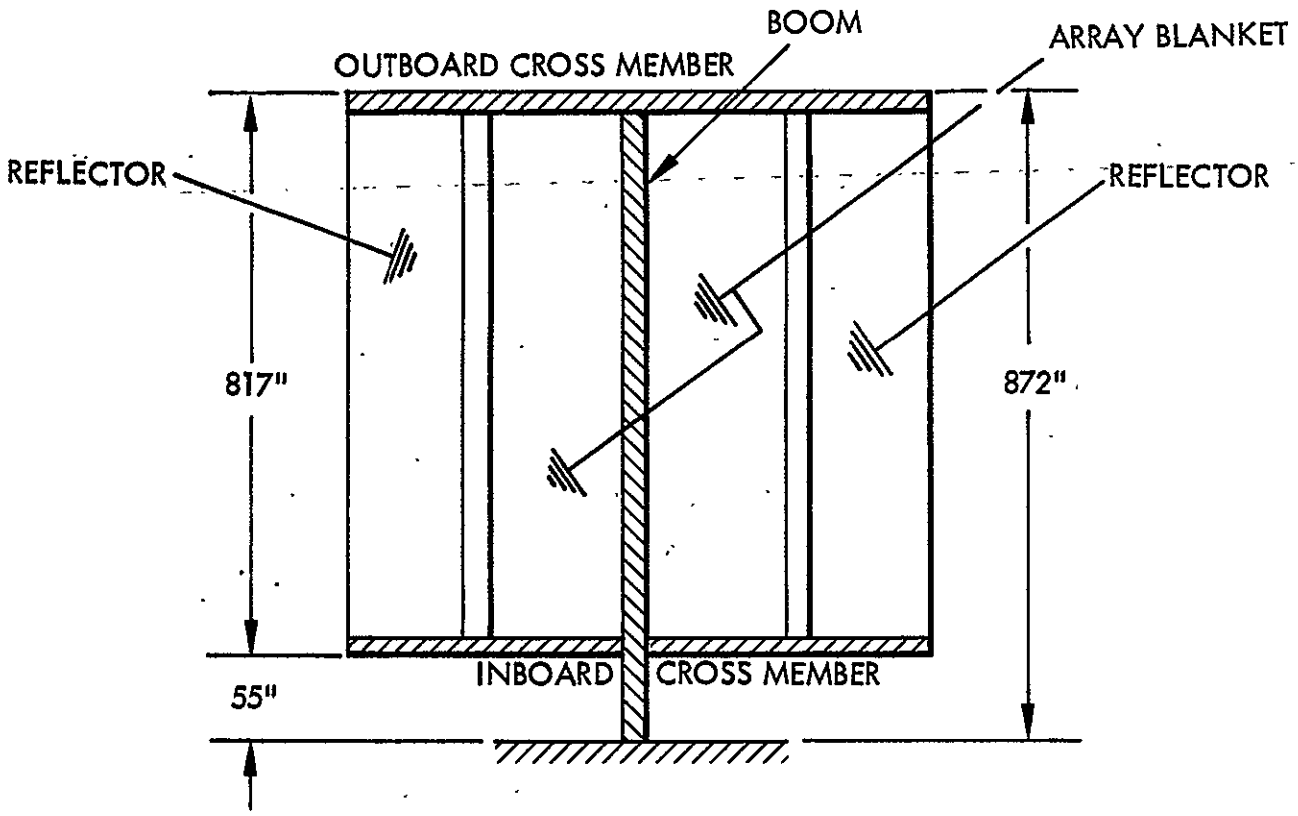

Figure 3-15 Array-Reflector Dynamic Model

The plot of frequency versus preload and boom radium, Figure 3-16, show that for a radius of 4.5 inches the desired frequency of .04 Hz cannot be reached. Higher values of preload tend to stiffen the solar array blanket, which would raise frequency, but tend to decrease the boom stiffness due to column action. Beyond a radius of 6.5 inches, the boom tends to act as a rigid support and so the required preload appears to approach an asymptotic limit. The low values of blanket preload (approximately 2-1/2 pounds for a frequency of .04 Hz) as compared with PCR (Euler load) indicates that the fundamental mode is essentially a blanket mode with very little deflection of the boom. The reflectors with a pretension of 12 pounds and a combined weight of only 3 percent of the blanket weight have a much higher resonance than the values investigated in this study.

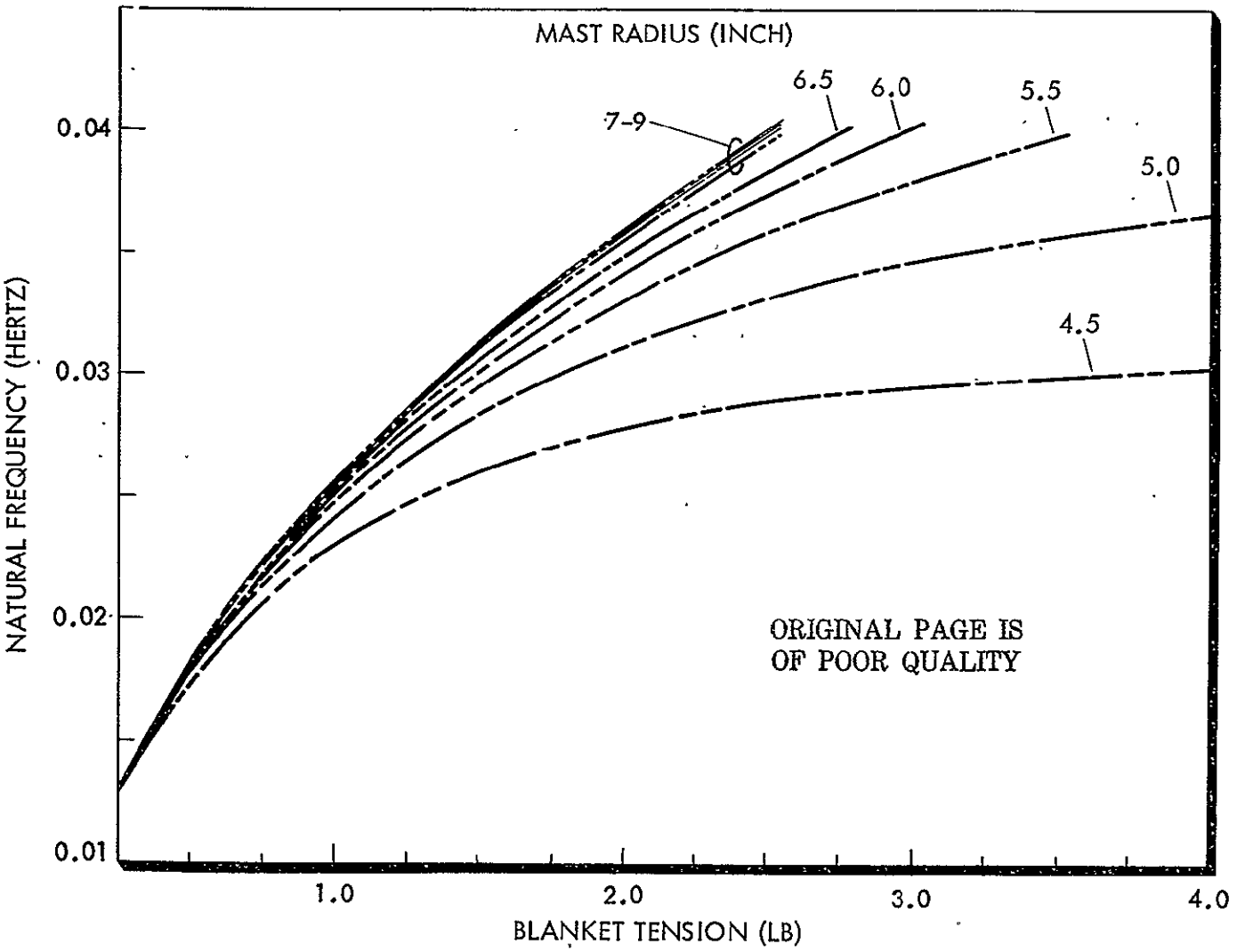

Figure 3-16 Array Natural Frequency

3.2.3 Thermal Analysis

Mathematical models were developed to calculate the distribution of solar energy entering the cavity, temperatures of reflectors and solar cell blanket, and electrical output. These models incorporate the details of geometry, solar distance, optical properties, and solar cell efficiency which is in turn a function of temperature and solar flux density. The specific assumptions and ground rules which define the relationship of the mathematical model to the physical problem or which limit the range of the parameters are: (1) All surfaces are flat and are assumed to be isothermal, (2) Constant surface optical properties are used (no angular dependence), (3) Solar vector deviates off normal only in the direction of the primary reflector with the maximum angle limited to the angle of the reflector, (4) Solar cells were

assumed to be perfectly diffuse (specular reflectance), (5) All incident energy is divided into three components upon striking a surface $Qi = \alpha Qi + \rho_s Qi + \rho d\, Qi$. The absorbed energy (Qi) is used directly in the thermal energy balance. The reflected energy is divided into diffuse (ρdQi) and specular (ρsQi) components. The diffuse portion is assumed to stay diffuse and will be absorbed and reflected by other surfaces. The specular portion is treated as incident energy which strikes another surface(s) and again assumed to divide into three components, (6) The geometric view factors for the simple trough are calculated directly by the program, (7) No conduction heat transfer between reflectors and solar cells. Conduction through the cell and backside has been included, (8) Steady state conditions only, (9) Solar cell efficiency curves with an input bias factor are based on data representative of the solar cells to be used. Figure 3-17 is a simplified sketch of the array thermal model.

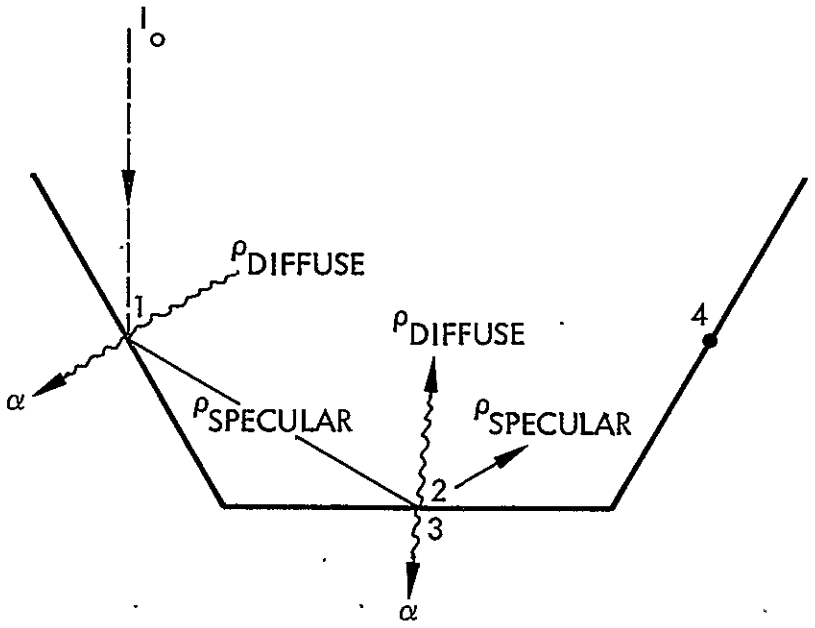

- 4-NODE THERMAL MODEL
- SPECULAR AND DIFFUSE COMPONENTS ACCOUNTED FOR
- 57° REFLECTOR GEOMETRY USED FOR VIEW FACTOR CALCULATIONS

Figure 3-17 Array Thermal Model

Shape Factor Variation Across Array

An analysis was done to determine the maximum temperature variation across the cell blanket width due to a non-uniform shape factor. Two cases were considered: (1) perfectly diffuse reflectors and (2) reflectors with an IR emittance of 0.04. The results of the analysis, plotted in Figure 3-18, show the perfectly diffuse reflectors to cause a maximum blanket ΔT of 2.5°C while the specular reflectors caused a maximum blanket ΔT of 2°C.

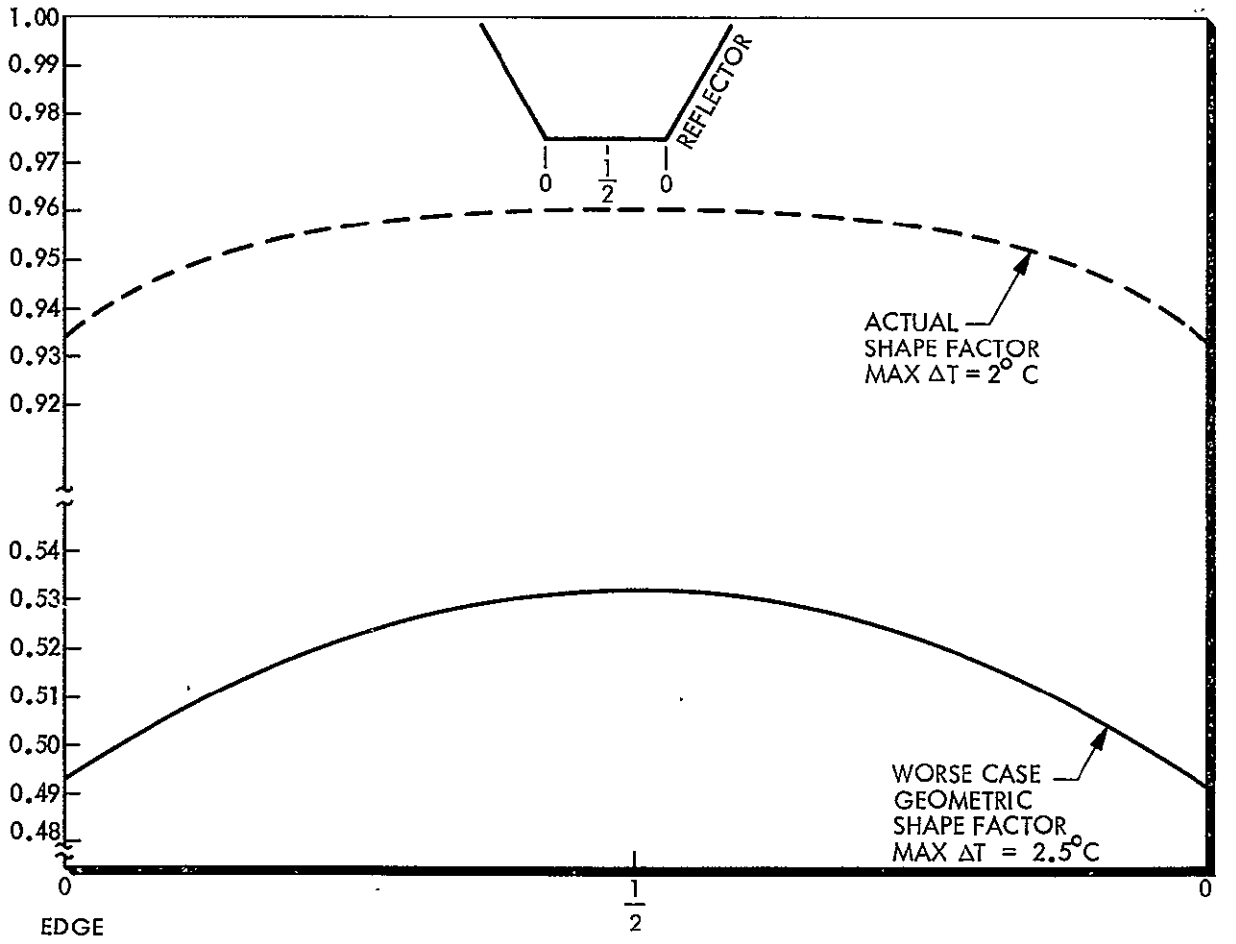

Figure 3-18 Thermal Shape Factor Variation Across Array

Solar Cell Temperature Predictions

The concentrated and planar array cell temperatures were estimated using LMSC developed multi-nodal thermal analysis computer programs and are shown in Figure 3-19. The cell's α/ϵ was assumed to be 0.74/0.81 and the blanket backside emittance was assumed to be 0.80. For the thermal analysis, the light intensity on the cell blanket was $1.7/(A.U.)^2$ for the 57 degree concentrator design. The cell efficiency at the various distances were factored into the overall energy balance. An accounting was also made of the specular and diffuse portions of the light reflected from the concentrators. The reflector material had an ρ, ϵ, and α of 0.92, 0.04, and 0.08, respectively. For a variation of 1 to 3 AU, the concentrated solar cell temperatures ranged from approximately 100°C to -60°C, respectively. The planar solar cell temperatures ranged from 45°C to -90°C for the same distances.

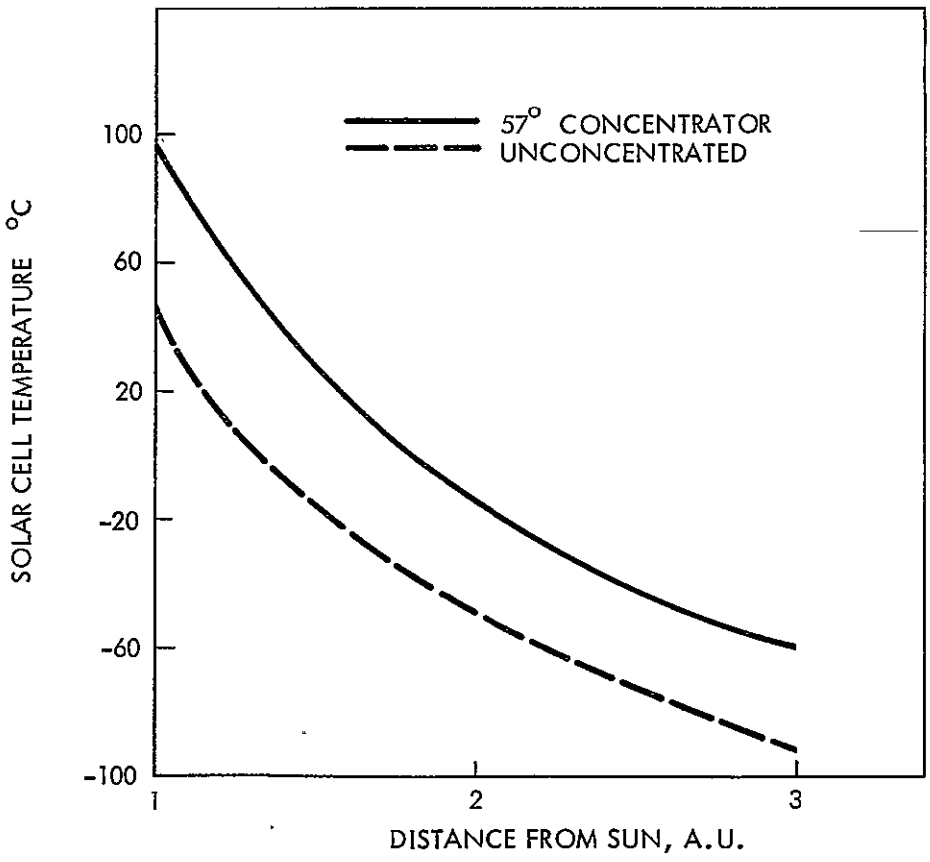

Figure 3-19 Solar Cell Temperature Predictions

3.2.4 Electrical Power Analysis

System Voltage Compliance. Several factors must be considered in analyzing electrical power output from a concentrator solar array as a function of distance from the sun. A primary set of variables is the change in solar cell parameters under changing solar intensity and corresponding temperature changes. Extensive SEP wraparound cell characterization tests were run by Boeing under NASA-MSFC Contract NAS8-31670. The results of this program are incorporated in report No. D180-20573-1, "Solar Cell Selection and Characterization for Solar Electric Propulsion." From this report the Vmp, maximum power voltage, for OCLI and Spectrolab SEP wraparound cells, corresponding to distance from the sun are referenced. This data was used directly to assess acceptability of the SEP baseline series-parallel panel circuit design to evaluate operational panel voltage ranges.

The desired array operating voltage range is 200 to 400 volts. Below 200 volts the power conditioning equipment weight becomes a concern and above 400 volts factors of corona, plasma leakage, etc. must be considered. The cell blanket electrical design will have to be configured so that given a cell's V_{mp} range, the array's voltage will stay in the desired range. Figure 3-20 plots the V_{mp} behavior for three cells over a temperature/intensity range with a 57° concentrator. At 1 A.U. the baseline 306 cell series string (module) operates at about 107 volts and so it will be necessary to series two circuits (panel) for a voltage of 214. At 3 A.U. each string operates at 180 volts (Boeing data) and 2 circuits will be at 360 volts. The SEP circuit/power layout can be used without change for the CESA 1 to 3 A.U. application.

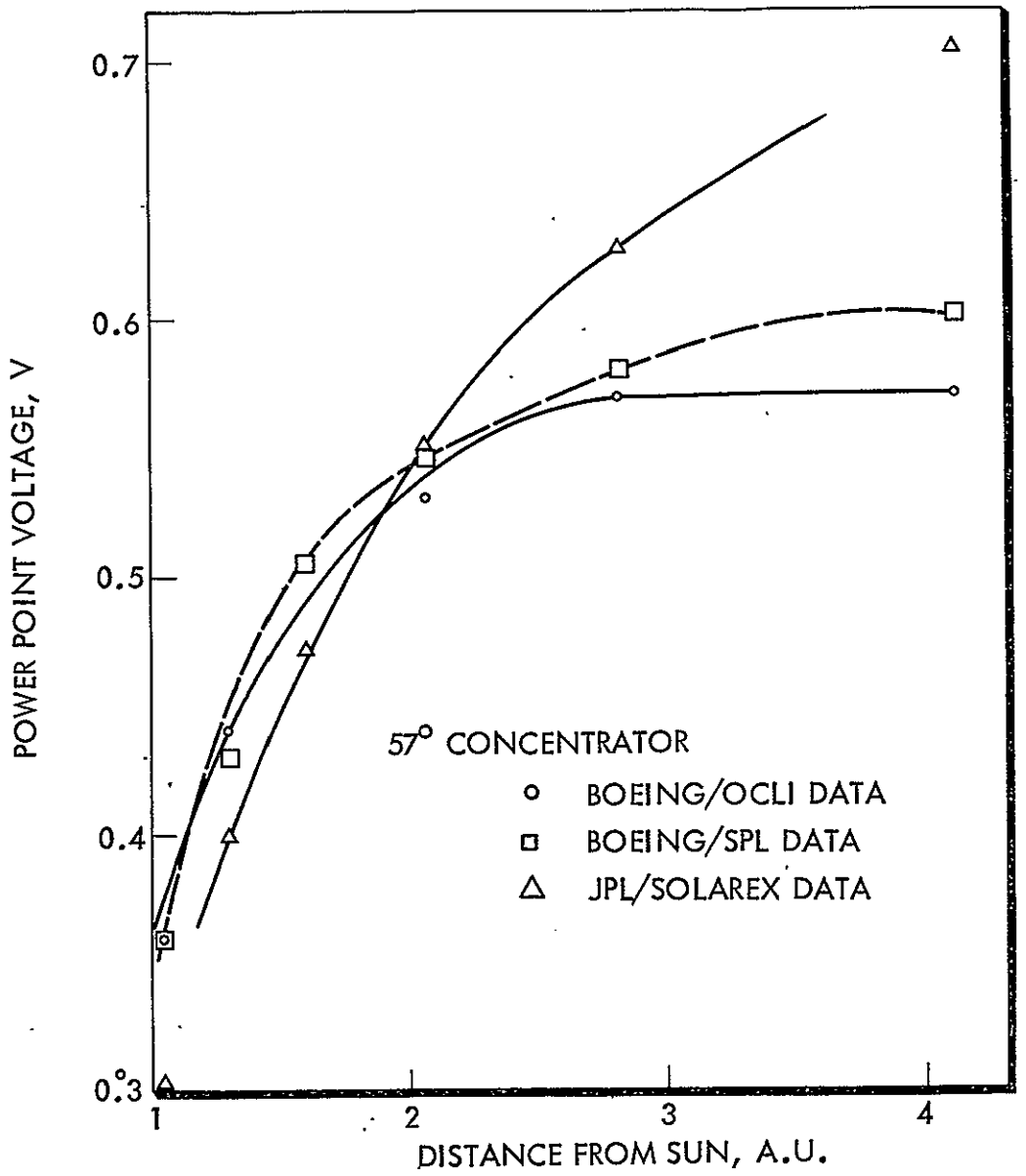

Figure 3-20 Solar Cell Maximum Power Voltage versus Distance

Array Panel Configuration. The nomenclature associated with the SEP solar array panel design is depicted in Figure 3-21. A panel, made up of two modules, contains 3060 each 2 x 4 cm wraparound electrode solar cells. Power feeder harnesses run down the outboard edges of the panels and each module is brought inboard as an electrically independent unit. The placement of the harnesses along the edge of the array blanket simplifies the incorporation of reflectors by allowing an offset (gap) at the point of intersection of the array plane and reflector planes. It also diminishes the criticality of reflector container length, helping to keep reflector assembly length within the same profile length as the stowed solar array.

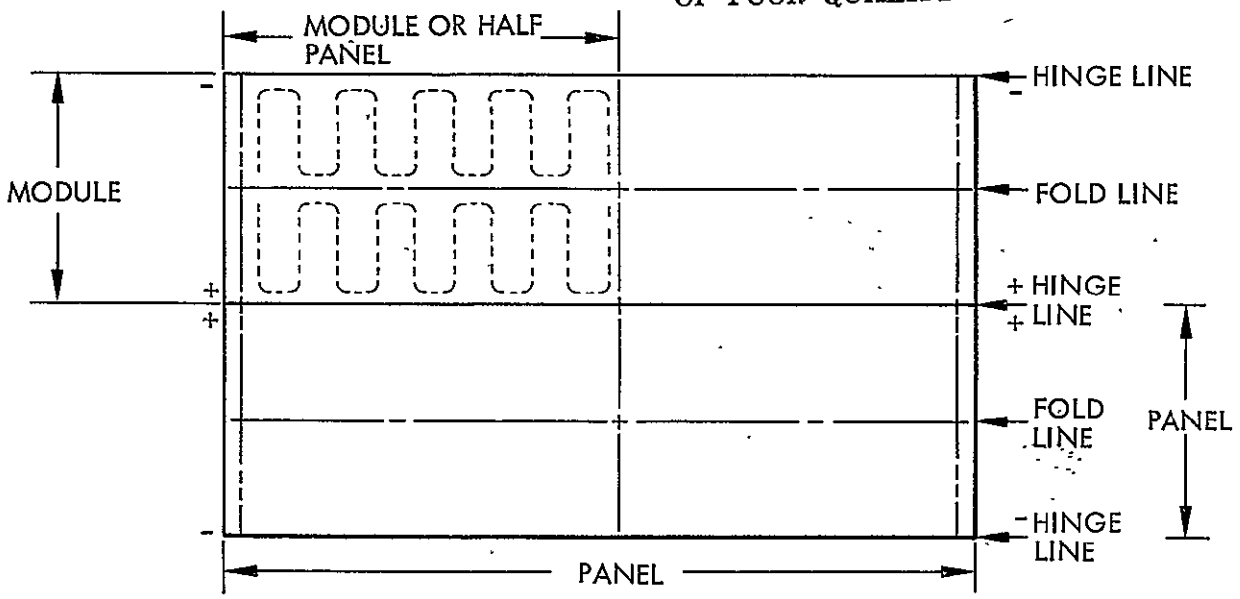

SOLAR ARRAY MODULE

5 CELLS IN PARALLEL BY 306 IN. SERIES
1,530 CELLS TOTAL

SOLAR ARRAY PANEL

2 EACH MODULES
3,060 CELLS TOTAL

Figure 3-21 Array Panel Configuration

Array Power Projections. The array power projections were made based on the previously developed temperature data and the Boeing solar cell characterization data cited above. A 57° concentrator with an effective CR of 1.7 was assumed. A 7.2 percent loss was included to account for assembly, isolation diode and harness losses. In order to provide a 1 AU crossover of 25 kW minimum the concentrator array contains two each 27 panel wings and the planar array contains two 38 panel wings for total array complements of 54 panels and 76 panels respectively. The planar SEP array is reduced from 82 panels (41 panel wings) to 76 (38 panel wings) by going from an old baseline 11.4% efficient wraparound to a conservative 12 percent cell. Significant improvements in cell efficiency have occurred since designation of the 11.4% baseline. The power available from the CESA (concentrator) and the SEP (planar) array systems are depicted in Figure 3-22. It is very significant that the concentrator type array is much more efficient at higher distances from the sun than the planar array.

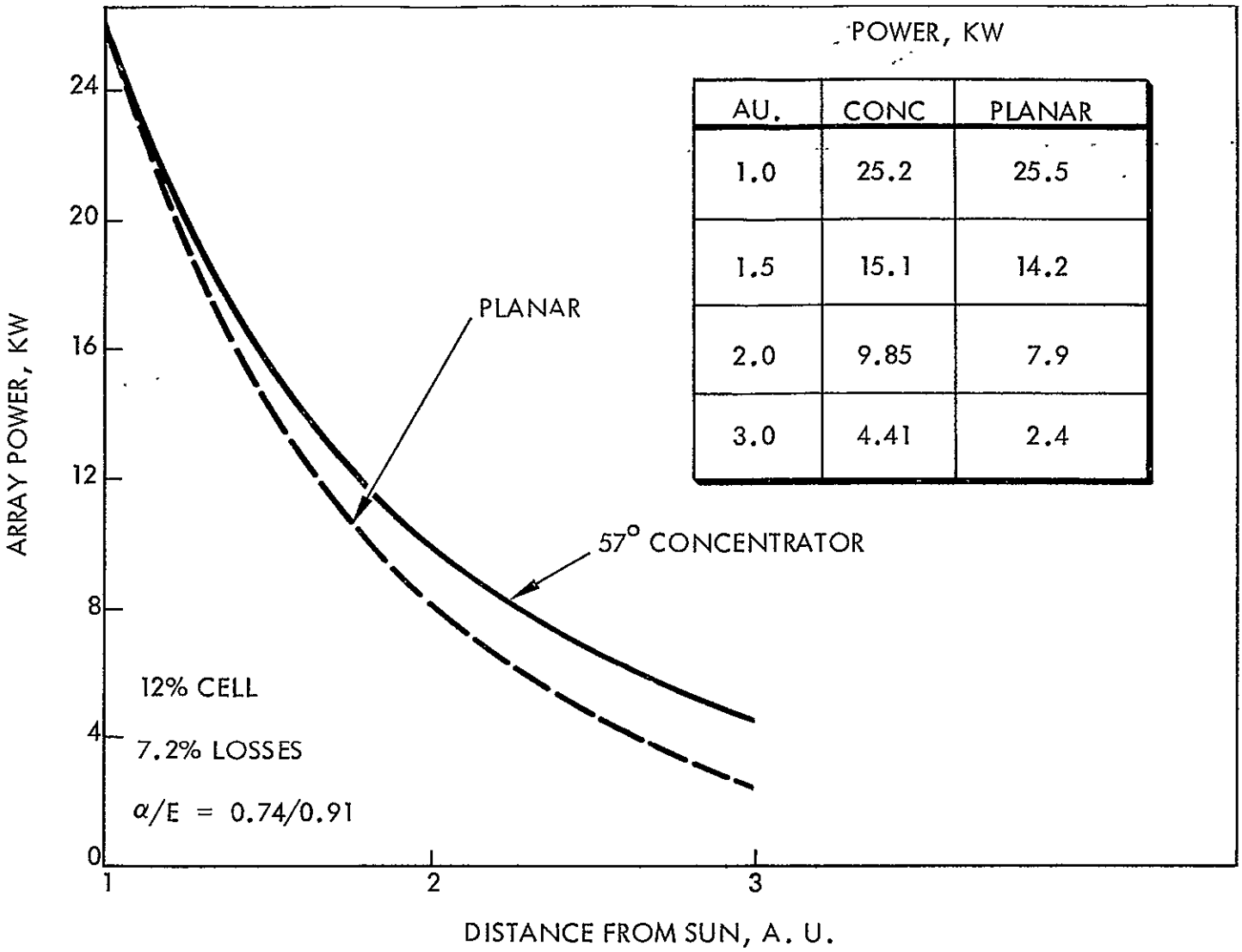

Figure 3-22 Estimated Array Power

Electrical Analysis Tests. Two investigative tests were run with a small solar cell/trough reflector assembly to assess the effects of imbalanced illumination and the effects of misalignment with the solar vector.

The first investigative test was run using a small solar cell assembly, 5 each 1 x 2 cm solar cells in series by 2 cells in parallel, to evaluate the effects of incremental, unbalanced illumination on the cell assembly. Using an X-25 light source and with both right hand and left hand reflectors of the test unit set at 60° and initially shrouded with black covers, the increase in short circuit current was monitored while the

shrouds were removed such that the cells in the string received reflected light--one cell at a time. After the L.H. reflector was fully working a 36% increase in power occurred and the add in of the R.H. reflector resulted in a 73 percent increase in power overall. The most significant finding of this test was the dramatic increase (or decrease) in power associated with illumination of the last cell in the string showing the impact of imbalanced illumination. even though hard shadowing was not occurring. The results of this test are depicted graphically in Figure 3-23.

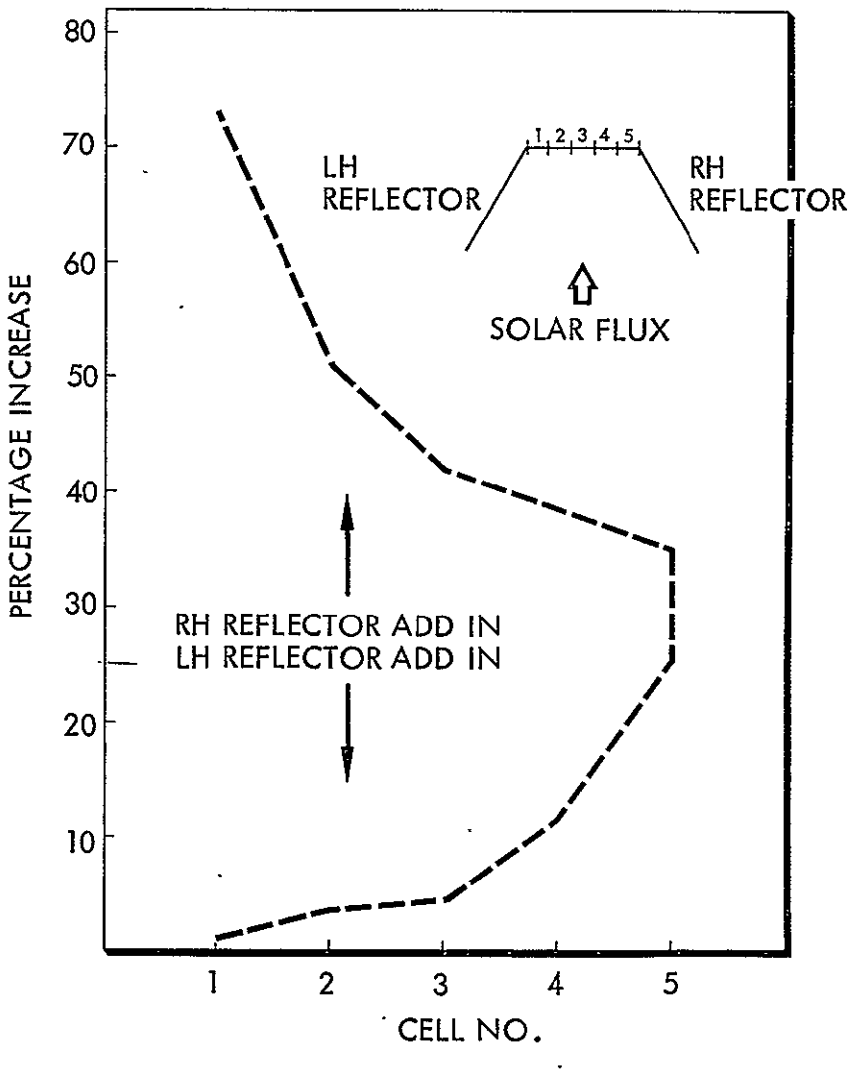

Figure 3-23 Increase in Power vs Reflected Illumination Cell by Cell

The second investigative test was also run with a small cell assembly with reflectors set at 60° and the effective reflector length precisely adjusted so that there was no reflected light overshoot beyond the edge cells. The assembly was then rotated through ± 5° one degree at a time and the associated reduction in I_{SC} was plotted as shown in Figure 3-24. The lack of symmetry in the data was attributed to reflections of an adjacent light colored wall. With a 5° off angle power is reduced almost 20 percent whereas for a planar unconcentrated array response is very flat with less than 1/2 percent change at 5°. From these two tests and from the concentrator analysis it is very important in concentrator array design that reflector positioning and length is such that imbalanced illumination does not occur due to tracking error. It is better to open up the angle from 60° or greater to less than 60° such as the 57° baseline, take some reduction in CR, but be less sensitive to tracking errors, misalignment and imbalanced illumination.

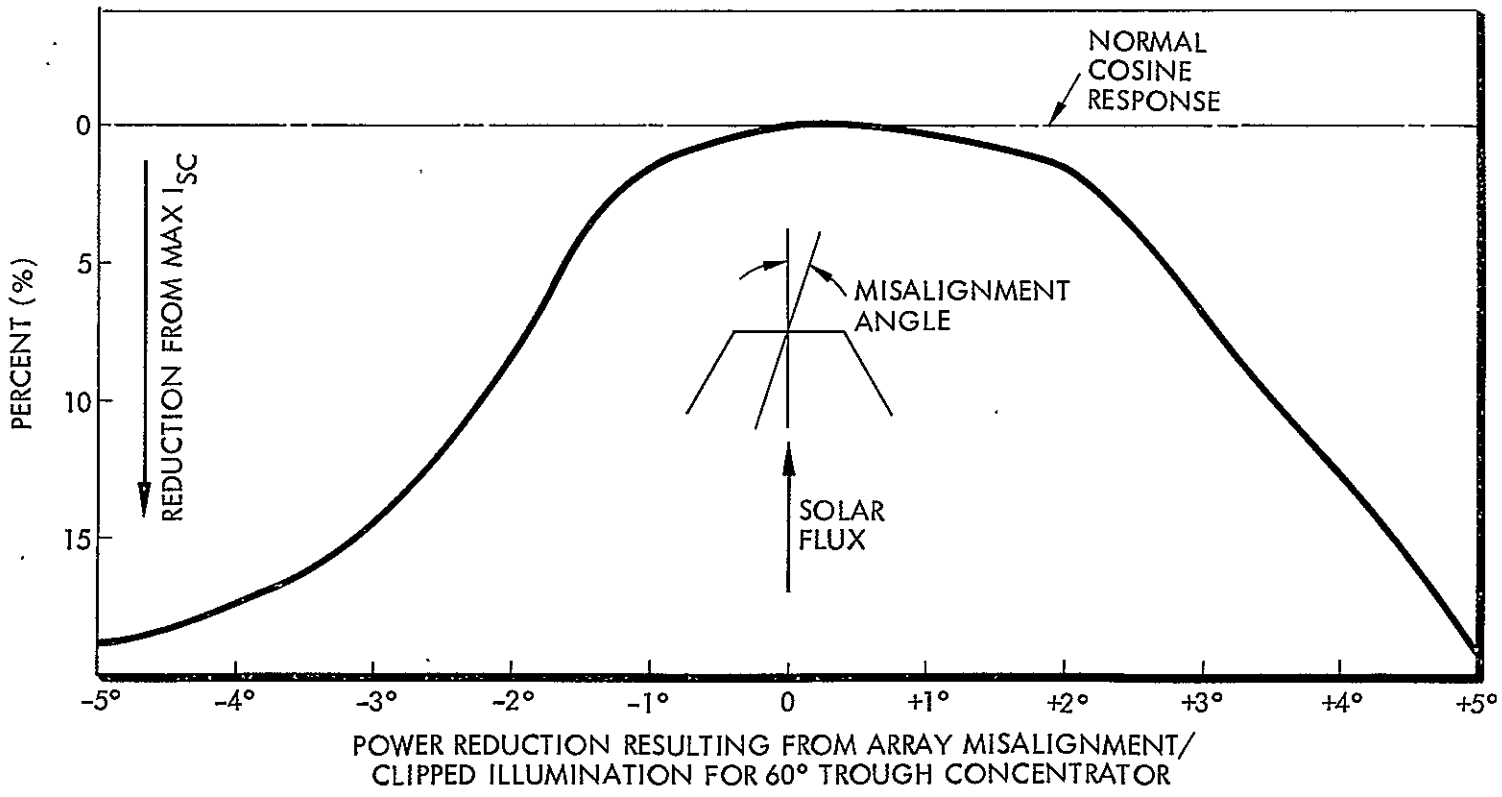

Figure 3-24 Power Reduction Resulting from Array Misalignment

3.2.5 Structural Analysis

Structural analysis considers the loads imposed on the system throughout its service life, the failure modes that elements of each concept might experience, and safe sizing of each component.

3.2.5.1 Loads. Ground handling loads expected during integration of the spacecraft and its subsystems into the Space Shuttle are limited to ± 1 g laterally and 1 ± 1.3 g vertically dependent upon the type of transportation employed.

Launch loads caused by events such as gust loading, engine ignition and cutoff, separation and docking will induce low frequency transient responses in the Space Shuttle vehicle. Sinusoidal vibration will achieve a frequency range of 10-200 Hz at a level of 1.5 g peak with a sweep rate of 1 octave/minute in all 3 principal axes. Random vibration arises mainly from engine generated acoustical noise plus, to a minor degree, structural transmitted vibration. A definitive random vibration environment must be determined on a case by case basis. Preliminary values for a 200 kg stowed array are as shown in Table 3-3.

TABLE 3-3
LOAD LEVELS

Frequency (Hz)	Level
50-200	+9 dB/oct
200-450	0.1 g^2/Hz
450-900	-6 dB/oct
900-1200	0.024 g^2/Hz
1200-2000	-6 dB/oct
Composite	8.4 g RMS

duration - 180 seconds per flight

Acoustic sound pressure within the cargo bay can be considered reverberant. The spectrum varies during launch with respect to level and shape achieving an overall peak sound pressure of 149 dB within one second of liftoff. It then decreases rapidly to 119 dB at t = 21 sec, but increases once more reaching a peak of 135 dB at t = 51 sec.

Shock loads are imposed by pyrotechnics, landing, and on-orbit operations. Pyrotechnics may be involved in the ejection of the spacecraft from the cargo bay, in the release of the solar array from its stowed position, and in some of the deployment sequences thereafter. Although the basic mission is non-return, the possibility of shuttle abort exists and landing loads of 0.2 ± 1.3 g axial, ± 0.7 g lateral, and 2 ± 2 g vertical should be successfully resisted without equipment failure. In case of Shuttle crash, all payload equipment must resist impacting the flight crew upon experiencing ultimate loads of 9 g forward, 1.5 g aft, 1.5 g lateral, 4.5 g up, and 2 g down. On-orbit shock loads are a function of the payload handling and jettisoning procedure which is TBD.

Acceleration loads at liftoff are: 3 ± .15 g axial, ± 1 g lateral, and ± 1.65 g vertical. On-orbit maneuvers may produce accelerations up to 1.3 ft/sec^2 (0.04 g).

Once placed in independent orbit, the IUS provides attitude control and thrust to the spacecraft. The IUS configuration chosen for this mission is a two motor propulsion system with a hydrazine attitude control subsystem. The maximum accelerations experienced during its burn is 5.09 g axial and ± 2.09 g lateral. The dynamic limit load (composite sum of all dynamics and quasi-static accelerations) for the stowed solar array is 13.0 g.

The solar array is deployed prior to IUS separation to capitalize on the relatively stiff attitude control capacity of the IUS. Deployment of the solar array involves functioning of at least four pyrotechnic devices per wing impacting shock loads to the spacecraft. Sequential events requirements of the total deployment procedure may involve additional pyrotechnics.

When the array is fully extended, the IUS is separated by functioning explosive nuts. The maximum shock imparted to the payload is 4000 g at 10 kHz due to pyrotechnic spacecraft separation events.

Finally, the electric propulsion system is turned on producing 0.26 to 1.3 lb of thrust to the spacecraft dependent on the number of ion engines energized.

Besides the loads imposed on the solar array by the various environments and transportation devices, certain other loads must be imposed to produce a viable concentrated array system. An analysis was performed to determine the tension field in a Kapton panel with loads applied at the 4 corners as shown in the figure. Since there is symmetry around both the X- and Y-axis only 1/4 of the reflector was modeled (reference Figure 3-25). Seams every 47 inches were included in the model and treated as small bean-like stiffeners (area = 0.006 sq. in.). Only one area of compression was found near the loaded corner. The rest of the panel was in biaxial tension except for the seam/stiffeners which are each under axial compression. A 2 lb force was chosen as the baseline corner force pulling at 30° from the Y-axis. For a 0.0003 inch thickness, the X and Y stress are 6 and 75 psi, respectively.

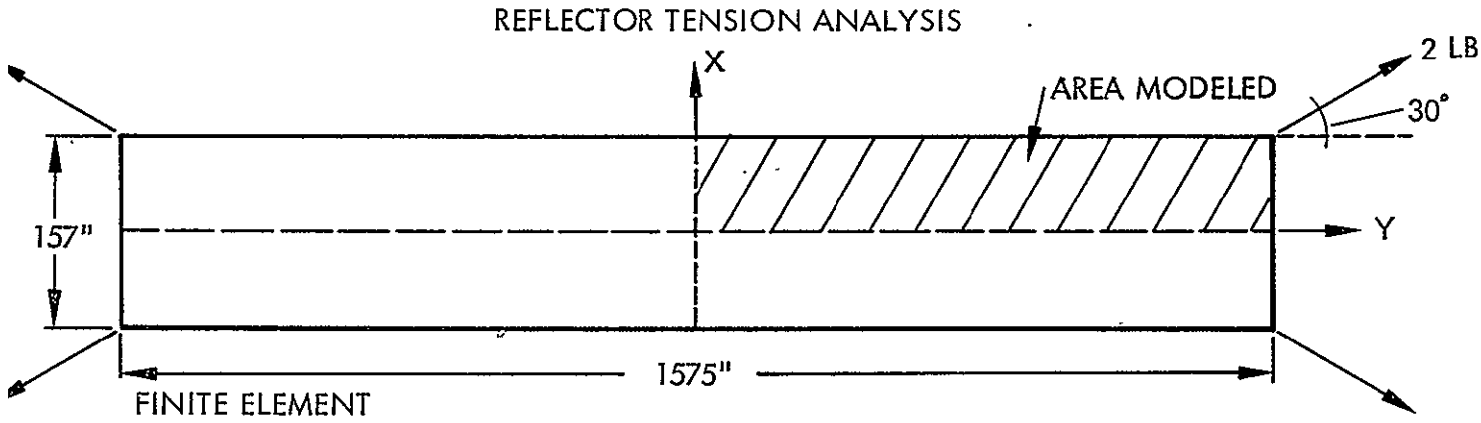

Figure 3-25 Reflector Tension Analysis

The dynamic analysis discussed in section 3.2.2 developed the need for 0.75 lb of array blanket tension in addition to the 6 lb of force in each reflector system (2 lb each corner plus 2 each 1 lb guidewires) to meet the minimum lateral fundamental natural frequency requirement.

3.2.5.2 Structural Failure Modes. The primary structural failure mode of the reflector is in ultimate tension originating most likely at a stress riser and propagating rapidly across the entire sheet. Introduction of the corner loads must be accomplished

carefully with adequate doublers. Raw edges should be doubled over and bonded to eliminate rip propagations from minute discontinuities in the sheared edge. Splices should be accomplished so that load transfer is uniform. Ultimate tension in the reflector is probably limited to the capability of the splice joint adhesive. Tensile yield strength of unreinforced polyimides (Kapton) range from 7.5 to 13 ksi or 2.25 to 3.9 lb per inch for 0.0003 inch thick film. Peel strength for dry film adhesive is 2.5 lb per inch.

The booms which support the deployed reflector are quite long (152.9 in) and necessarily cantilevered. Although the loads are small, the bending moment is large (~410 lb-in) and the small available cross section indicates a high bending stress at the root. Deflection of the boom tip must be restricted, or compensated for, to maintain adequate reflector tension. The root moment must be successfully transferred from the reflector boom through the boom rotation hinge into the array blanket outer support beam. An analysis of the hinge lugs must be made to insure no bearing or hinge pin shear failures occur.

The array blanket outer support beam transfers all reflector and blanket tensions, guidewire forces, and moments into the deployment mast.

The deployment mast, which is a coilable lattice structure consists of 3 S-glass/epoxy resin composite longerons joined into bays by battens constructed of the same material. Six flexible diagonals of stainless steel cable stabilize each node of each bay. The nominal mast radius (R) refers to a circle through the centerlines of the three longerons.

In addition to the mast parameters listed in Table 3-4 the following stiffness characteristics are representative for the continuous longeron mast.

Mast torsional stiffness	$GJ = 0.020\ EI$	EI in $lb\text{-}in^2$
Mast shearing stiffness	$GA = 301\ R^2$	R in inches

The mast stiffness is normally sized by the extended array natural frequency requirement. Failure of the mast either as an euler column, combination loaded beam, or in local crippling must be investigated for each application.

TABLE 3-4

DEPLOYMENT MAST PARAMETRIC DATA

BAY SPACING	1.25 R	
MAST WEIGHT	$7.19 \times 10^{-3} R^2$ (LB/FT)	R IN IN.
MAST STIFFNESS	$EI = 7530 R^4$ (LB-IN.^{2})	R IN IN.
CRITICAL AXIAL LOAD	$P_{CR} = 5.348 R^2$ (LB)	R IN IN.
MINIMUM BENDING STRENGTH	$M_{CR} = 2.675 R^3$ (LB-IN.)	R IN IN.
CANISTER HEIGHT	$H_{can} = 0.022L + 3.3R$ (IN.)	L&R IN IN.
CANISTER DIAMETER	$D_{can} = 2.36R$	R IN IN.
CANISTER WEIGHT	$W_{can} = 5.21 \times 10^{-4} LR + 0.553 R^2$ (LB)	L&R IN IN.
MAST/CANISTER INTERFACE BENDING STIFFNESS	$K = 0.729 (EI)^{3/4} \left(\frac{\text{IN.-LB}}{\text{RADIAN}}\right)$	EI IN LB-IN.^{2}

Protection of the solar array blanket and the reflectors from the launch and staging loads is accomplished by flat pleat folding them and separately squeezing the pleated stacks between two resilient pads. When sufficient normal force is developed, the resultant static friction retains the folded blankets from lateral movement.

The backup structure for the squeeze pads provides a point of integration for deployment devices and spacecraft attachment.

The major mass of the assembly is in the solar array blanket and containment box. Consequently the containment box is chosen as the main structural support member. It is directly fastened to the spacecraft, and all other items are supported from it.

3.2.5.3 Component Sizing. Preliminary sizing of certain elements has been accomplished. These include the reflector boom, hinge, tensioning unit, and the mast and counterbalance. The original SEP array containment design was not examined except where major changes were made.

The reflector boom is 152.9 inches long with reflector tensioning loads at the ends, and guidewire loads at quarter spans. It is supported at one end by a hinge/actuator/latch system in a cantilever mode. The beam cross section available to resist these

loads is limited to less than four inches wide by one inch deep. Volumetric demands in the inboard reflector boom for storage of the flat folded reflector and a cable passageway reduce this area to 3.38 inches wide by 0.88 inches deep. The outboard boom requires no cable way so its available cross section is 4 inches wide by 0.88 inches deep. Boom loading is shown in Figure 3-26.

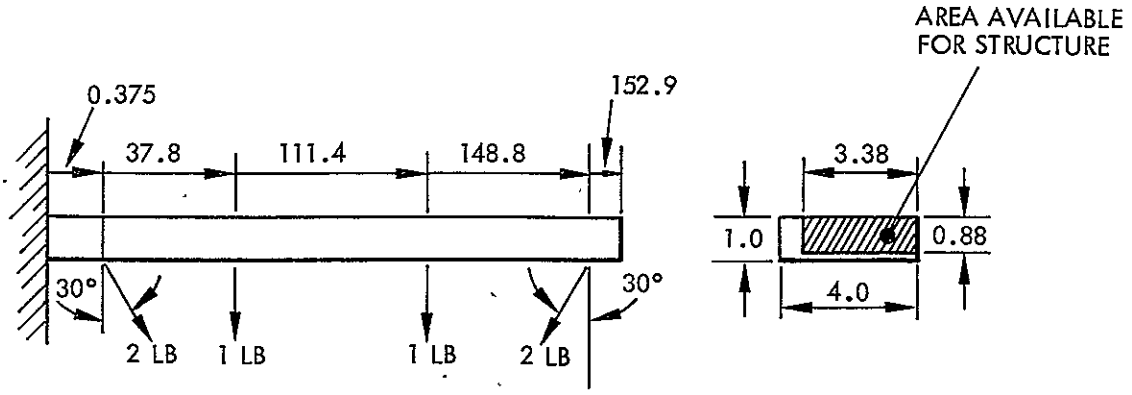

Figure 3-26 Reflector Boom Loading

Concern over stress and deflection of the reflector boom caused various outrigger and guy wire concepts to be postulated. However, the complexity of erecting these devices caused them to be considered as a last resort. Consequently, the boom was designed with a known 3 inch tip deflection which could be compensated for by either trimming the reflector or adjusting the outboard fixed tethers to match the deflected boom. The former was chosen so as to better maintain the 30° off angle tension.

Design of a honeycomb sandwich structure involves determination of the required flexural rigidity and then selecting combinations of total sandwich thickness and facing thickness for various types of facing materials. Hexel Corp. document TSB121 describes the process in detail. The bending deflection constants (K_B) tabulated in this document did not cover the case of multiple loaded cantilever beams.

Therefore, a constant was derived using Castigliano's first theorem. From this theorem we know that

$$Y_{total} = \sum_{n=1}^{4} Y_n = \sum_{n=1}^{4} \frac{1}{6} \frac{W_n}{EI} (3 a^2_n - a^3_n)$$

Loads and deflections are summarized in Table 3-5.

TABLE 3-5

LOADS AND DEFLECTIONS DATA

n	W_n (lb)	a_n (in)	Y_n (in)	M_n (lb-in)
1	1.73 (2 cos 30°)	0.4	20.6/EI	0.7
2	1	37.8	97,304.0/EI	37.8
3	1	111.4	692,889.2/EI	111.4
4	1.73	148.8	1,899,912.6/EI	257.4
Total	5.46		2,690,126.4/EI	407.3

and from TSB121

$$K_B = \frac{EIY}{W\ell^3}$$

Substituting data from the table into the expression for K_B we find:

$$K_B = \frac{EI\,(2,690,126)}{EI\,(5.46)(148.8)^3} = 0.15$$

Using this derived constant, a flexural rigidity was obtained and for a total sandwich height of 0.88 inches, facing thickness of various materials were determined and presented in Table 3-6 and Figure 3-27.

TABLE 3-6

HONEYCOMB SANDWICH FACING MATERIAL CANDIDATES

Material	E (10^6 psi)	t_f (in)
Aluminum	10	0.070
Titanium	15	0.050
Graphite/epoxy	25	0.030 (by interpolation)
Steel	30	0.023

Of these candidates, graphite epoxy was chosen as the least weight candidate.

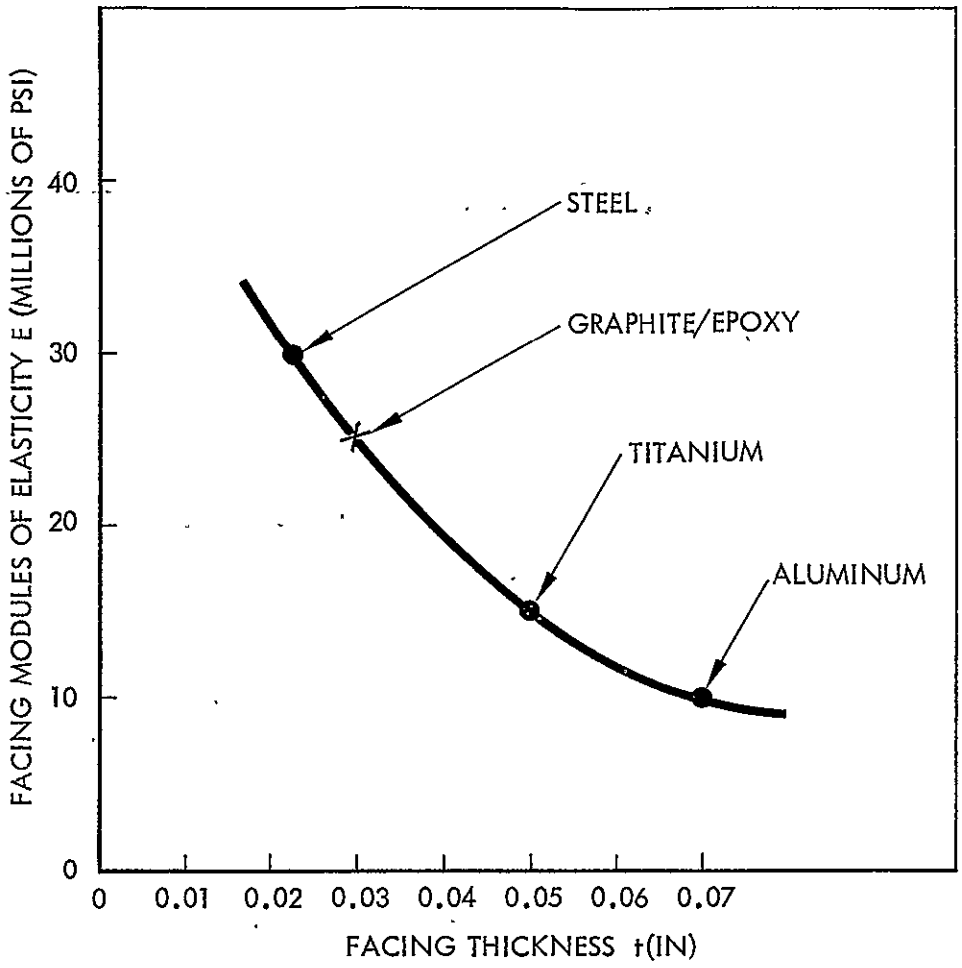

Figure 3-27 Effect of Facing Stiffness On Facing Thickness Requirements

The next step was to select a honeycomb core. Based on the total shear load of 5.64 lb, 3.38 inch beam width, and core thickness of 0.82 inch, the minimum required honeycomb shear strength is less than 10 psi. The lowest density aluminum core material commercially available (1.0 lb per ft^3) has a minimum shear strength of 20 psi. Suitable core materials would be 0.0007 inch thick 5052 or 5056 aluminum foil configured in 0.38 inch hex cells.

As a final step, the stress in the facings was checked. For an allowable compressive stress of 55,000 psi, a maximum bending moment of 407.3 lb-in, and a core thickness of 0.82 inch, the required facing thickness is 0.010 inch. The facing thickness of 0.030 inch selected earlier is more than adequate to resist the bending stresses.

The reflector boom hinge must react 407.3 lb-in of moment. The hinge pin is 0.25 inch diameter and is placed in quadruple shear. The maximum lug shear, S, is:

$$S = \frac{M\,Y_{max}}{\sum_{n=1}^{3} Y_n^2} = \frac{407.3 \times 1.75}{4.60} = 155 \text{ lb}$$

$Y_1 = 0.825$ in.
$Y_2 = 0.925$ in.
$Y_3 = 1.75$ in.

The lug bearing stress is 6200 psi. These values represent a safe design, so a more rigorous analysis is not pursued.

Analysis of the tensioning unit involves selection of a spring, output drum, take up drum and a cable reel which do not exceed allowable strength values. The total extension of the tensioning unit is 40 inches, which when applied to a 1.0 inch diameter reel results in 12.75 revolutions. The force required is 1.73 lb, or a torque of 0.86 lb-in. The smallest spring available which equals or exceeds this torque is 0.31 inch wide and 0.007 inch thick. This spring is high carbon steel rated for a life of 4000 cycles when used on a takeup drum 1.09 inch diameter and output drum 1.82 inch diameter.

The mast radius for the SEP solar array is 7.2 inch. Shortening of the solar array blanket from 41 to 27 panels per wing stiffens the system considerably. However, an end couple produced by the eccentric tension loads of the array blanket, and reflectors counters some of this benefit.

The dynamic analysis (paragraph 3.2.2) not only established blanket tension (0.75 lb), but also showed that minimum frequency (0.02 Hz) could be met by mast radii as small as 4.5 inch. If a 4.5 inch radius mast is elastically stable, then considerable weight may be saved.

Figure 3-28 shows the manner of loading of the mast where moment M results from the various tensioning loads in the system.

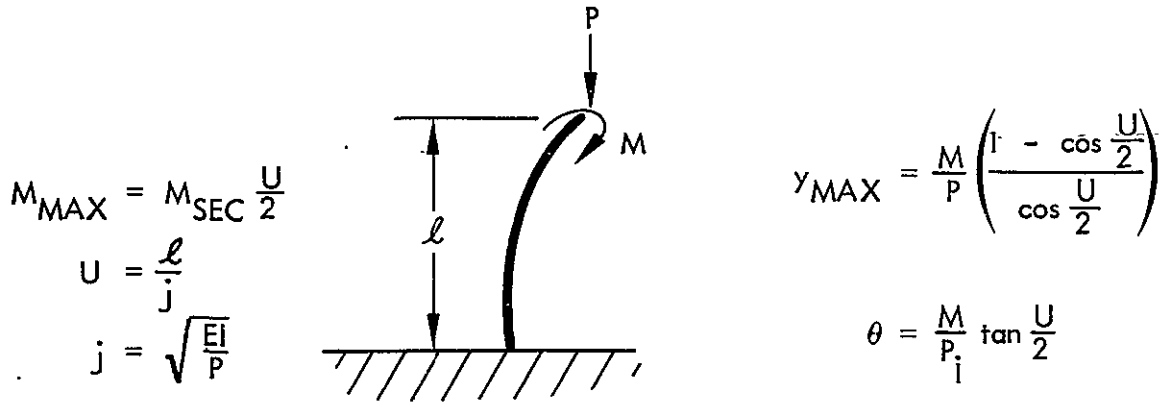

Figure 3-28 Combination Loaded Mast

The moment is derived from the individual loads acting about the mast centroid as shown in Figure 3-29. The total moment is 943.52 lb-in. The root moment is amplified from the tip moment loading because of the combined nature of the applied loads. This amplified moment must be compared with mast minimum bending strength.

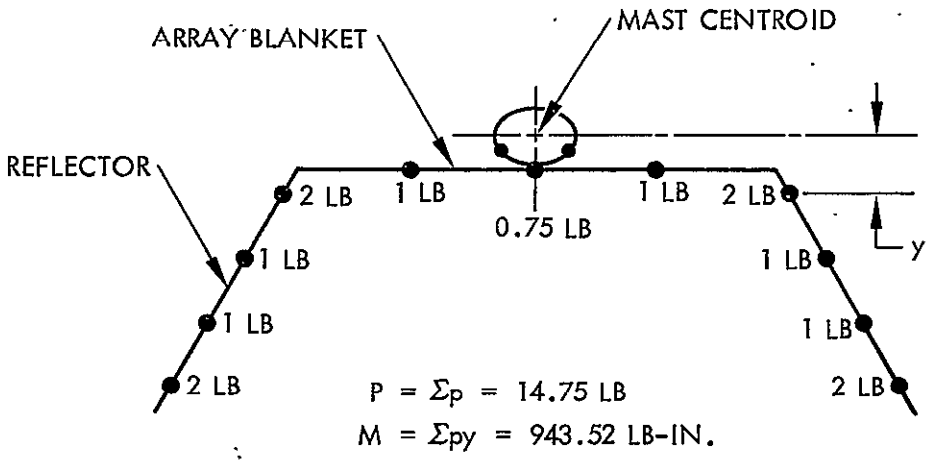

Figure 3-29 End View Array Tension Loads

Using 1.25 as a safety factor, an expression for R may be written using the parametric data of Table 3-4.

$$R = \left[\frac{1.25\,M}{2.675 \cos\left[\frac{L}{2\sqrt{\frac{7530R^4}{P}}}\right]}\right]^{1/3}$$

M = 943.52 lb-in
L = 943 in
P = 14.75 lb.

And a solution for R is 7.9 inches.

A smaller mast radius can be achieved by reducing the end couple either by reducing blanket/reflector tensions, or by counterbalancing. Reducing reflector corner tension from 2 lb to 1 lb results in an end couple of 639 lb-in. P declines to 10.75. The expression for R becomes:

$$R = \left[\frac{1.25 \times 639}{2.675 \cos \left[\frac{943}{2\sqrt{\frac{7530\ R^4}{10.75}}} \right]} \right]^{1/3}$$

With a solution R = 6.9 inch.

If the reduced corner tension in the reflectors cannot be accepted, then a counterbalance erected on the opposite side of the mast centroid could be mechanized to alleviate all end couple.

With the elimination of end couples, the mast system now becomes a straight forward column design problem.

From Euler

$$P_e = \frac{C\ \pi^2\ EI}{L^2}$$

P_e = Critical Buckling Load (lb)

C = End fixity coefficient

EI = Column stiffness (lb-in^2)

L = Column length (in)

C = 0.25 for one end fixed, one end free

The most practicable counterbalance design produces an additional load of 9 lb on the column. Thus

P_e must = 1.25 (14.75 + 9)

Inserting mast parameters in the Euler equation and solving for R we find:

$$1.25\,(14.75 + 9) = \frac{0.25\,\pi^2 \times 7530\,R^4}{(943)^2} = 29.7 \text{ lb.}$$

$R = 6.2$ in.

All that remains is to check for crippling

$$P_{CR} = 5.348\,(6.2)^2 = 205 \text{ lb.} \qquad 29.7 \text{ lb}$$

The counterbalance is illustrated in Figure 3-30 showing how the composite reflector and array blanket tensions (P_1) acting at an effective eccentricity (e) are balanced by load P_2 acting at the end of the counterbalance mast.

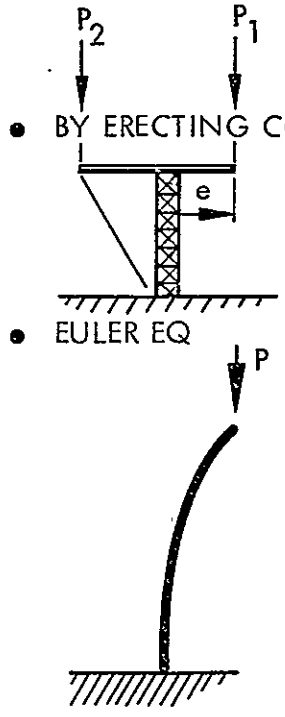

COUNTERBALANCED MAST

- BY ERECTING COUNTERBALANCE, $M \rightarrow 0$, BUT $P \rightarrow 25$ LB,
  ALTHOUGH $P \ll P_{CR}$, SLENDERNESS RATIO INDICATES CLASSIC EULER COLUMN ACTION
- EULER EQ FOR ONE END FIXED, ONE END FREE, $C = 1/4\,P_C = \frac{C\pi^2 EI}{L^2}$

Figure 3-30 Counterbalanced Mast

The choice of alternatives must be based on weight, complexity, and reflector performance considerations as summarized in Table 3-7.

TABLE 3-7

MAST CANDIDATE WEIGHT COMPARISON

R (IN.)	W_M (LB)	W_{can} (LB)	OTHER (LB)	ΣW (LB)	REMARKS
7.9	35.26	37.14	0	72.40	HEAVIEST
6.9	26.90	28.77	0	55.67	REDUCED REFLECTOR TENSION
6.2	21.72	23.53	5	50.25	COUNTERBALANCE COMPLEXITY

The counterbalanced design (R = 6.2) is selected on the basis of least weight and delivery of adequate reflector tension at the cost of some deployment complexity.

3.3 BASELINE MECHANICAL DESIGN

The baseline mechanical design uses the basic Solar Electric Propulsion (SEP) solar array technology which has been under development since 1973. This solar array provides a departure point from which the unique requirements of this study may be applied. Through relatively minor modifications it was found that the SEP array may be utilized for Concentrator designs.

3.3.1 SEP Array Description

The SEP solar array wing shown in Figure 3-31 extends and retracts either fully or partially to a predetermined point depending on the specific mission requirements. It tensions a flat-folding blanket of solar cells, 31.6 m by 4 m, to provide a natural frequency equal to or greater than 0.04 Hz. It is capable of automatically restowing the blanket and preloading it for return to earth via a shuttle spacecraft.

The wing consists of five major components; array blanket, mast, tensioning mechanisms, containment box, and box cover. The blanket is folded in 81 layers and stowed in the container for ascent. The padding on the individual blanket panel halves serves as separation between the cell-coverslide assembly surfaces and as protection against cell damage during ascent loading in the shuttle bay. The folded blanket is preloaded (compressed) between the storage containment box floor and the containment box cover to prevent slippage during the ascent phase of the mission. Preload force is maintained to the cover by four levers which are integrated to the mast tip by an interface fitting, pivoted by a linkage to the box cover assembly, and which bear against fixed lugs on the containment box. The preload is released by actuating the mast for extension. The mast is a continuous longeron lattice structure, 32 m (105 ft.) long designed by AEC-Able Engineering Company, Inc., Goleta, California. The coilable truss structure is stowed in a canister and is extended by a rotating nut driven through a gear system by two electric motors. The rotating nut interfaces with small rollers mounted on the longerons at each bay (every 9 inches of longeron length) to extend or retract the mast. As the mast extends, the levers release the preload and then become the load path from the tip of the mast to the cover. The box cover now serves as support for the outer end of the array blanket when tensions

ORIGINAL PAGE IS
OF POOR QUALITY

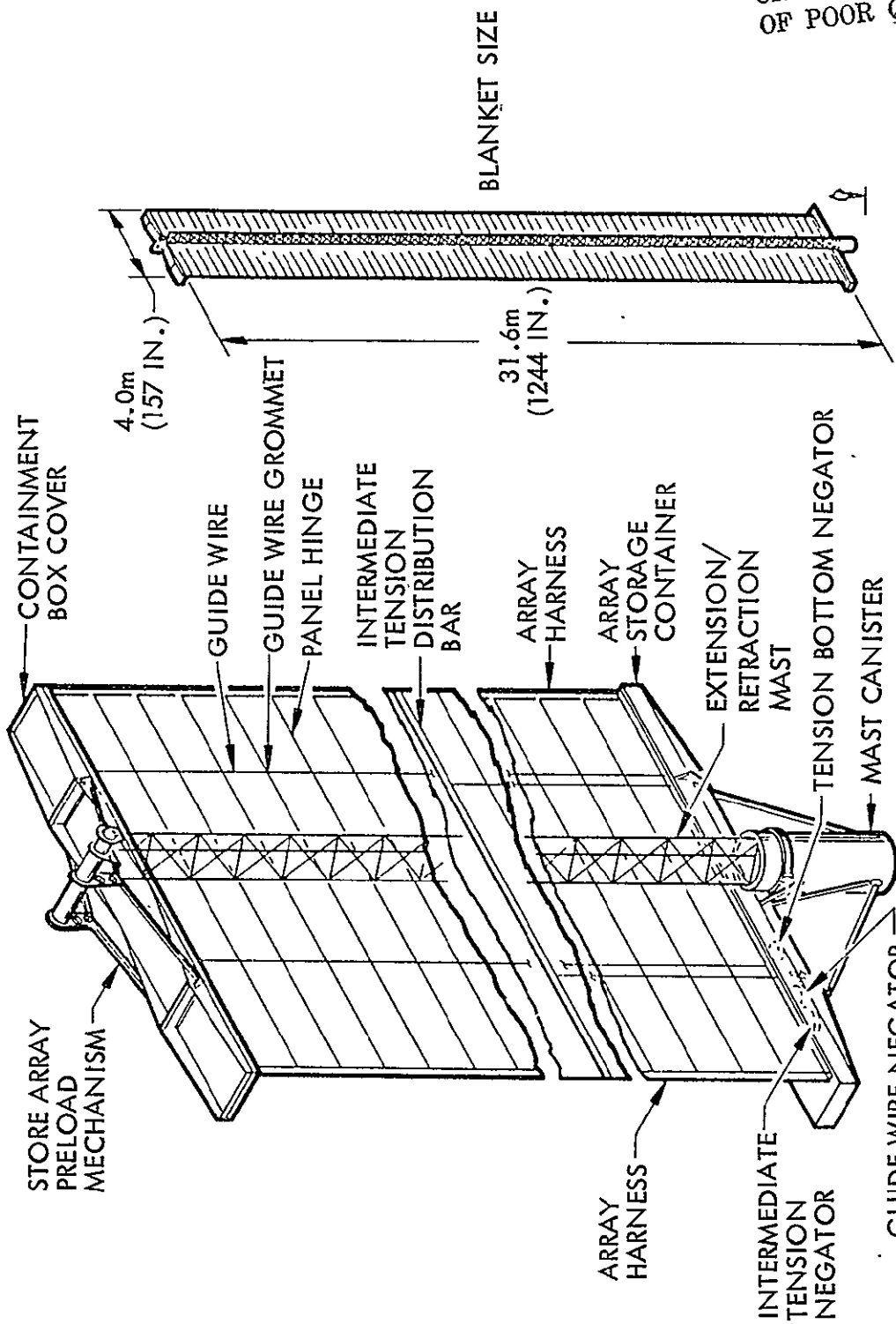

Figure 3-31 SEP Solar Array Wing

are applied to the blanket. Two guide cables attached to the cover and tensioned by negator powered reels are used to maintain a positive position of the unfolding blanket in zero-gravity. Continued mast extension unfolds the stowed array panels as shown in Figure 3-32 until a predetermined intermediate tension point is reached. Two negator powered reels and tension cables provide up to 37.8N (8.5 lbs) force for tensioning the blanket sufficiently to meet the 0.04 Hz minimum natural frequency requirements.

Further mast extension will eventually fully extend the blanket. At this point two more negator-powered reels and cables will tension the blanket to assure the 0.04 Hz minimum natural frequency requirement. Upon command the mast will retract either back to the intermediate tension point or to the fully retracted position. Retraction will result in folding of the untensioned individual blanket panels in a random sequence below the intermediate tension point. After the partial extension point is passed, folding of the remaining outboard array panels occurs in random sequence to the fully stowed position where the cover locking levers will again preload the stowed blanket and the mast will be automatically stopped. The wing will then be ready to survive the reentry loads applied within the shuttle bay.

3.3.1.1 Blanket. The blanket assembly shown in Figure 3-33 consists of 41 panel assemblies which are folded into 82 half panels for ascent stowage. Each panel contains 3060 solar cell and cover assemblies welded to a copper interconnect system. For ascent and reentry phases of the SEP mission a form of cell protection from the environment is provided by criss-cross padding as shown on the panel assembly. The criss-cross padding alternates between adjacent panel halves so that, when they are folded in the stowed position, the pad patterns cross each other providing cell separation.

Stiffening of the panels is necessary for zero-gravity fold-up. The baseline concept provides stiffening along the fold and hinge-lines and at the guide wire positions. The stiffener elements near the wire harnesses were removed because sufficient support was given by the harness. Although the height of the stiffeners is limited to the cell/coverslide height due to stacking limitations, the stiffener element width capabilities have been increased from .064 to .13 inches along the hinge and fold areas and from 0.064 to 0.3 inches at the guide wires. Each panel is also thermally set into a crease at its fold-line to enhance proper fold direction.

ORIGINAL PAGE IS
OF POOR QUALITY

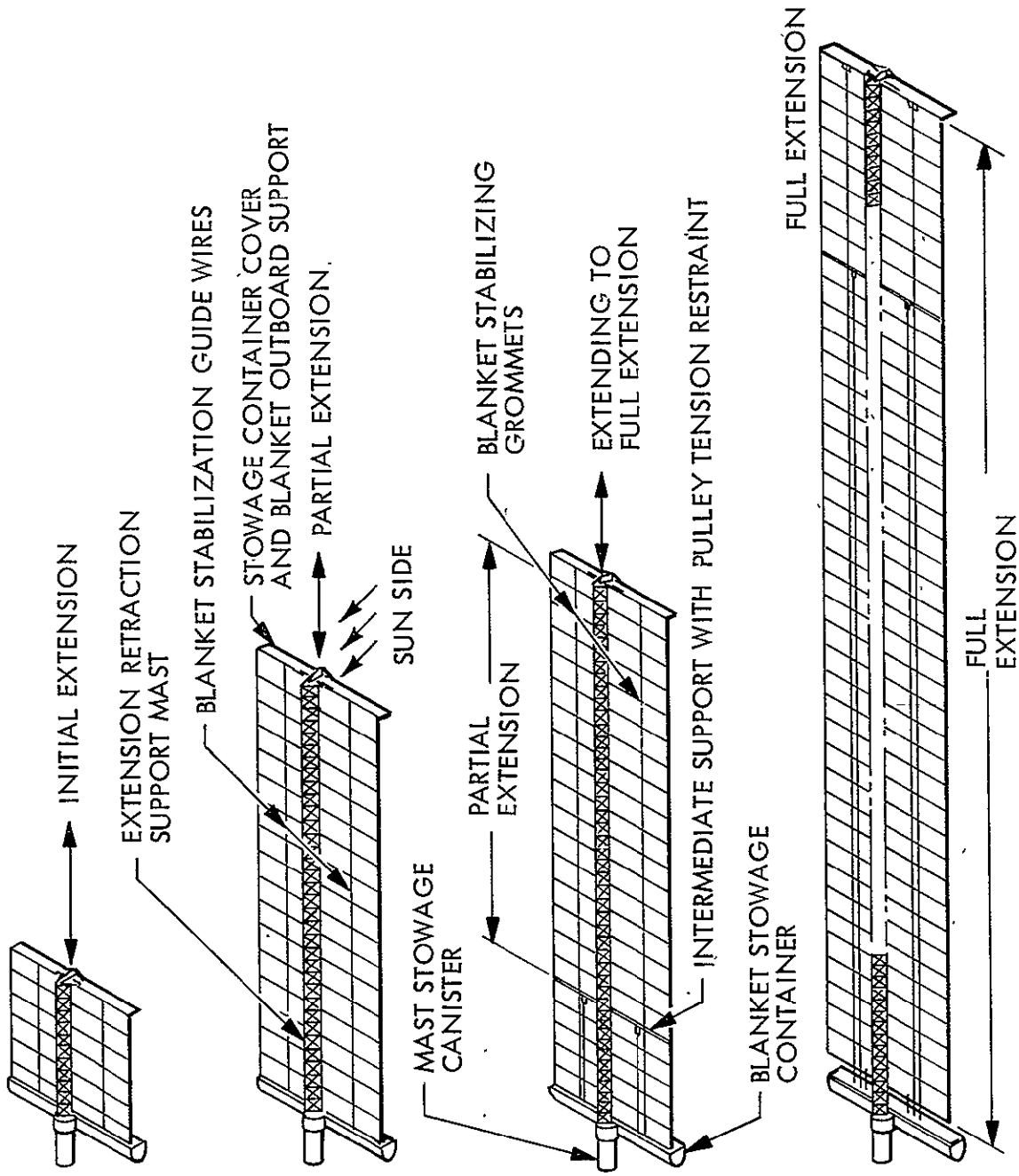

Figure 3-32 SEP Solar Array Extension Sequence

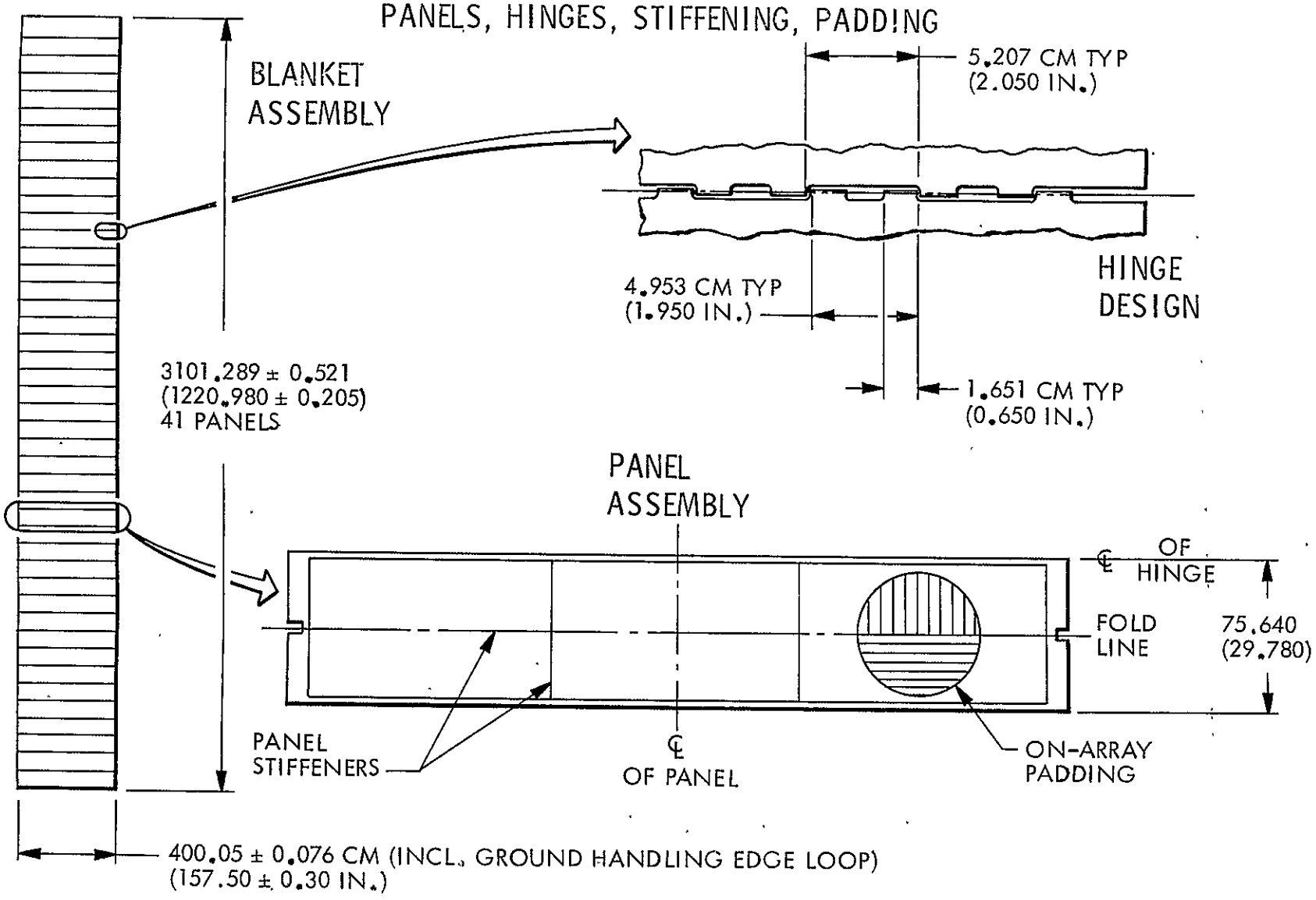

Figure 3-33 SEP Solar Array Blanket Design

Along the mating edges of each panel is a fiberglass cloth hinge with alternating long and short cutouts between equal length hinge lobes. As shown in Figure 3-3, the short cutout and its adjacent lobes are spaced to fit between the long cutout of its mating hinge and are spaced on 4.00 in. centers. The short cutouts then accept the attachments of the intermediate and bottom tension distribution bars. The 41 panels are attached to each other mechanically by a hinge pin ("S" glass-epoxy rod, 0.032 in. in diameter).

At the outer end of the blanket, where it interfaces with the cover, a leader of Kapton with a fiberglass hinge, configured the same as those on the panels, provides sufficient distance from the cover to preclude shadowing by the cover up to angles of 23.5 degrees with the sun vector.

At each hinge line there are two tabs with eyelets for the guide wires which provide control of the blanket position during extension and retraction in zero-gravity.

3.3.1.2 Tensioning System. The blanket tension and guide cable systems are all negator powered. They differ in the amount of cable travel and force required. There are 3 pairs of mechanisms; 2 guide, 2 intermediate tension, and 2 bottom tension. Each guide cable mechanism provides a 4.4 N (1 lb.) force to a cable which passes through an eyelet at each hinge line in the foldable blanket. Two negators power a central cable reel which is appropriately sized based on the length of cable necessary to guide the panels to their fully deployed position. The negator spring lengths and the two negator drum diameters are sized to provide sufficient tension and revolutions to the cable take-up reel. The shafts for each reel end drum are directly attached into the containment box honeycomb floor to minimize the system weight. Inserts are tooled into the floor to provide parallelism to the mechanism shafts. Solid film lubricants are used throughout to minimize friction within the assembly. The components are fabricated from the materials listed below.

Negator springs - 301 stainless steel
Negator support drums - beryllium
Shaft - A286 stainless steel
Cable - braided dacron 0.025 in. dia.
Cable Reel - beryllium

The tension mechanisms provide tension to the extended blanket. Each mechanism applies a force to a tension distribution system (see Figure 3-34) which distributes the two local loads over the blanket width. The local loads from the mechanism are introduced to a graphite-epoxy tube through a fitting. The loads from the tube are then transferred to a blanket hinge line by 38 spring assemblies. The spring rates of the assemblies are sufficiently low such that straightness tolerances in the blanket and tube, and tube deflections will not represent large tension variations across the blanket. One end of the spring assembly is permanently fixed to the graphite tube, while the other end is clipped to a blanket hinge-pin. In the stowed position, the tubes are guided to rest on stops within the container by the tension mechanism cables as shown in Figure 3-35. The tension distribution springs conform to the blanket hinge-line position. The tension mechanism uses the same principles, construction, and materials as the guide wire mechanism. The reels and drums are appropriately sized for the forces and lengths involved and the number of negator springs used per cable reel is five.

The bottom tension mechanisms located at the bottom of the blanket each provide a force of 37.8 N (8.5 lbs.) to this tension distribution system. The reels and drums are appropriately sized for the forces and lengths involved and here the number of negator springs per cable used are four.

3.3.1.3 Array Blanket Support. The array blanket is supported in the folded condition during ascent and reentry phases of the SEP mission to ensure its survival for satisfactory performance. In orbit it is also supported and tensioned to assure a system minimum natural frequency of 0.04 Hz and proper alignment to the sun vector. The mast described in paragraph 3.3.1 is a major support element in these mission phases along with the box cover and containment box.

A preload of 1.03 N/cm^2 (1.5 psi) average is created over the folded blanket between the box cover and the container floore. This force is created by the mast during retraction. It is transferred from the mast through a tip fitting to four levers which pivot on the mast tip fitting and engage 4 strikes as shown in Figures 3-36 and 3-37.

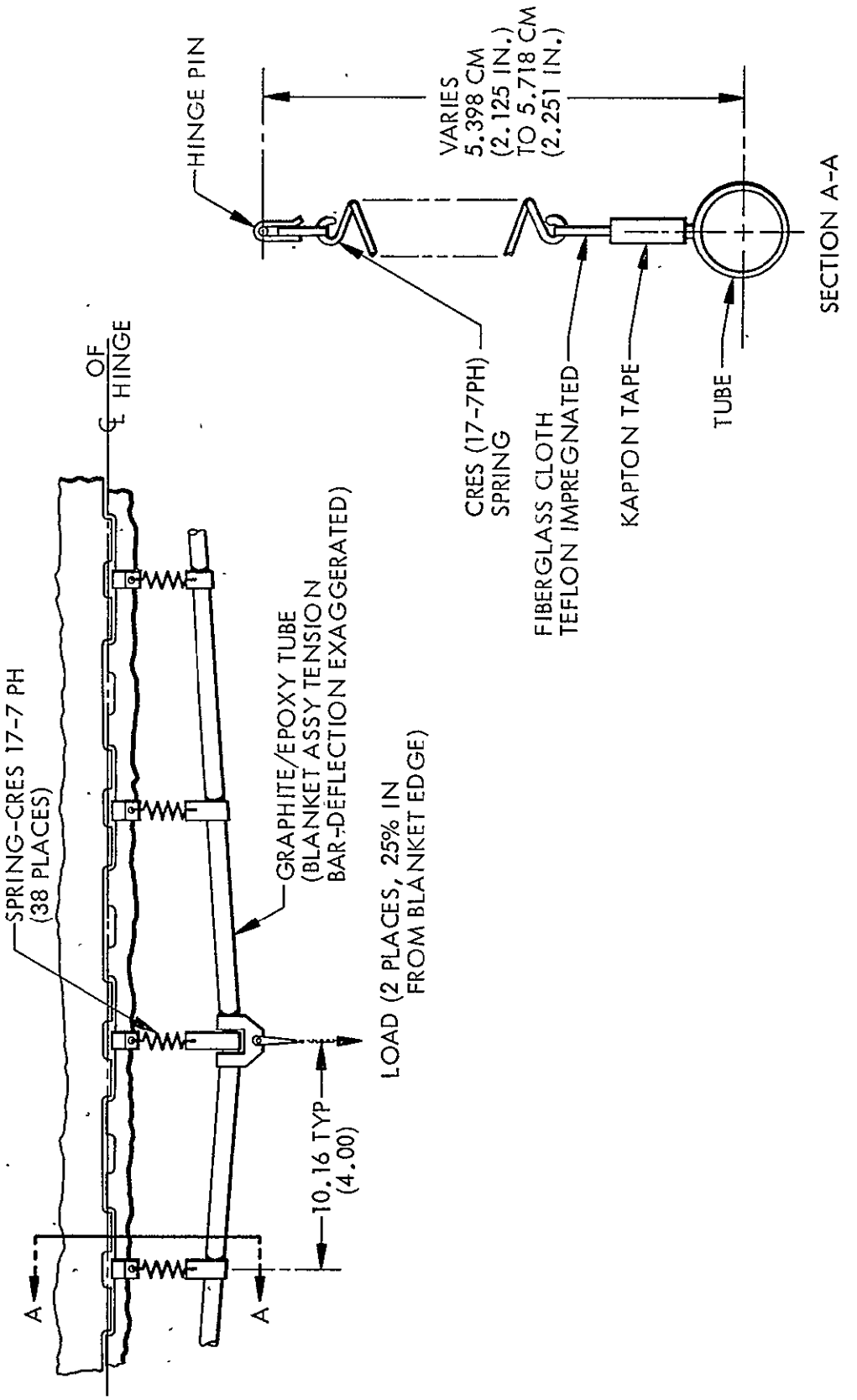

Figure 3-34 Blanket Tensioning

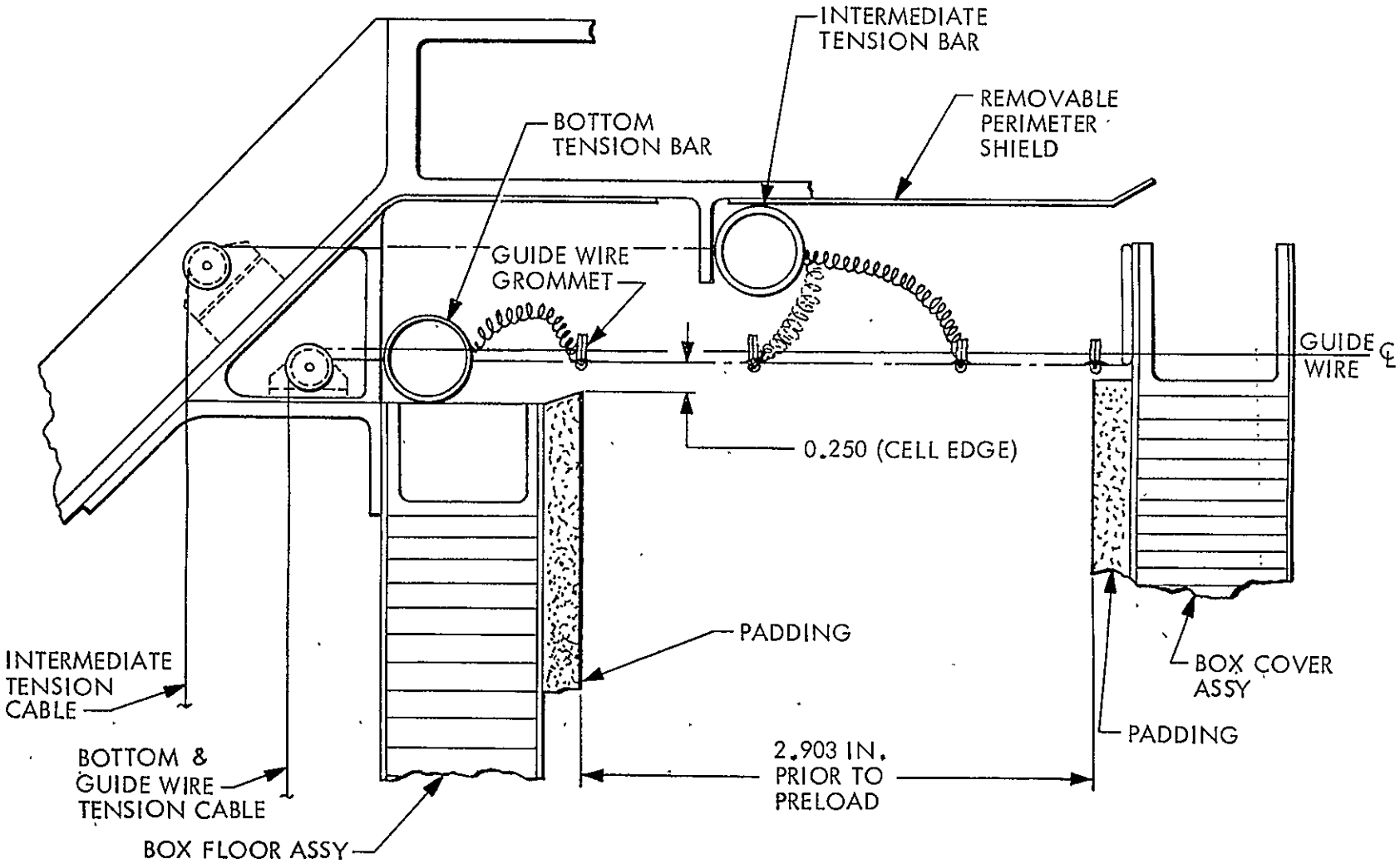

Figure 3-35 Blanket and Tension Bar Stowage

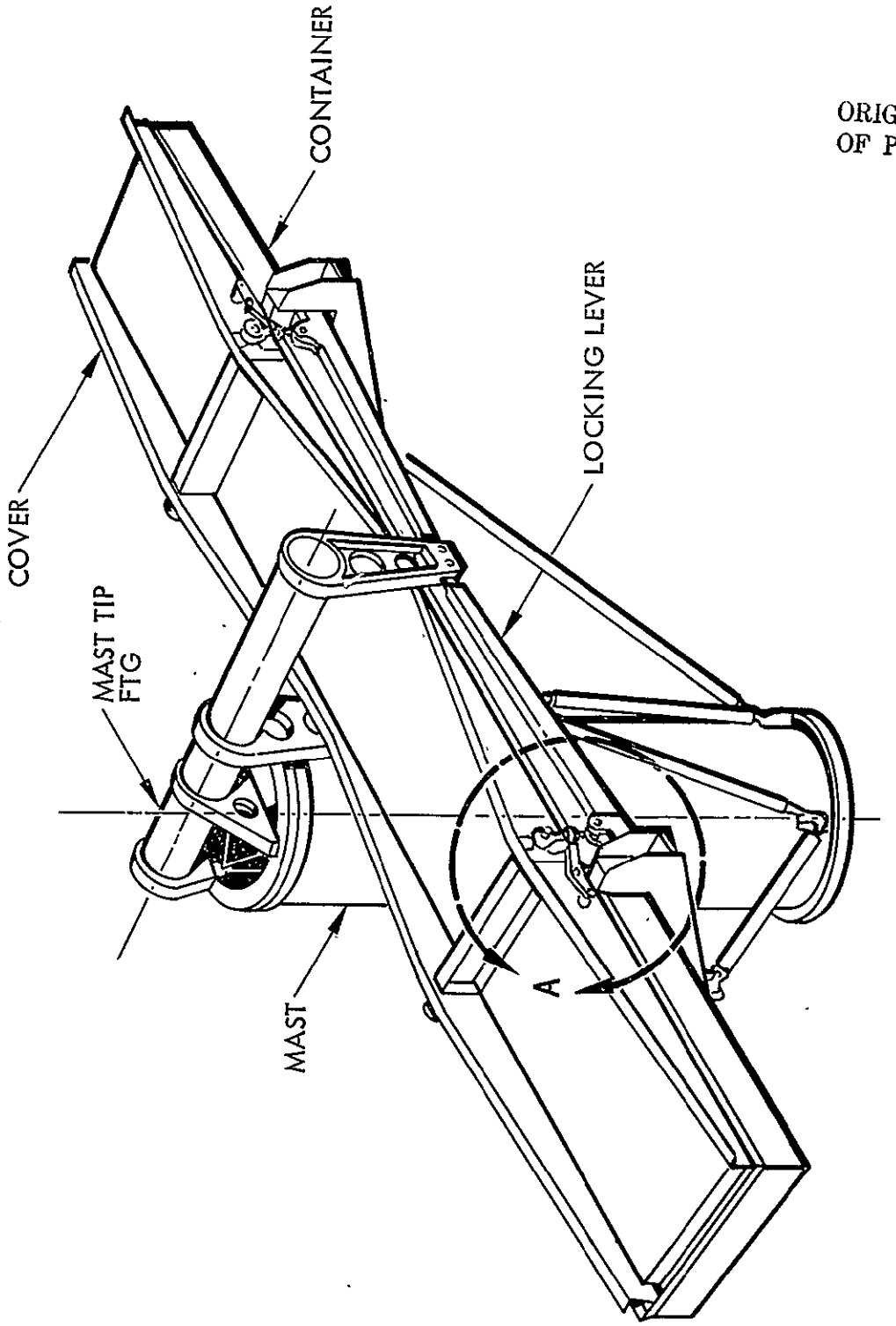

Figure 3-36 Blanket in Stowed Condition

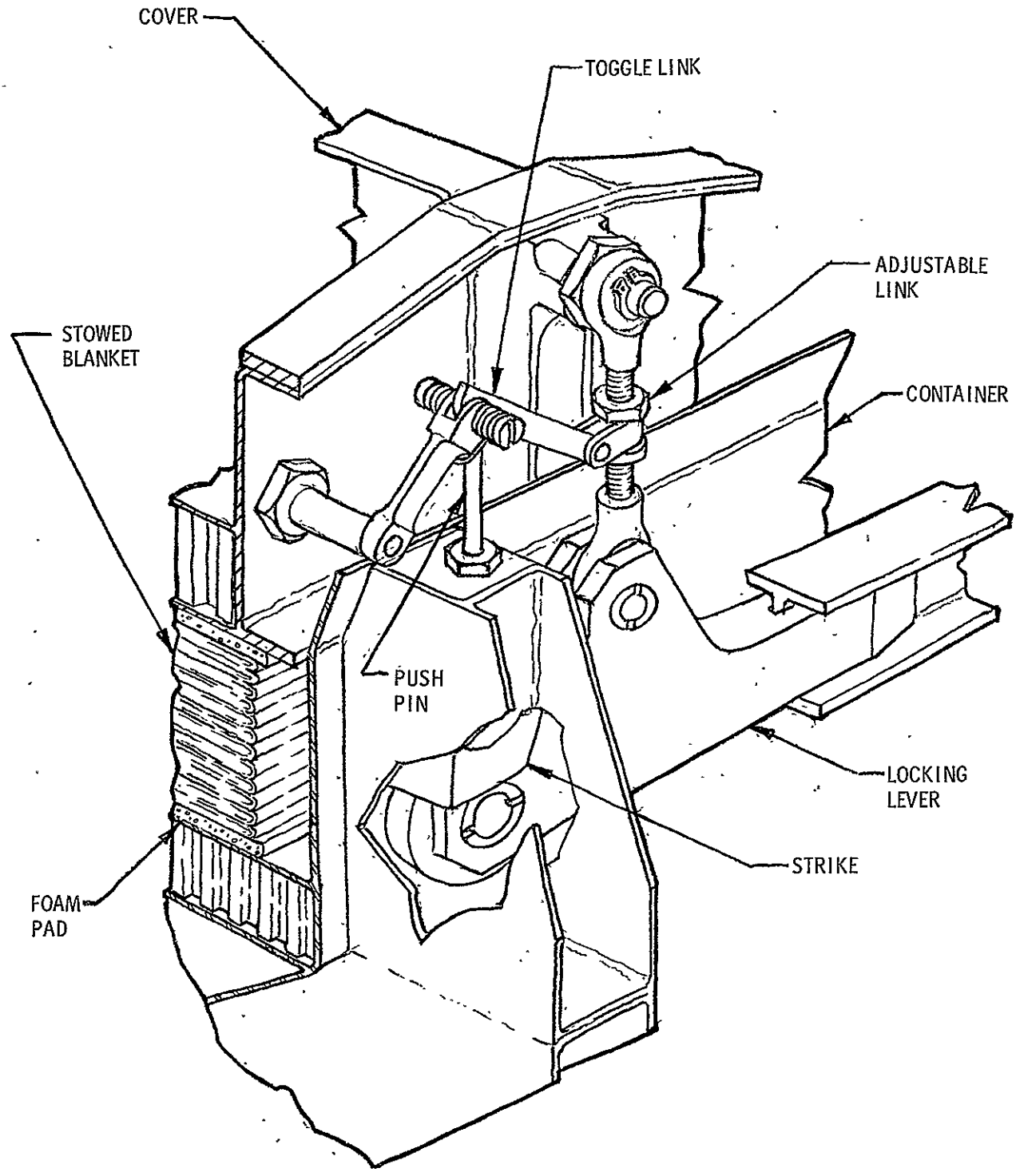

Figure 3-37 Blanket In Stowed Condition, Detail A

The cover, shown in Figure 3-38, is made up of graphite-epoxy channels laminated to that thickness that produces a reasonable balance between stiffness and weight. An aluminum honeycomb core with graphite skins is the cover base for pressure distribution. The blanket side of the cover is faced with 0.5 cm (0.19 in.) thick polyurethane foam covered with Kapton to prevent UV degradation.

The array containment box (Figure 3-39) provides an equal and opposite reaction capability in stiffness to work together with the box cover. It supports the mast and tension mechanisms and interfaces with the spacecraft. The floor of the container is a 2.54 cm (1.00 in.) thick honeycomb panel with graphite skins and aluminum core. The blanket side is faced with polyurethane foam for cell protection with the blanket stowed. The guide wire, intermediate, and full tension mechanisms are mounted on the underside of this honeycomb panel. The central section of the container is triangular with graphite-epoxy skins and formers. The main support fittings are also made of a laminated graphite-epoxy construction.

The perimeter of the honeycomb floor is a shield for large contaminant protection during ground operations with the stowed array wing. One end of the shield is removable for attachment of supports for ground extension of the wing. The shield is also fabricated from graphite-epoxy laminate.

The mast support struts and end fittings are fabricated from graphite-epoxy. They interface with the graphite epoxy container and an aluminum canister with graphite-epoxy gusset fittings.

The mast tip fitting is also fabricated from graphite epoxy laminates. It interfaces at the three mast longeron fittings at the mast tip and the inner locking lever ends.

The array wing-assembly container configuration is shown in Figure 3-40.

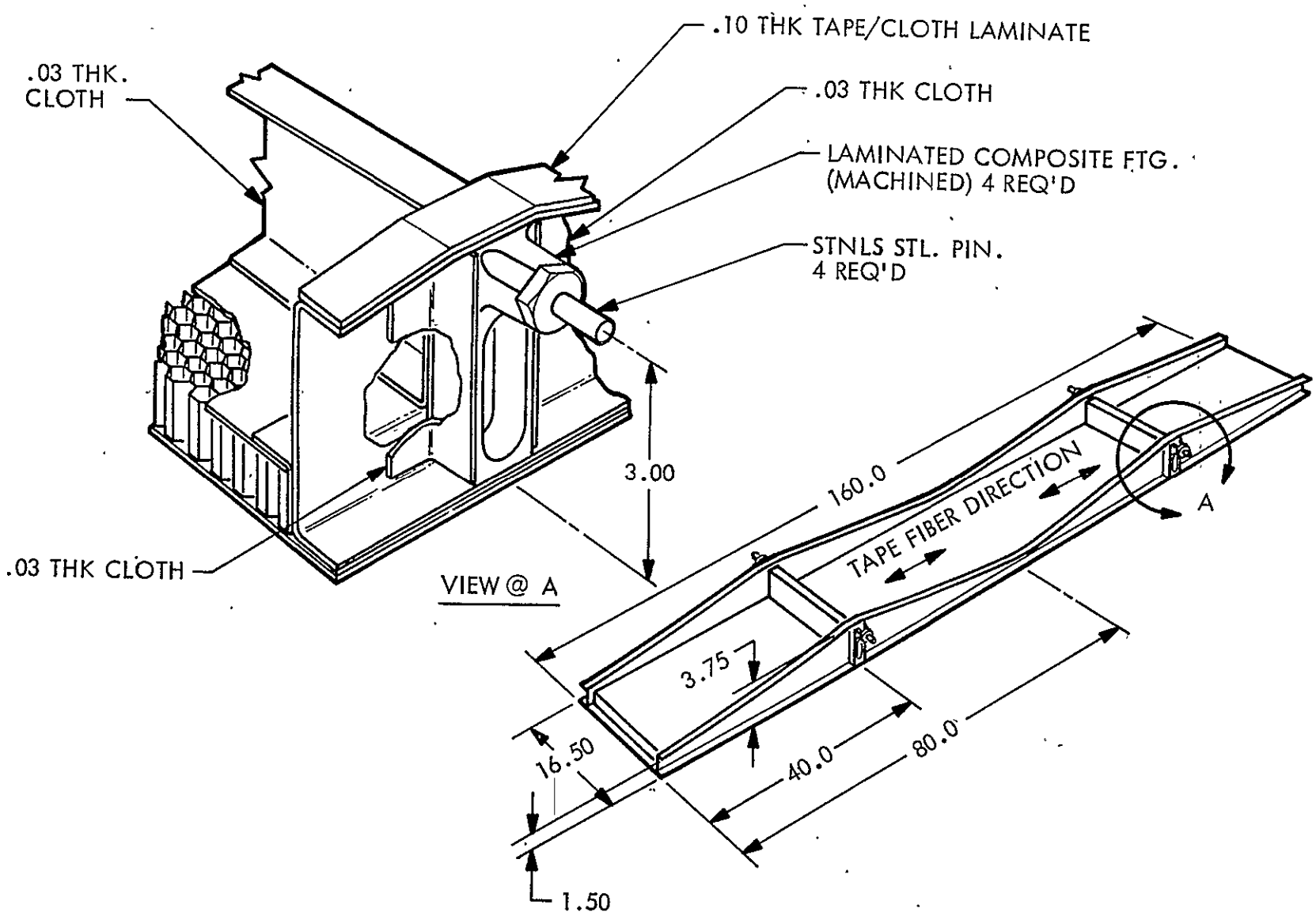

Figure 3-38 Array Box Cover-Graphite Composite

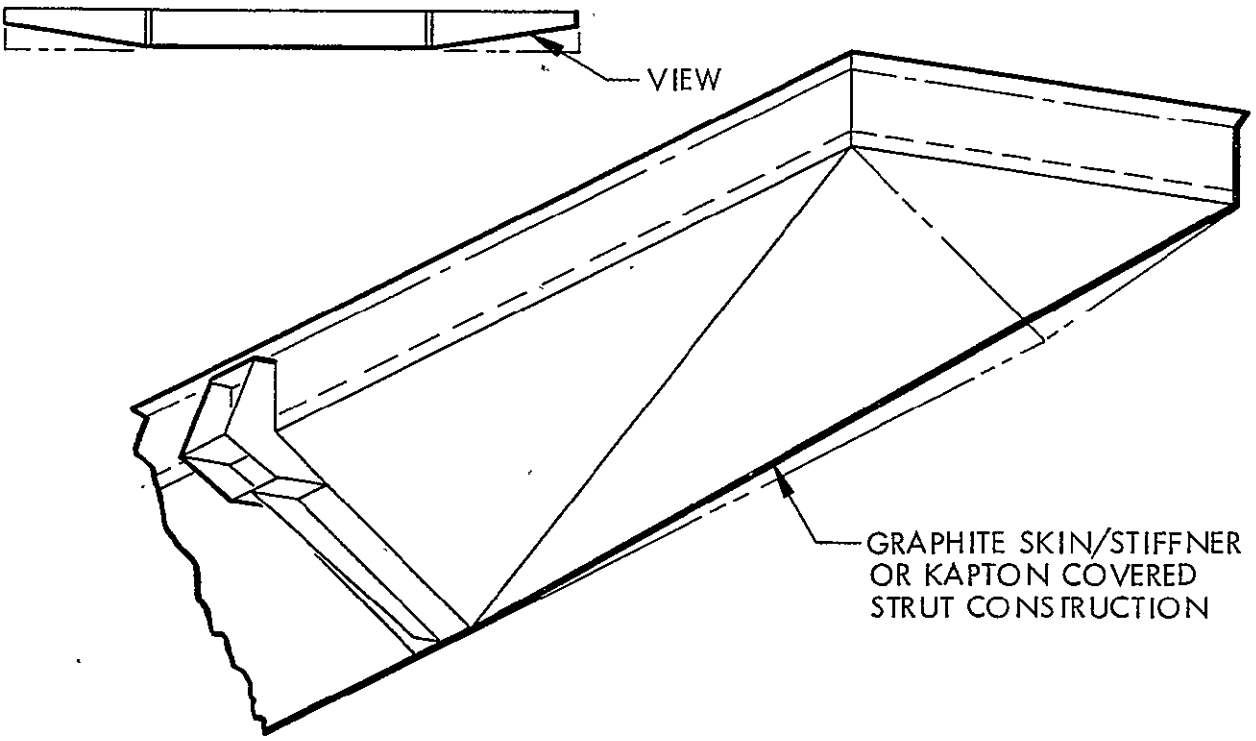

Figure 3-39 Containment Box Configuration

3.3.1.4 Extension Mast. The selection of a continuous coilable longeron mast for the SEP Solar Array was based on its minimum weight for the application. An additional advantage of this mast is the minimization of dead band around zero deflection as compared to a metal articulated lattice structure design. The development of a high temperature polyimide resin system in the coilable longeron and batten material was accomplished by Able Engineering Co., Inc. Mast survival has been greatly enhanced by increasing the mast temperature capability from 93°C (epoxy resin) to 302°C (polyimide resin). The extension mast design developed by Able Engineering Co., Inc. is illustrated in Figure 3-41.

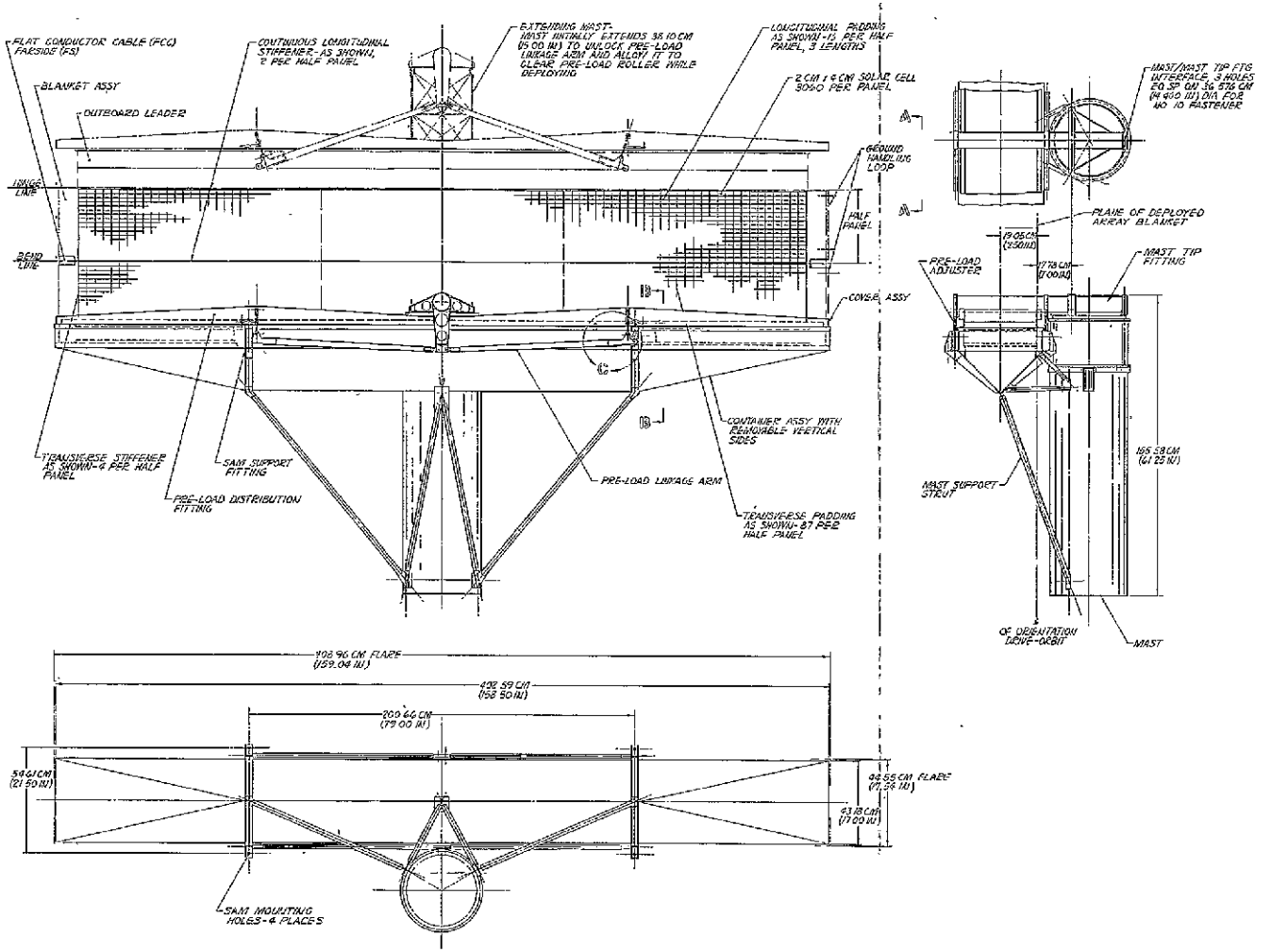

Figure 3-40 SEP Solar Array Wing Assembly Container Configuration

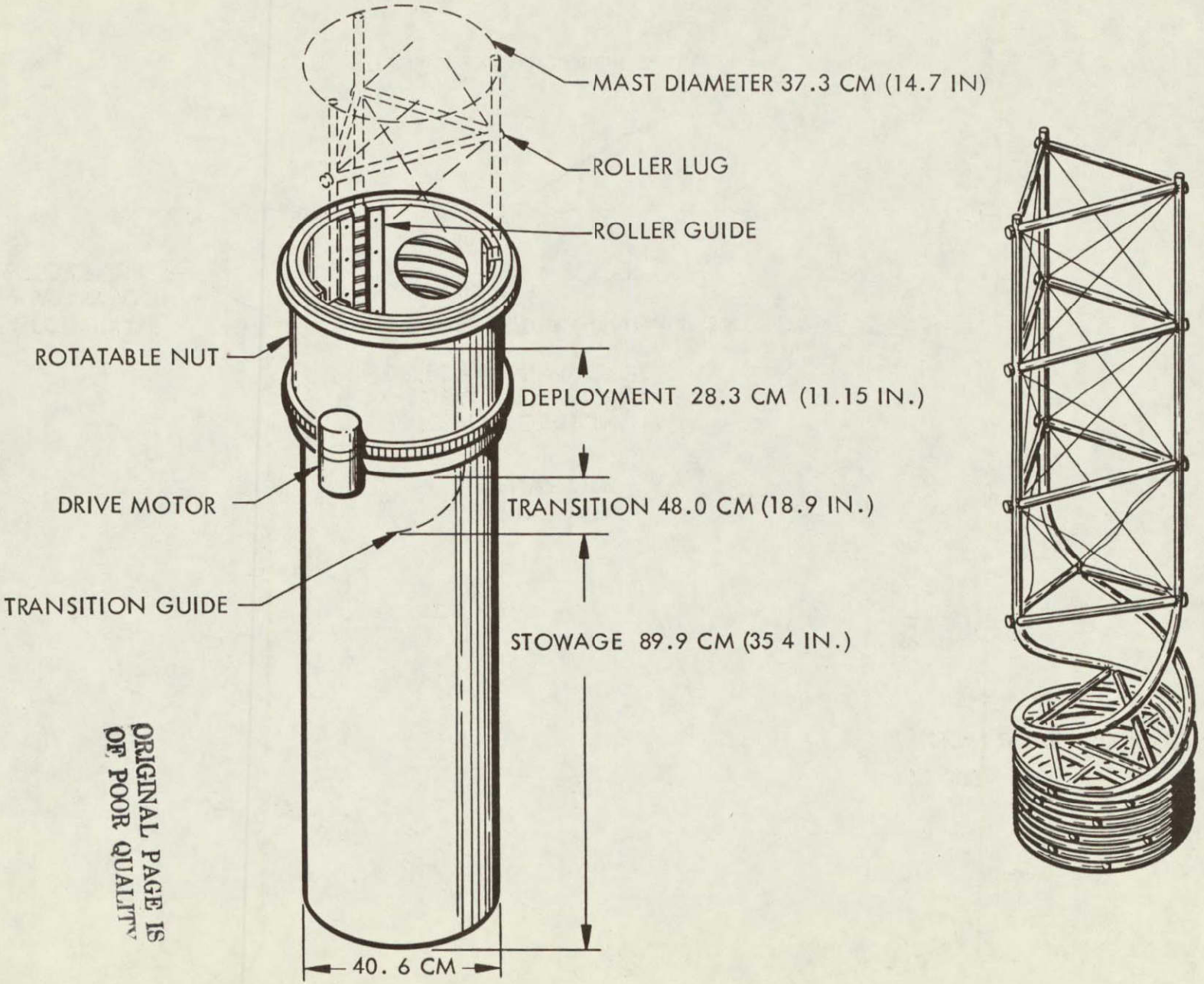

Figure 3-41 SEP Solar Array Extension Mast

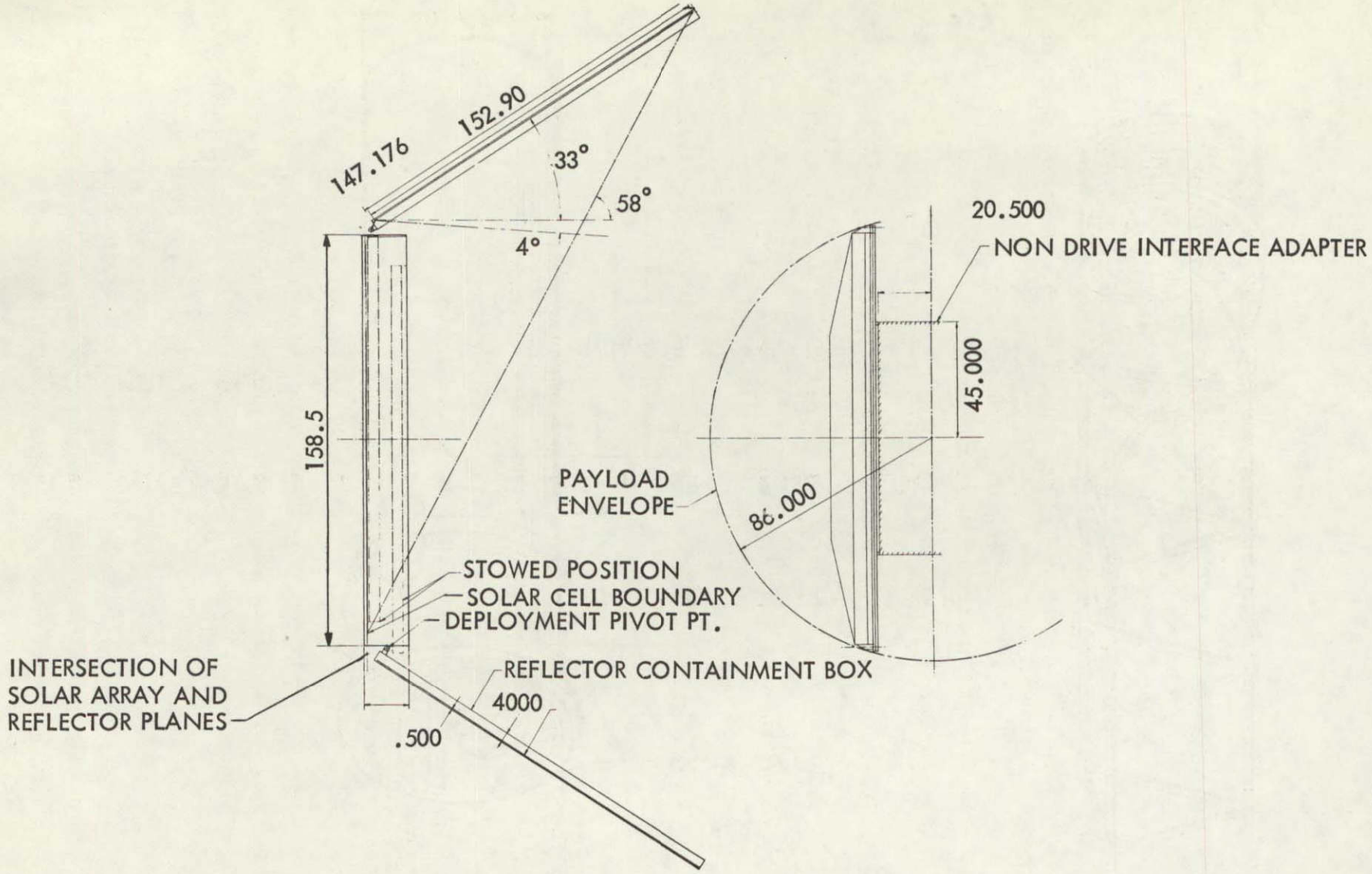

Figure 3-42 Mechanical Design

This procedure resulted in a reflector length of 147.176 inch as shown. The reflector is contained (and deployed) between two sections of a honeycomb beam 4 inches wide by 152.9 inches long. The ends of the reflector are tethered to take a final position 0.5 inch from the edge of these members. Guidewires and splices are on the shaded side of the reflector. Deployment hinge axes locations are chosen to result in symmetrically stowed reflector containers when swung onto the solar array containment box. The stowed locations of the reflector containment boxes do not exactly line up with the edge of array containment box cover. The sunward unit overhanges 2.848 inches and the shadeward unit underhanges 0.529 inches. This variation results from the need to pivot the reflectors from different stowage locations to arrive at symmetrically equal deployed locations. Neither reflector box, when stowed, reaches the full length of the array containment cover. Growth potential is 5.071 inches.

When stowed, the complete system must fit within the confines of Space Shuttle Oribter Cargo Bay. Payload envelopes, including all dynamics, within this vehicle are limited to a cylinder 180 inches in diameter. For purposes of preliminary designs, an arbitrary limit of 172 inches (86.0 inch radius) has been imposed.

The Ion Drive Interface Adapter is represented by a 90 inch by 41 inch cross section. An additional 1.0 inch allowance for array tiedown structure results in the array being located 21.5 inches from cargo bay centerline. The transverse alignment of the stowed array is required by spatial requirements of other elements of the spacecraft both forward and aft of the Interface Adapter. Sufficient space exists between the payload envelope and the stowed concentrated array to install hinges, actuators, and other mechanisms necessary for reflector deployment. Since all SEP preload hardware has been discarded, it is necessary to compress the entire assembly against the Interface Adapter to develop the 1.5 psi stowage pressure on the folded array blanket, and the folded reflector. This pressure is transmitted first to the reflector containment boxes, then through the solar array containment cover to the solar array containment box.

Three concepts for deploying the reflector stowage boxes were examined. In Figure 3-43 the two reflector boxes must be sequentially rotated to position. In Figure 3-44 the boxes are first translated and then rotated to position. An attempt to produce a flat surfaced array cover is shown in Figure 3-45. In this concept, the reflector

ORIGINAL PAGE IS
OF POOR QUALITY

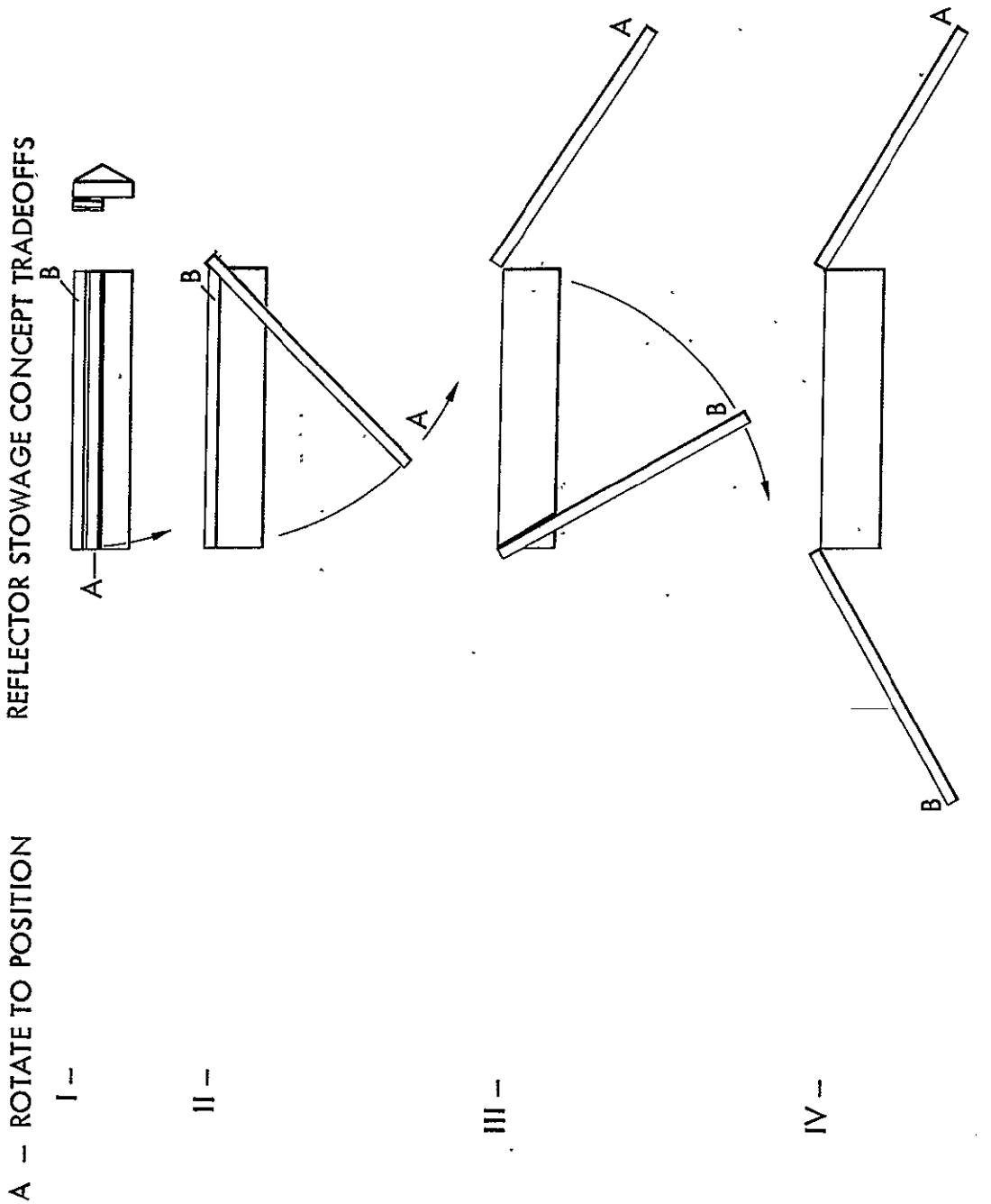

Figure 3-43 Reflector Stowage Concept Tradeoffs - Option A

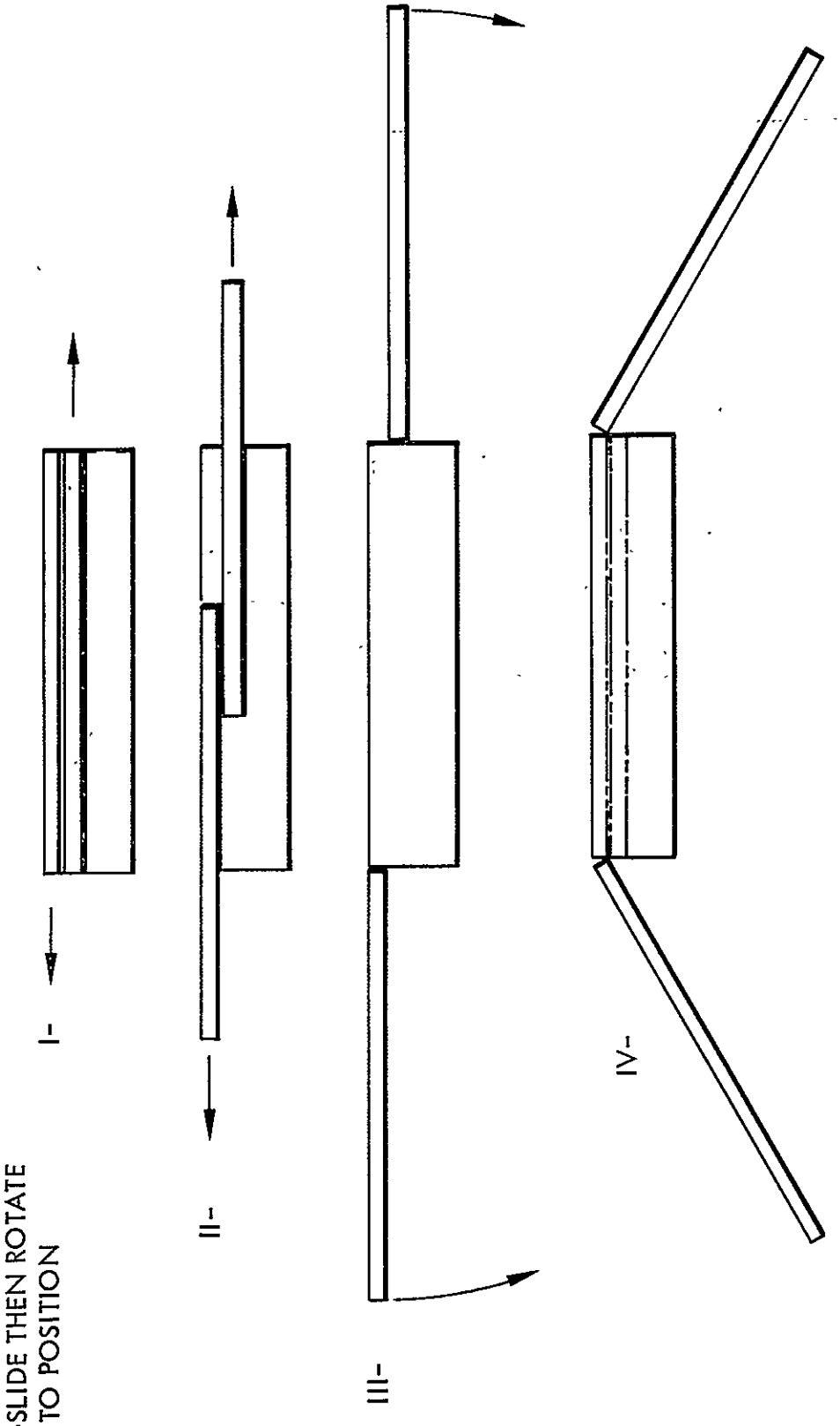

Figure 3-44 Reflector Stowage Concept Tradeoffs - Option B

ORIGINAL PAGE IS
OF POOR QUALITY

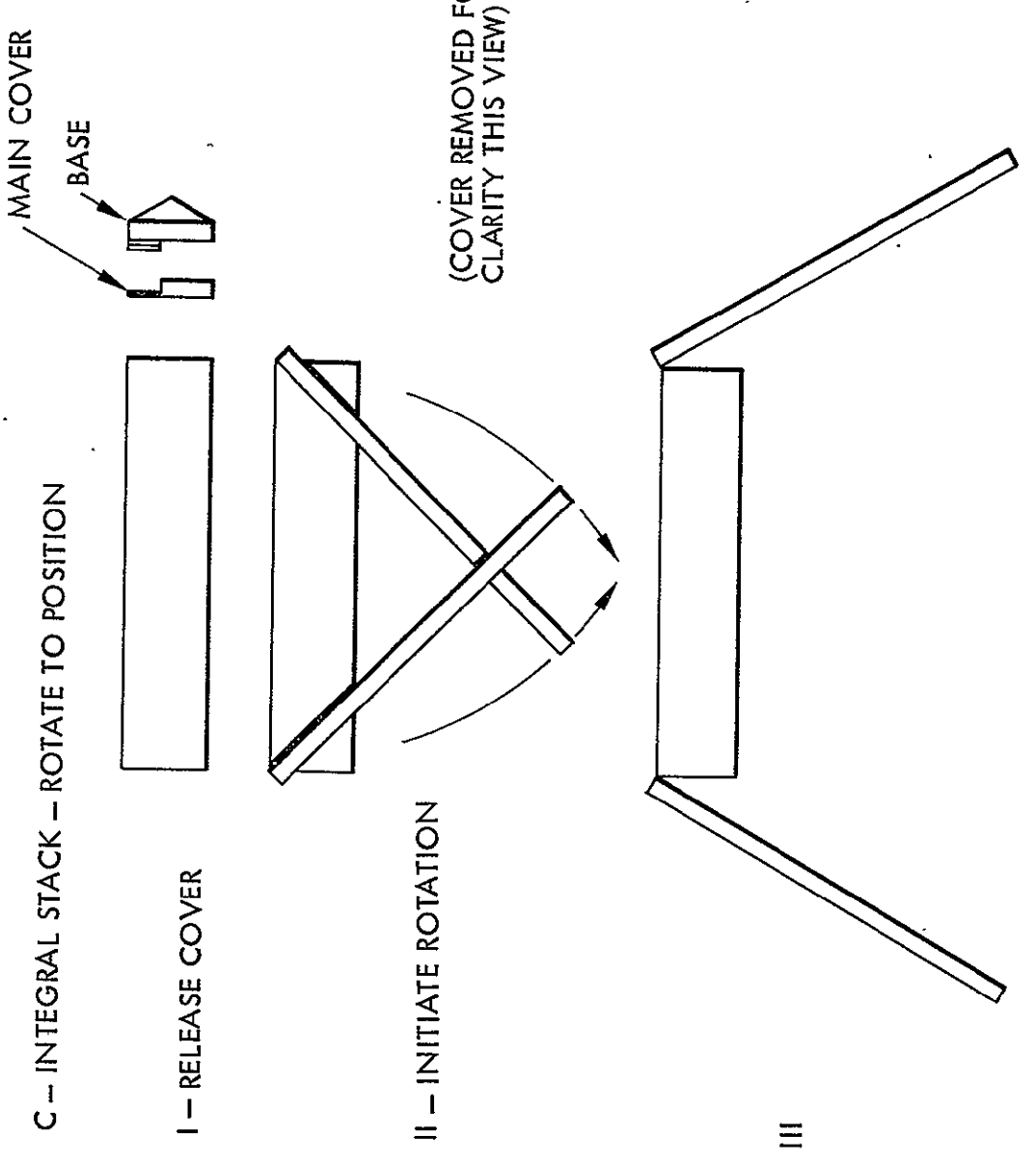

Figure 3-45 Reflector Stowage Concept Tradeoffs - Option C

containment boxes are integrated into a notch in the array cover. The first concept was chosen to be developed by this design.

Details of the reflector hinges are shown in Figure 3-46.

Rotation, or swing out, of the reflector containment boxes is accomplished by action of a combination spring actuator and viscous damper. An externally adjustable orifice on the damper permits fine tuning of rotation rate. One actuator is required for each reflector and is mechanized to drive the inboard half of the reflector stowage box. Synchronism of the inboard and outboard halves of the reflector containment boxes during swing out is provided by tapered indexing pins. These pins disengage during the first events of reflector deployment.

Due to the variation in hinge axis location, and reflector stowed locations, each hinge set is different. The sunward reflector containment, shown in Figure 3-46, is supported from the overhanging section on the bottom (inboard half), and the side (outboard half). Offset structure built into the moving halves of these hinge sets transfer loads to the stationary halves via quadruple shear of a 0.25 inch diameter hinge pin. Dry film lubricants are used throughout the reflector system to minimize frictional loads.

Rotation is stopped and locked by an over center 4 bar linkage set in each hinge. These links are nested within the hinges before rotation commences. At the limit of rotation, they are taut, and slightly overcenter providing firm and accurate control of final rotational position. An adjustment in the linkage mounting provides fine tune capability of reflector angle during assembly procedures. The outboard half of the reflector containment box which must deploy with the array cover, is affixed to the edge of the cover. The other half of the reflector containment box is affixed to the array containment box end. Whenever possible, items which could be located on either the outboard or inboard halves of the reflector containment boxes were selected to be located inboard. This helped to minimize tip mass and consequently increase array natural frequency. Following this philosophy, the reflector guidewire mechanisms were installed in the array containment box in the same manner as array guidewire mechanisms. As mentioned earlier, the array intermediate tensioning system was discarded. In its place, and elsewhere on the honeycomb panel are located

ORIGINAL PAGE IS
OF POOR QUALITY

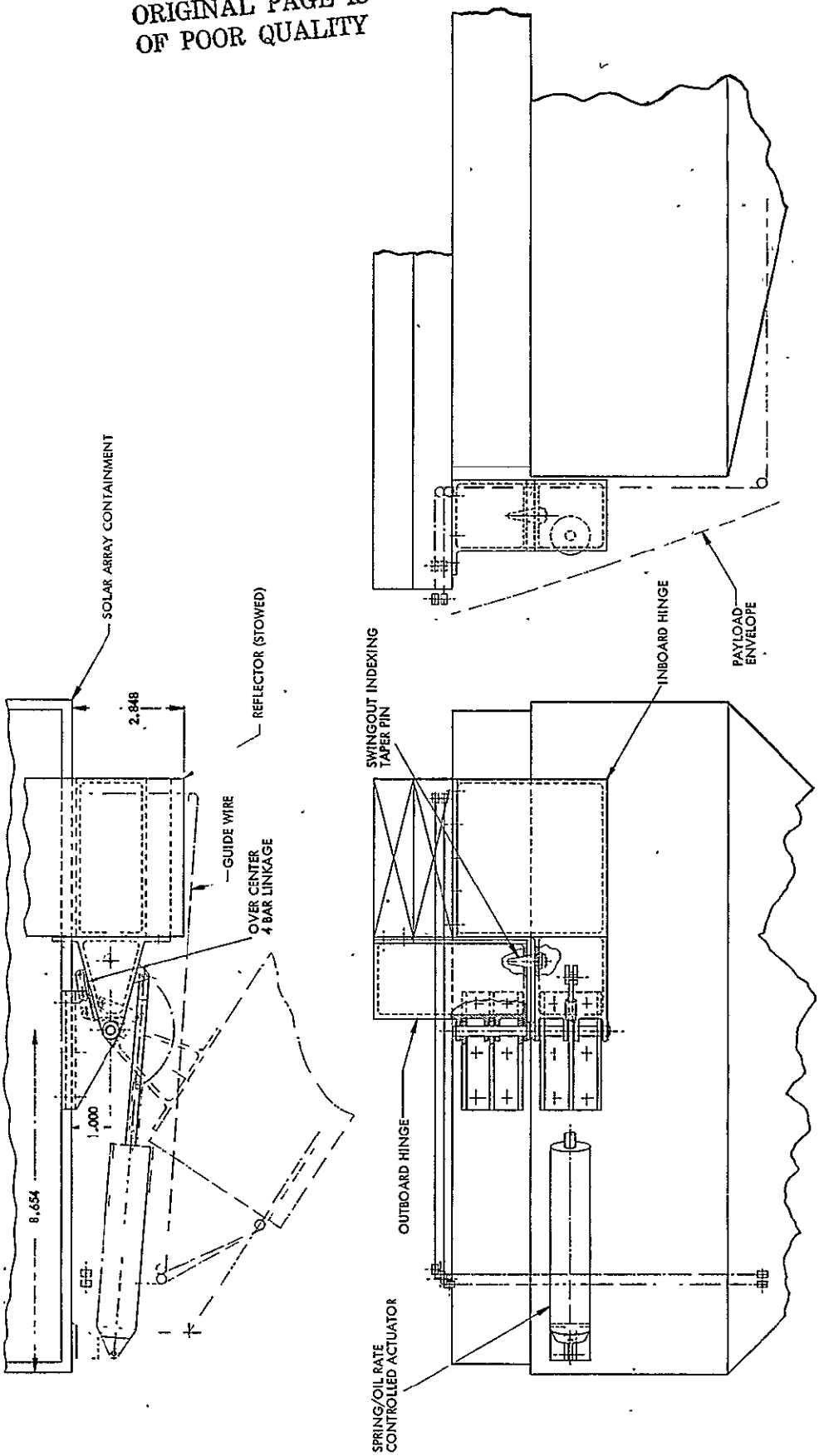

Figure 3-46 Sunward Reflector Joint Detail

the four new guidewire mechanisms engendered by the reflector additions. Two guidewires are directed out of each end of the array containment box. The wires are threaded through a series of pulleys to route them around the hinge axis and into the inboard half of the reflector containment box. The routing within the containment box will be discussed below. The guidewire tension is arbitrarily set at 1 lb each. This tension provides assistance to the actuator during swing out. The shortening of the guidewire is taken up by the storage reel.

The linkage on the shadeward stowed reflector box, shown in Figure 3-47, is similar in function to that of the sunward reflector. It differs only in that the interface between hinge and box is on the box end rather than side or base as described earlier. The other major difference is in the arrangement of the actuator. In this case, the actuator is located below the hinges and provides rotation counter-directional to the sunward assembly. The rotational stops, guide wire routing, indexing taper pins, and hinge arrangements are all functionally similar to the sunward reflector. However, the unique geometry produced completely different moving hinge designs.

Figure 3-48 shows the details of the reflector blanket. The blanket is composed of 17 full panels, and one short panel spliced in 17 places. Total length of the reflector is 815 inches with the ends being trimmed at a slight angle to compensate for the deflection of the reflector stowage box halves. Each panel is 47 inches long by 147.176 inches wide by 0.0003 inch thick constructed from a 48 inch width roll of aluminized Kapton. The material is produced by numerous vendors to commercial specifications.

The splices are shown in section D-D and incorporate a stiffening member 0.012 inch by 0.5 inch. These stiffeners contribute to the absence of reflector edge curl.

The edges of each panel are reinforced by folding back 0.5 inch of the material and bonding to itself with dry film adhesive as shown in section C-C. This procedure precludes edge tears from propagating from micro-irregularities in edge shearing. The ends are reinforced as shown in section B-B by inclusion of a 0.012 inch stiffeners in a 0.5 inch fold back of reflector material. The outboard end is

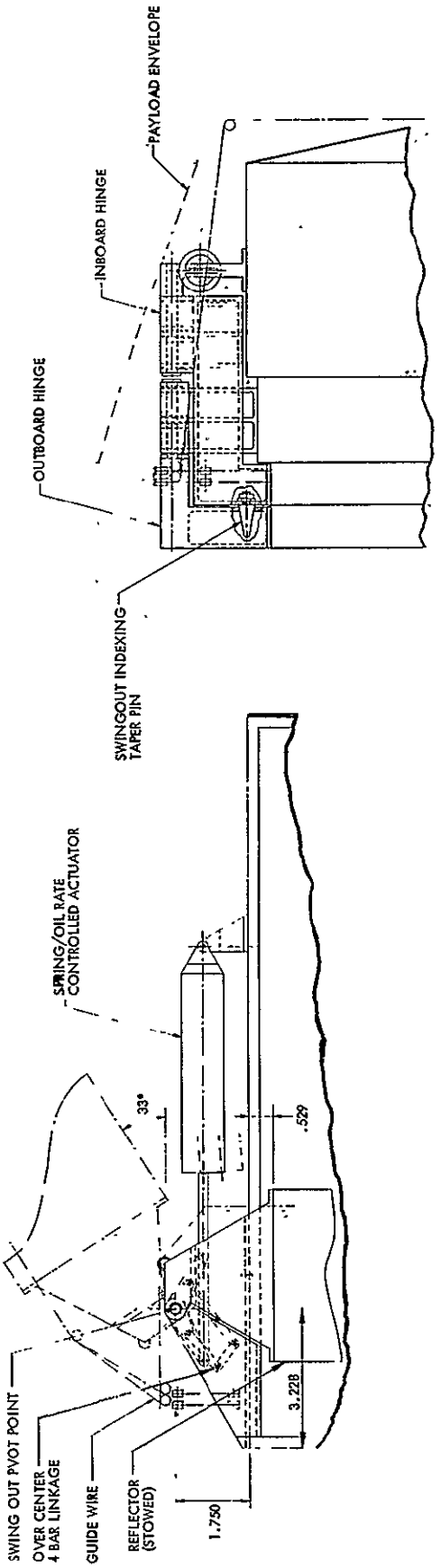

ORIGINAL PAGE IS
OF POOR QUALITY

Figure 3-47 Shadeward Reflector Joint Detail

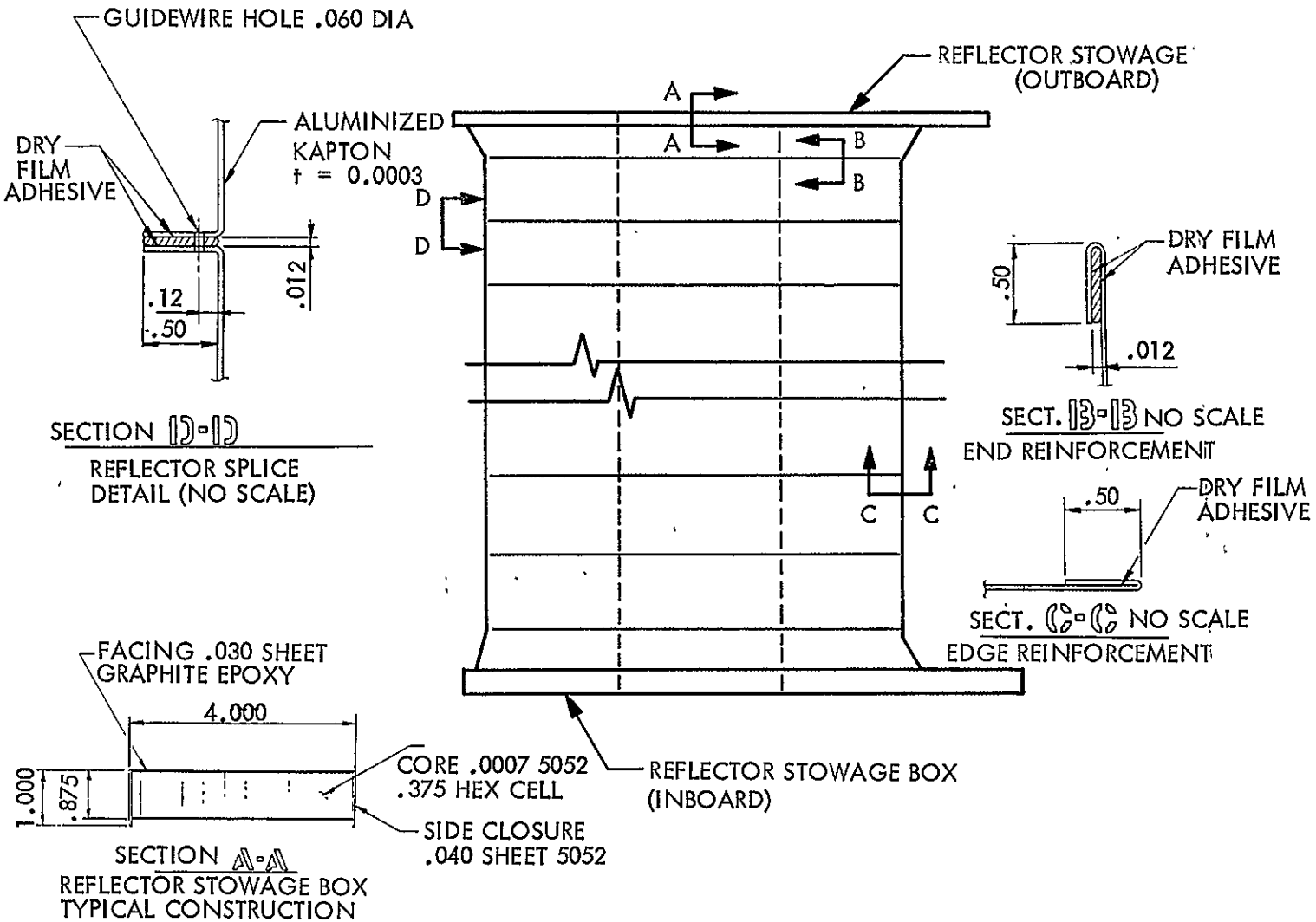

Figure 3-48 Reflector System Detail

C-2

tethered with fixed length tethers cut to maintain the 30° off angle tension relationship after stowage box deflection has occurred. Guidewires are fastened to this same box and pass through holes in the splices providing control over the blanket as it is being deployed. As previously mentioned, the guidewires are fed from storage reels located in the array containment box and routed around the hinge area by a system of pulleys. The inboard reflector end is tensioned by tethers directed 30° off angle and connected to a full deployment blanket tensioning mechanism located in the inboard reflector containment box tip.

This device is shown in Figure 3-49. The tensioning cables are routed to two separate cable reels. Connected to, and sharing the same mounting post is the negator output drum. Feeding the negator spring material to it is a negator take up drum. The capacity of the tensioning system as well as the guide wire and other systems permits the fully deployed array and reflector to be moved outboard at least one meter to fine tune spacecraft center of pressure.

The folded reflector has 244 folds and is 147.176 inches long by 3.857 inches wide when folded. Each panel is folded 14 times between splices. Due to the increased thickness of edges, ends, and splices, the folded reflector thickness varies. A sculptured resilient pad covered with Kapton, accommodates the thickness variation while developing the required 1.5 psi packing pressure. Cable routing and pulley installations are located in the inboard stowage box directly under the tethers and guidewires. A root hinge attach insert provides a universal fitting for interfacing the various hinge attachments whether it be from end, side, or base. An alternate design involves placement of one full deployment cable tensioning mechanism in the outboard and one tensioning mechanism in the inboard halves of the reflector containment box. The fixed tethers would be changed to accommodate this alternative. The benefit of this alternate would be twofold. First, the box length could be reduced 1.5 inches from 152.9 to 151.4 inch. Second, the box halves could then be made identically, reducing the part count by a factor of 2.

The stowed CESA solar array module is shown in Figure 3-50. The similarity to SEP is clearly indiciated. The same array containment to mast canister arrangement is retained. The containment cover is different with the upper surface being completely

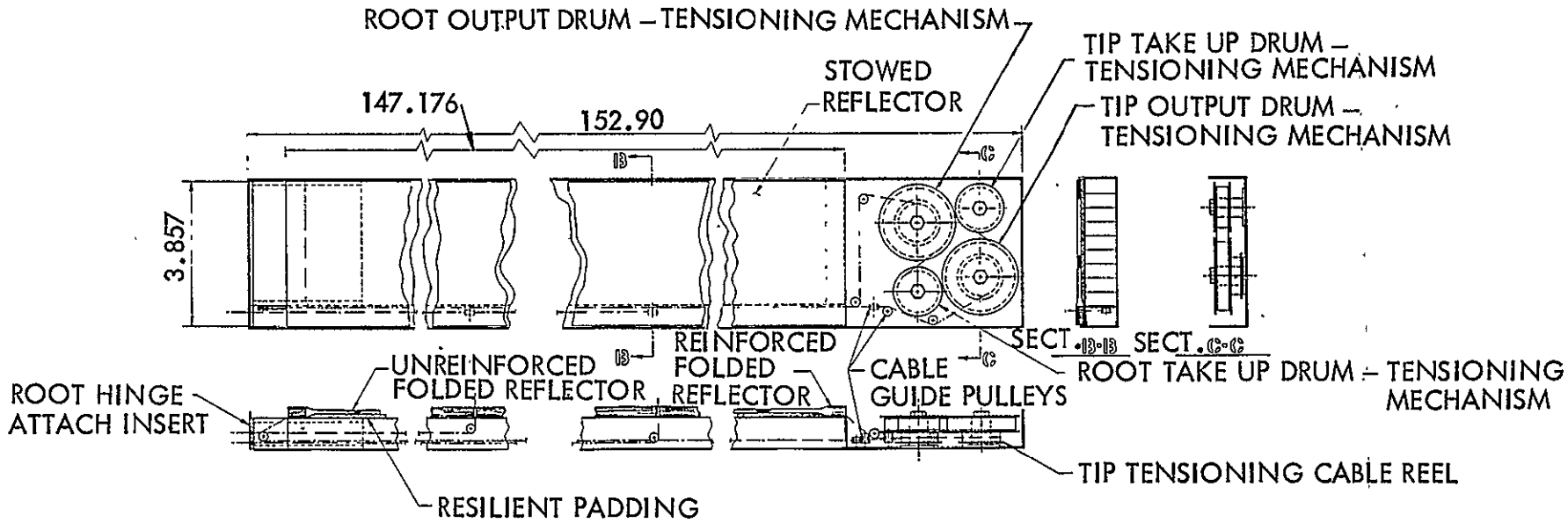

Figure 3-49 Detail - Inboard Reflector Stowage Box

ORIGINAL PAGE IS
OF POOR QUALITY

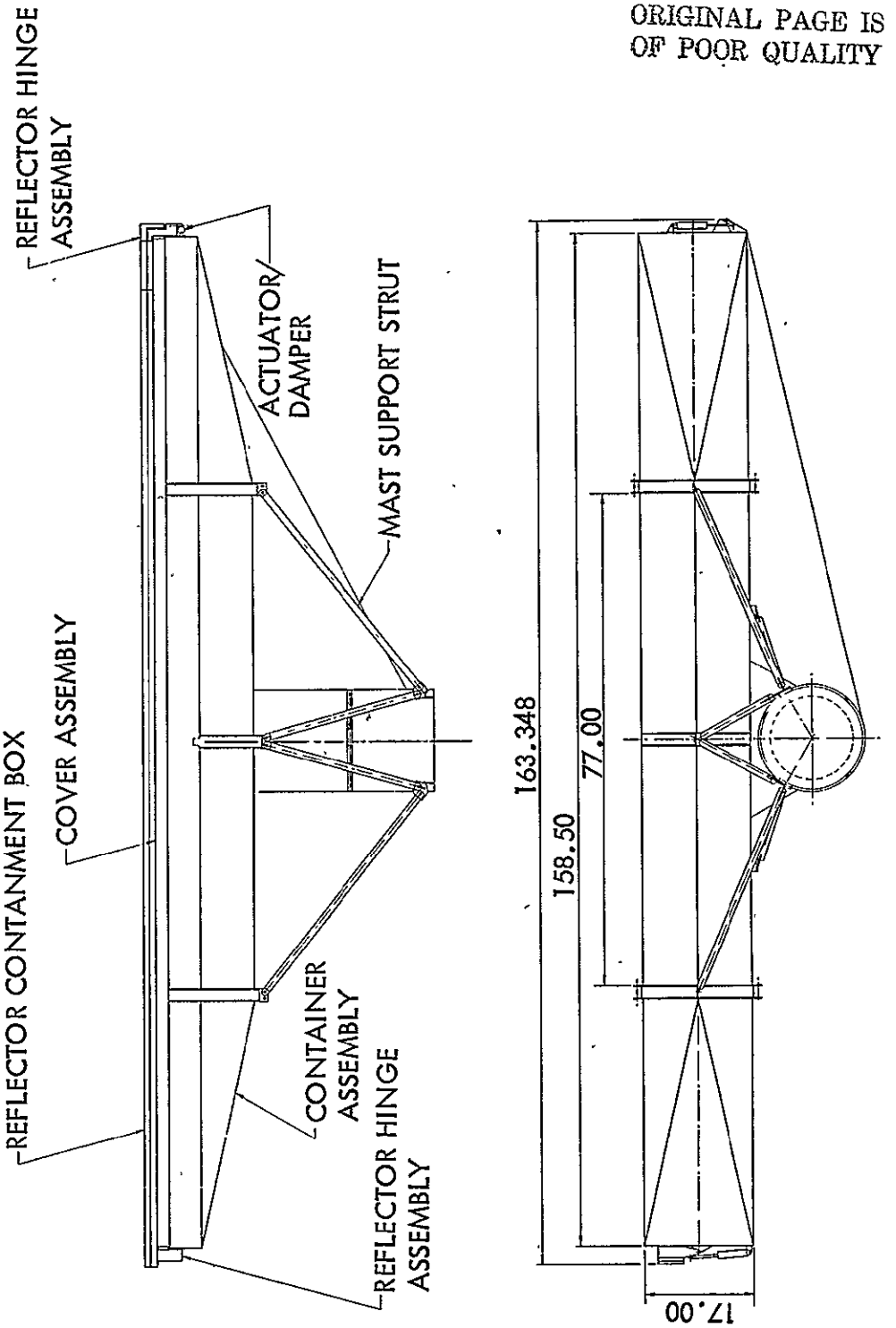

Figure 3-50 Stowed CESA Solar Array Module

flat. An extension of the cover to the side provides the structural connection to the mast tip. The preload mechanism and strikes are removed and launch preload of both solar array blanket and reflector blankets is provided by compressing the module against the Interface Adapter and retaining this compression until hold downs are released.

The mast counterbalance system is shown stowed in the top view in Figure 3-51. It consists of a two piece telescoping tube assembly held in the stowed position by a bumper bearing against the shadeward stowed reflector box.

A spring driven actuator/damper, similar to those of the reflector system, rotates the counterbalance 90° to a position directly away from the sun. An over-center 4 bar linkage controls ultimate position, similar to the reflector mechanisms. The inner telescoping member is extended by an internal spring. Near the root of the counterbalance a tensioning mechanism is installed. This mechanism is designed to produce the ultimate tension and to provide for 1 meter excursions for C.P. adjustment as mentioned earlier.

The tension cable from this mechanism is led through ferrules mounted on the counterbalance over a pulley at the tip. When swung out, the cable is in alignment from the ultimate tensioning mechanism to the tip pulley. The tension cable is directed to the base of the mast canister where it is wound on a negator powered cable storage reel similar to a guidewire mechanism. The tension produced by this mechanism is 1 lb. As the array is deployed, cable pays off the storage reel until a predetermined stop is encountered. From this point on, the full tension mechanism comes in effect and counter balances the full tension couples created in the reflector and solar array blankets.

A detailed mass summary of the CESA solar array module is presented in Table 3-8.

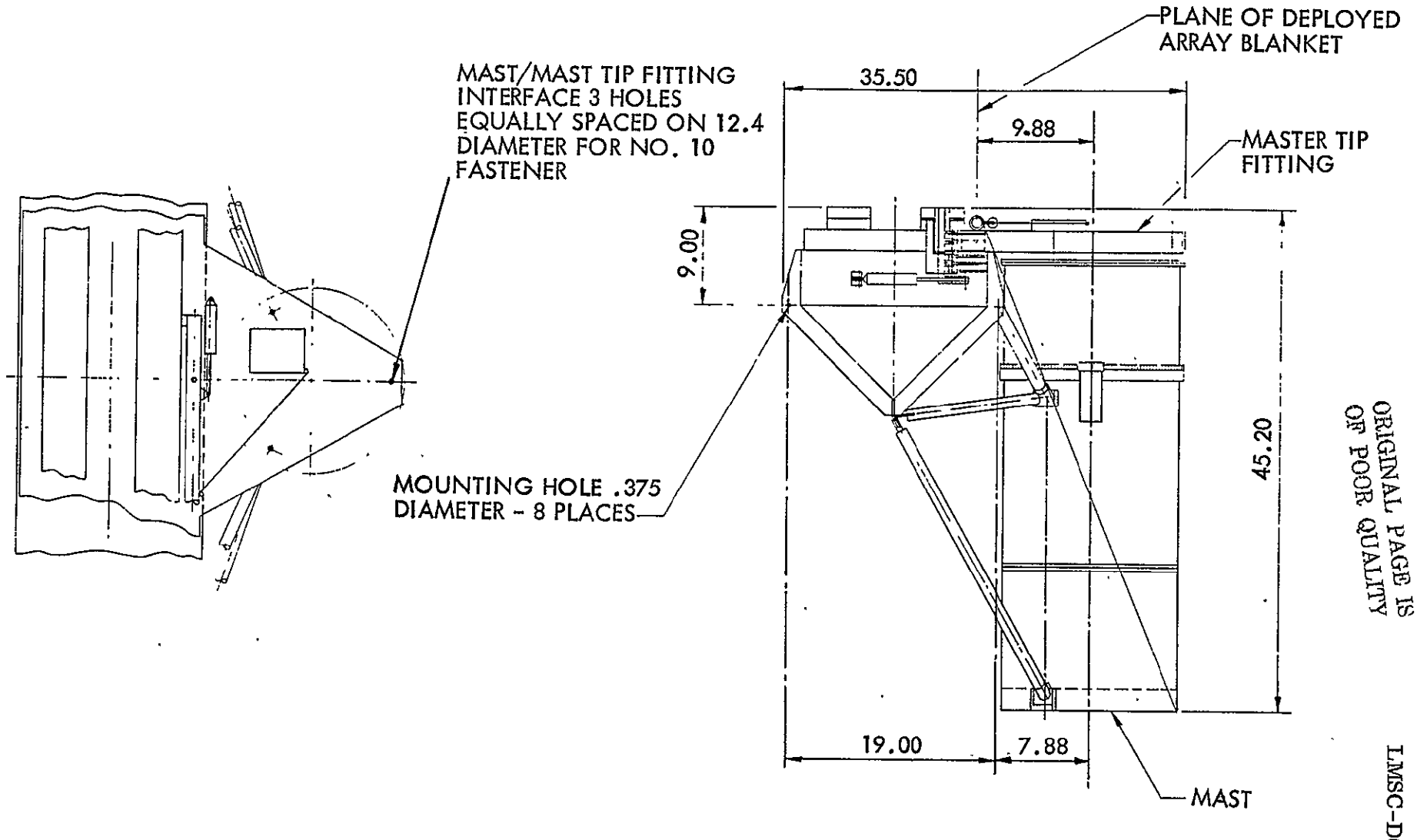

Figure 3-51 Stowed Mast Counterbalance System

TABLE 3-8
DETAILED CESA MASS SUMMARY

Item No., Description, & Estimated Mass (kg)			Contingency Factor	Contingent Mass (kg)	Remarks
	Total Module (one wing of 27 panels)			153.46	
1.0	Mast (1)	23.164	1.15	26.64	
1.1	Canister (1)	11.034			
1.2	Mast Element 23.95 m (943 in.) (1)	9.860			R = 6.2"
1.3	Mast Balancing System	2.270			
2.0	Array Guidewire Mechanism (2)	1.327	1.15	1.53	
2.1	Wire 22.28 m (877.06 in.) (2)	0.048			
2.2	Negator (4)	0.641			
2.3	Wire Reel (2)	0.222			
2.4	Negator Hub (2)	0.132			
2.5	Negator Reel (2)	0.106			
2.6	Shaft (6)	0.156			
2.7	Washers	0.014			
2.8	Panel/Wire Retainer (56)	0.008			
3.0	Reflector Guidewire Mechanism (4)	2.478	1.15	2.85	
3.1	Wire 23.04 m (907.06 in.) (4)	0.099			
3.2	Negator	1.327			
3.3	Wire Reel (4)	0.444			
3.4	Negator Hub (4)	0.264			
3.5	Negator Reel (8)	0.212			
3.6	Shaft (12)	0.104			
3.7	Washers	0.028			
4.0	Full Tension Mechanism (2)	0.650	1.15	0.75	
4.1	Wire 1 m (2)	0.002			
4.2	Negator (8)	0.278			
4.3	Wire Reel (2)	0.026			
4.4	Negator Hub (2)	0.090			
4.5	Negator Reel (8)	0.148			
4.6	Shaft (10)	0.096			
4.7	Washers	0.010			
5.0	Tension Transfer (8)	0.024	1.20	0.03	
5.1	Pulleys (8)	0.004			
5.2	Brackets (8)	0.016			
5.3	Pins (8)	0.004			

TABLE 3-8
DETAILED CESA MASS SUMMARY (Cont)

Item No., Description, & Estimated Mass (kg)				Contingency Factor	Contingent Mass (kg)	Remarks
6.0	Cover Assembly (1)		6.373	1.15	7.33	
6.1	Skin (2)	3.385				Graphite/ Epoxy
6.2	Core (1)	1.507				
6.3	Sides	0.671				
6.4	Adhesive	0.470				
6.5	Pad (1)	0.130				
6.6	Adhesive	0.210				
7.0	Container		11.060	1.15	12.72	
7.1	Honeycomb Panel	3.760				
7.1.1	Skin (2)	1.800				
7.1.2	Core (1)	0.630				
7.1.3	Edging	0.440				
7.1.4	Inserts	0.450				
7.1.5	Adhesive	0.440				
7.2	Triangular Beam	6.230				
7.2.1	Skin (2)	2.660				
7.2.2	Bulkhead (2)	0.330				
7.2.3	Longeron (3)	1.000				
7.2.4	Support Fitting (4)	0.300				
7.2.5	Perimeter Shield (1)	1.130				
7.2.6	Pad (1)	0.350				
7.2.7	Adhesive	0.460				
7.3	Support Struts	1.070				
7.3.1	Long (2)	0.500				
7.3.2	Medium (2)	0.410				
7.3.3	Short (2)	0.160				
8.0	Solar Cell Blanket (1)		75.046	1.04	78.05	
8.1	Upper Leader (1)	0.140				
8.2	Upper Attach Bar (1)	0.160				
8.3	Bottom Tension Distr Bar (1)	0.650				
8.4	Lower Leader (1)	0.170				
8.5	Panel (27)	73.926				
8.5.1	Substrate w/Pad & Stiffening (27)	14.337				
8.5.2	Solar Cells (3060 x 27)	31.617				
8.5.3	Cover Adhesive (3060 x 27)	3.510				
8.5.4	Coverslide (3060 x 27)	22.815				

TABLE 3-8
DETAILED CESA MASS SUMMARY (Cont)

Item No., Description, & Estimated Mass (kg)					Contingency Factor	Contingent Mass (kg)	Remarks
8.5.5	Hinge (2 x 27)		1.566				
8.5.6	Hinge Pin (27)		0.081				
9.0	Interconnect Harness			3.808	1.05	4.00	
9.1	Flat Conductor Cable (Power)			3.438			
9.2	Flat Conductor Cable (Instr)			0.250			
9.3	Receptacles (4)			0.120			
10.0	Misc Nuts & Bolts			0.900	1.10	0.99	
11.0	Reflector Assy (KJ008) (2)			12.066	1.10	13.27	
11.1	Inboard Reflector Storage Box (2)		5.058				
11.1.1	Facings (2)	2.220					
11.1.2	Sides (2)	1.230					
11.1.3	Core (2)	0.244					
11.1.4	Liner (2)	0.450					
11.1.5	Adhesive (2)	0.260					
11.1.6	Root Hinge Attach Insert (2)	0.250					
11.1.7	Pad (2)	0.040					
11.1.8	Tensioning Mechanism (4)	0.350					
11.1.8.1	Cable Reel (4)	0.016					
11.1.8.2	Output Drum (4)	0.118					
11.1.8.3	Takeup Drum (4)	0.038					
11.1.8.4	Post (4)	0.086					
11.1.8.5	Guide Pulley/Brkt (12)	0.014					
11.1.8.6	Cable 6.3 m (4)	0.014					
11.1.8.7	Negator (4)	0.064					

TABLE 3-8
DETAILED CESA MASS SUMMARY (Cont)

Item No., Description, & Estimated Mass (kg)				Contingency Factor	Contingent Mass (kg)	Remarks
11.1.9	Guidewire Parts in 11.1	0.014				
11.1.9.1	Cable 4.1 m (2)	0.008				
11.1.9.2	Guide Pulley/ Brkt (4)	0.006				
11.2	Outboard Reflector Storage Box (2)		4.200			
11.2.1	Facings (4)	2.220				
11.2.2	Sides (2)	1.126				
11.2.3	Core (2)	0.264				
11.2.4	Adhesive (2)	0.268				
11.2.5	Root Hinge Attach Insert (2)	0.282				
11.2.6	Pad (2)	0.040				
11.3	Reflector (2)		2.808			
11.3.1	Aluminized Kapton 0.3 mil (2)	1.710				
11.3.2	Stiffeners (36)	0.866				
11.3.3	Adhesive	0.232				
12.0	Reflector Attachments			1.646	1.15	1.89
12.1	Outboard Sunward Hinge, Moving (1)		0.146			
12.2	Inboard Sunward Hinge, Moving (1)		0.379			
12.3	Sunward Hinge, Fixed (2)		0.098			
12.4	Indexing Tapes Pin (2)		0.013			
12.5	Pivot Pins (4)		0.054			
12.6	Actuator (2)		0.043			
12.7	Actuator Clevis (2)		0.004			
12.8	Guidewire Pulleys/ Brkts (14)		0.016			
12.9	Guidewire		0.003			
12.10	Over Center Linkage Set (4)		0.058			
12.11	Outboard Shadeward Hinge, Moving (1)		0.179			

TABLE 3-8
DETAILED CESA MASS SUMMARY (Cont)

Item No., Description, & Estimated Mass (kg)				Contingency Factor	Contingent Mass (kg)	Remarks
12.12	Inboard Shadeward Hinge, Moving (1)	0.177				
12.13	Shadeward Hinge, Fixed (2)	0.116				
13.0	Deployment Mechanism (1)		3.100	1.10	3.41	
13.1	Pin Puller (4)	0.640				
13.2	Trunnion (1)	0.920				
13.3	Actuator (1)	1.540				

Figure 3-52 a shows the spacecraft configuration after ejection from Space Shuttle until such time as IUS first stage is separated. The solar array modules are tucked in against the Ion Drive Interface Adapter, and held by four pyrotechnic devices. A trunnion links the mast canister to the solar tracking mechanism. The next Figure (3-52 b) shows the first step in deployment which occurs after IUS second stage burn. The pyrotechnic hold down devices are functioned releasing the solar array modules from the Interface Adapter. An actuator rotates the array module 180° and latches. In this position, the containment box will safely clear payload devices, and the shadowing effect on the spacecraft will be moderated. The IUS is retained until full array deployment to take advantage of its attitude control capability during deployment transients.

Figure 3-53 a shows an end on view of the solar array module while reflector boxes are being swung out. The sunward reflector is swung out first to clear a path for the shadeward reflector. After the shadeward reflector is swung out, the counterbalance is swung out.

At this stage, the deployment of the reflectors and solar array blanket is possible. Figure 3-53 b shows the module partly deployed. The near reflector is removed for clarity. The deployment mast driven by electric motors pushes the array containment cover outboard causing the folded reflectors and solar array to emerge from their containers. Cables are unreeled from storage reels to provide control of the blankets during this phase. Full deployment is shown in Figure 3-54. The 18 reflector panels are stretched taut. The solar array blanket is pulled flat, and in this view is shown edge on. Full tensioning mechanisms in the array, reflector, and counterbalance are in effect and the tip couple is nullified. The IUS separation pyrotechnic devices are functioned allowing the four bipods to open, and spring push offs establish a separation ΔV.

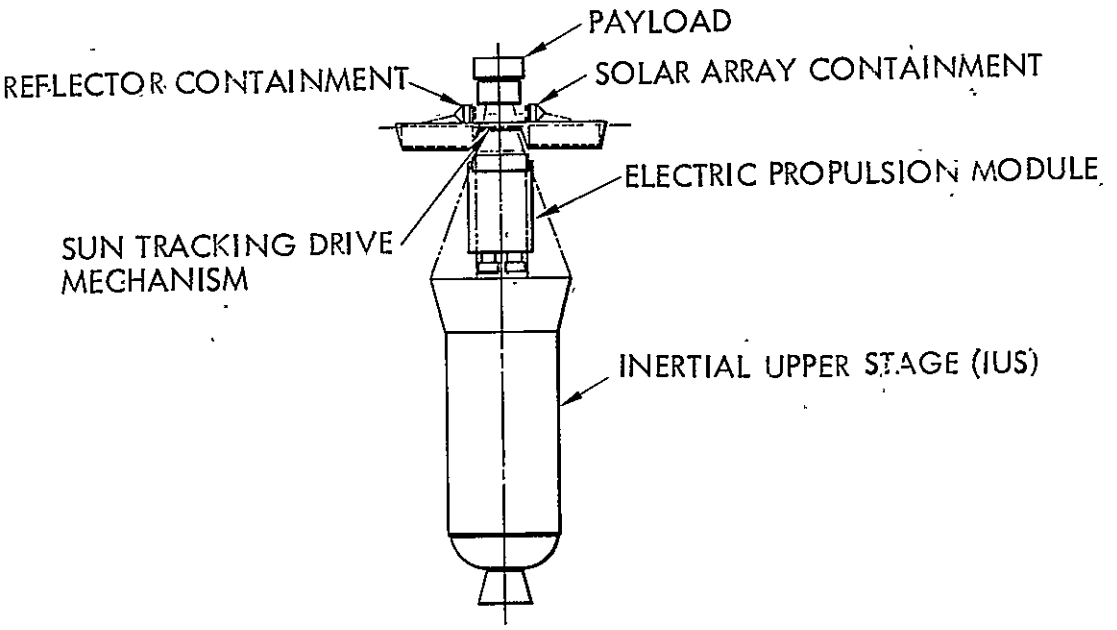

Figure 3-52 a Array/Reflector Stowed (Launch to IUS Thrust Termination)

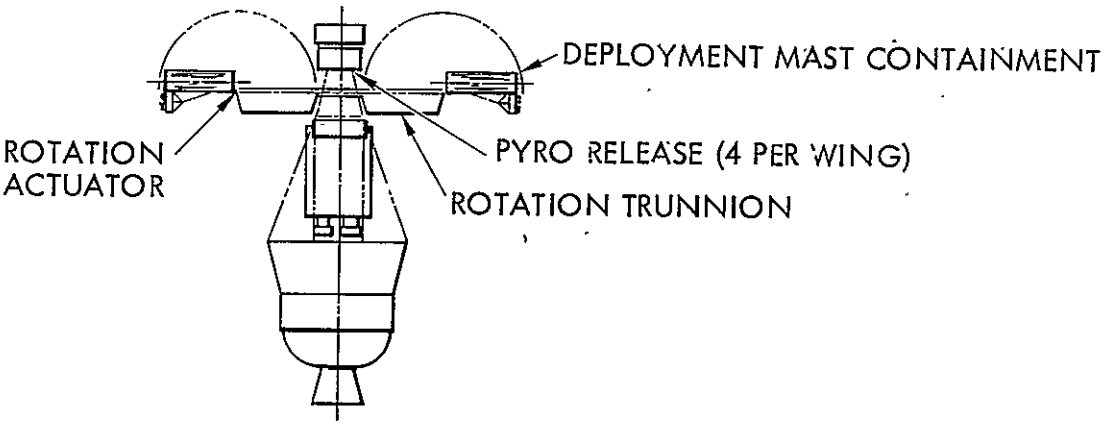

Figure 3-52 b Array/Reflector Release & Rotation (At Escape Velocity with IUS Stabilizing)

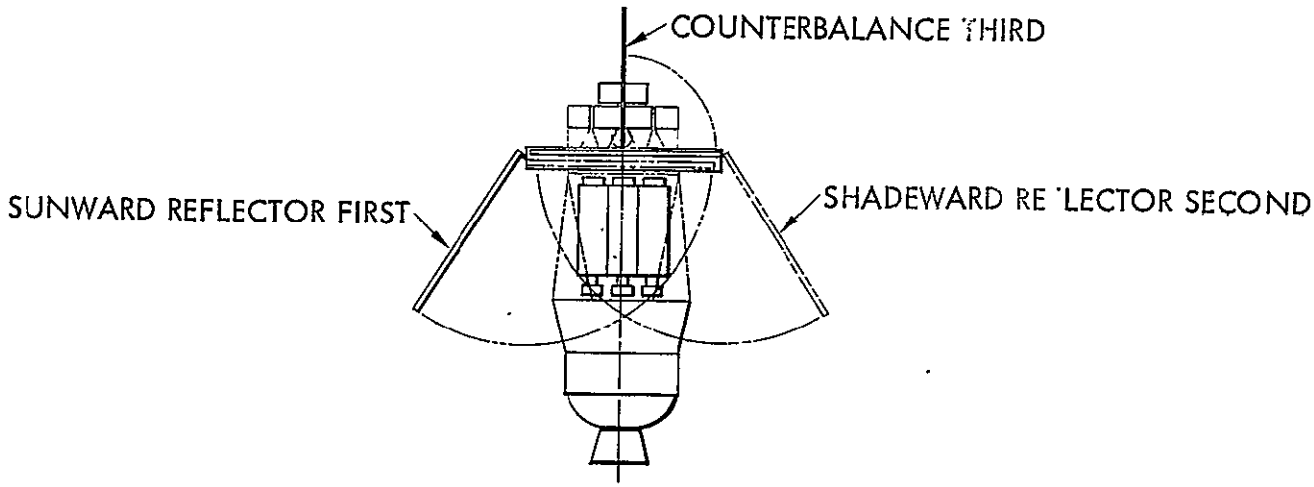

Figure 3-53 a Reflector & Counterbalance Release & Rotation (Sequential Events)

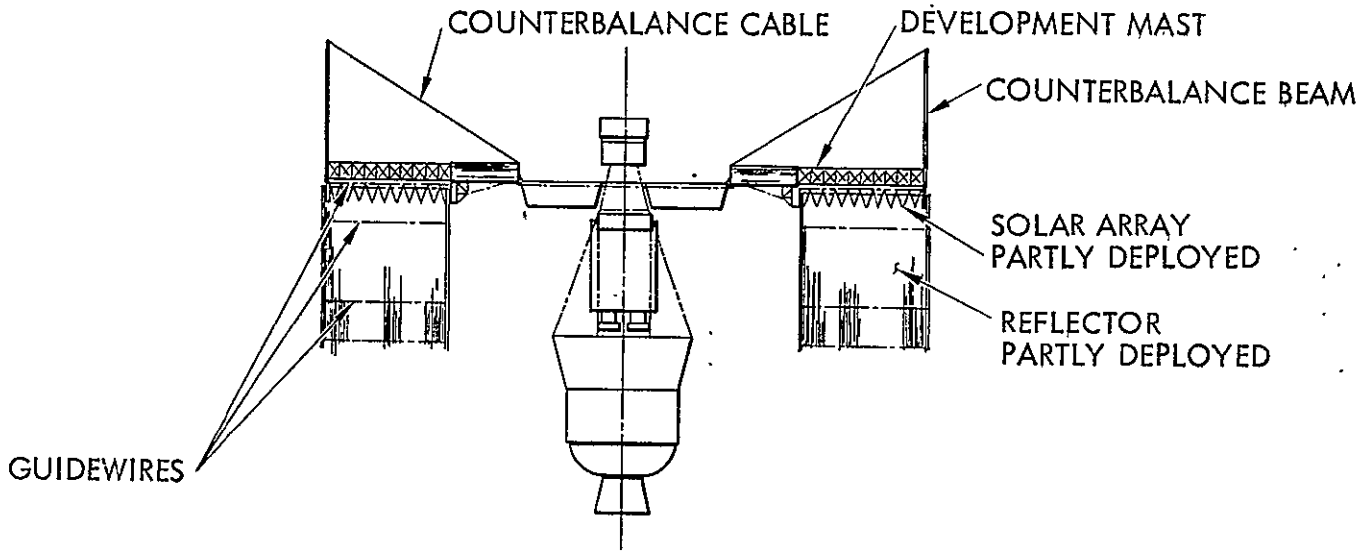

Figure 3-53 b Array/Reflector Partial Deployment Near Reflector Removed for Clarity

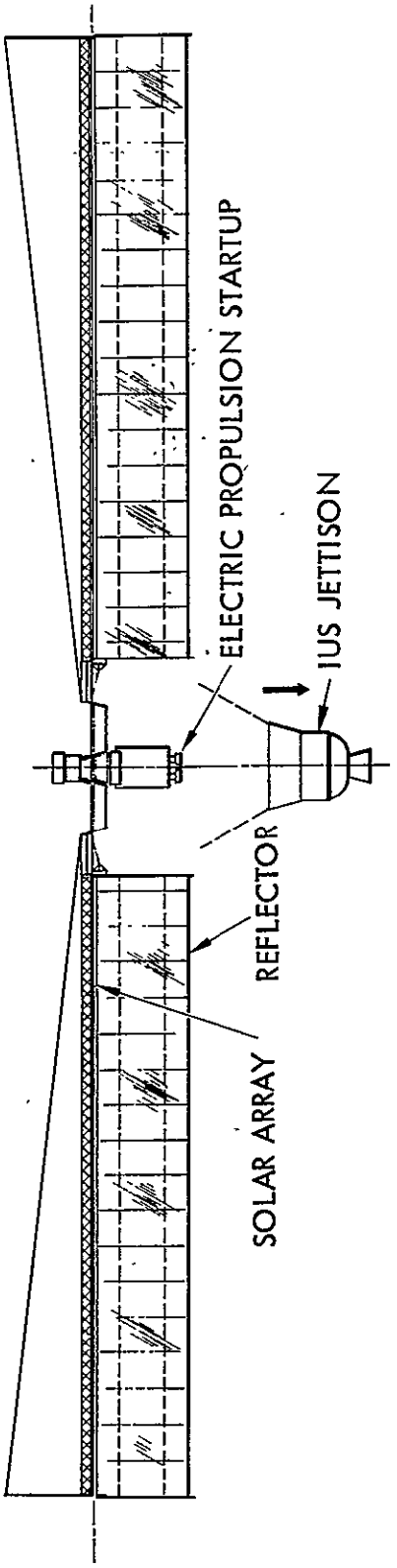

Figure 3-54 CESA Fully Deployed

Section 4

COST PROJECTION ANALYSIS

The groundrules and assumptions which were used in developing the cost projection figures for the CESA system are listed below.

- 1980 dollars
- Estimates include fee
- Estimates do not include swing out trunnions, tracking system or power transfer slip ring system
- Assume one development wing which is refurbed 30% for qual and one flight array (two wings)
- Assume basic SEP array is completely developed and qualified on other programs

Both the nonrecurring and recurring costs associated with the CESA solar array are depicted in Table 4-1. As noted total program cost would be in the range of 17 million which includes 8.548 million for one flight array incorporating two 27 panel wings. The equivalent recurring cost for a planar SEP type two wing array would be 11.057 million. The major increased cost is attributed to solar cell cost for the required 22 more panels, 67,320 solar cell assemblies plus spares. The concentrator type CESA array, though somewhat more complex mechanically, is much more cost effective costing 2-1/2 million less (22.6 percent) than its planar counterpart. It is noted that definitive formal pricing should be initiated at the time of program inception because of the fluidity of rates, burdens and inflation.

TABLE 4-1

		NON RECURRING	RECURRING
A	DESIGN, DRAWINGS, ANALYSIS AND SPECIFICATIONS	4,205K	
B	TOOLING DESIGN, FABRICATION AND CHECKOUT	765K	
C	MFG PLANNING, COORDINATION AND PRODUCEABILITY ENGR	331K	80K
D	ENGINEERING TEST HARDWARE – MATERIAL AND FABRICATION	351K	
E	DESIGN DEVELOPMENT TESTING	327K	
F	COMPONENT QUALIFICATION TESTING	127K	
G	MAIN UNITS – FABRICATION, ASSEMBLY, DEPLOYMENT AND ELECTRICAL TESTING	1,237K	8,153K
H	OTHER COSTS – GSE, QA, MFG IN PROCESS TESTS AND PROGRAM MANAGEMENT	1,113K	315K
	SUB TOTAL	8,456K	8,548K
	TOTAL	17 MILLION	

Section 5

NEW TECHNOLOGY

During the course of the study one innovative concept was developed during the concentrator analysis work that is in a new technology category. The pertinent data pertaining to this concentrator concept is as follows:

TITLE - Segmented Compound Reflector

This is an adaptation of a simple trough type reflector wherein a supplementary offset guidewire is incorporated on the deployed reflector such that each reflector contains two planes. This is a simple simulation of a parabolic reflector that provides significantly higher concentration ratios than trough or sawtooth concentrators. It is depicted in Figure 5-1.

INNOVATOR - W. R. Szmyd

PREVIOUSLY REPORTED - This innovation was formerly reported in the CESA Design Study Final Review brochure, 20 September 1978, on pages 12, 13, 34 and 35.

FINAL REPORT INCORPORATION - Discussions of the Segmented Compound Reflector concept are incorporated in this report, Section 3.2.1, pages

DATE OF INITIAL REPORTING - The Segmented Compound Reflector concept was first discussed with the JPL CTM at the second contract working review, 19 July 1978.

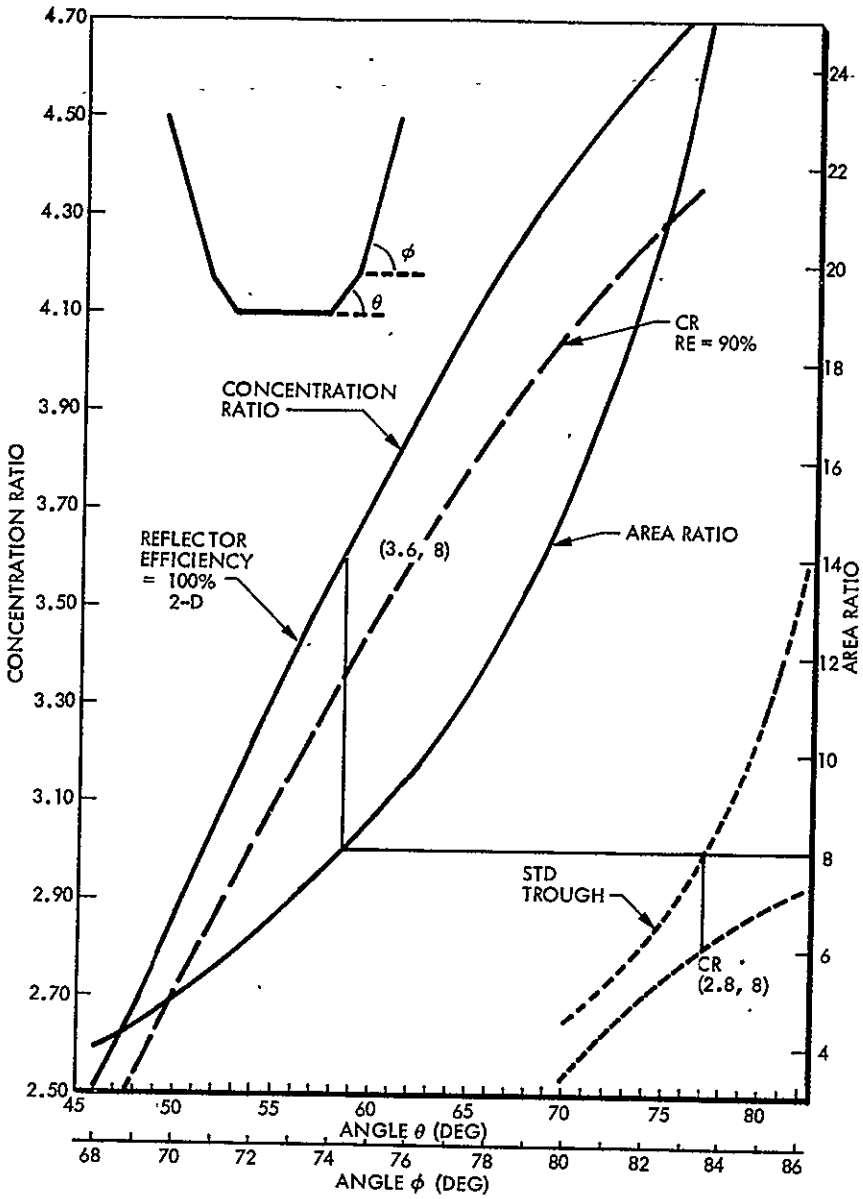

Figure 5-1 Segmented Compound Reflector